Electrodeposition of Ni-W Alloy and Characterization of Microstructure and Properties of the Deposits

Mizushima, Io

Publication date:
2007

Ph.D Thesis

Electrodeposition of Ni-W Alloy and Characterization of Microstructure and Properties of the Deposits

Io Mizushima

December 2006
Materials and Process Technology, MPT
Department of Manufacturing Engineering and Management, IPL
Technical University of Denmark, DTU

Preface

The present dissertation is submitted for acquiring Ph.D. degree at the Technical University of Denmark. The project has been conducted at the Department of Manufacturing Engineering and Management (IPL). Marcel A. J. Somers, Hans N. Hansen and Peter T. Tang have supervised the research activities.

The following papers are included in the thesis.

[1] I. Mizushima, P. T. Tang, H. N. Hansen and M. A. J. Somers, Electrochimica Acta, 51, 888-896 (2005)
[2] I. Mizushima, P. T. Tang, H. N. Hansen and M. A. J. Somers, Electrochimica Acta, 51, 6128-6134 (2006)

Acknowledgements

I gratefully acknowledge my supervisors. Professor Marcel A. J. Somers has kindly given me a lot of opportunities to be aware to consider deeply from some different points of view and improve skills in formulating. Professor Hans N. Hansen has given ideas of applications of electroplating. Dr. Peter T. Tang has provided many suggestions for resolving practical problems.

I thank Dr. Karen Pantleon and Dr. Anette A. Rasmussen for discussions of the present work.

I am grateful to Steffen S. Munch and Flemming B. Grumsen for the experimental assistance of the present thesis.

Professor Watanabe has contributed to discussions and arrangements for experiments with Focused ion beam (FIB) microscope and Glow Discharge-Optical Emission Spectroscopy (GD-OES).

Abstract

The subject of this thesis is an electrodeposition of Ni-W alloy and characterization of microstructure and properties of the deposits. In Chapter 3 background such as theoretical comments and literature reviews which provided suggestions for the way to tackle this subject, is described. The experimental results of the present work are given in the chapters 4-9. In Chapter 4 development of a new electrolyte for Ni-W alloys is described. In the chapters 5-9 the properties of the Ni-W alloys such as residual stress, microstructure, hardness and thermal stability are investigated. Furthermore, a paper on the fabrication of forming tool by electroforming of nickel based alloys is added as an appendix to this thesis. This serves as an example of an application of the material developed in this work. Details of the experimental procedures and the theories of unusual techniques such as cross-section observation with focused ion beam microscopy, compositional analysis with glow discharge optical emission spectroscopy and line broadening analysis of X-ray diffraction etc are given in Chapter 3.

In Chapter 4 the effect of the complexing agents citrate, glycine and triethanolamine (TEA) on the electrodeposition of Ni-W layers from electrolytes based on $NiSO_4$ and Na_2WO_4, is investigated. High W content and current efficiency could be realized by using electrolytes containing all of the three complexing agents. The results show that small amounts of glycine in a citrate-triethanolamine based electrolyte positively influence fractional current for Ni and Ni-W alloy deposition.

In Chapter 5 the residual stress in Ni-W layers electrodeposited from electrolytes based on $NiSO_4$ and Na_2WO_4, is investigated. The results show that the type of complexing agent and the current efficiency have an influence on the residual stress. In all cases, an increase in tensile stress in the deposit with time after deposition was observed. The increment depends on the applied current density.

In Chapter 6 Ni-W layers electrodeposited from electrolytes based on $NiSO_4$, Na_2WO_4 citrate, glycine and triethanolamine are characterized with glow discharge optical emission spectroscopy (GD-OES) and X-ray diffraction analysis (XRD). XRD showed the occurrence of an anomalous phase in the deposits, associated with the presence of an appreciable amount of carbon as identified with GD-OES. The anomalous phase is metastable and vanishes upon annealing at 550°C in air.

In Chapter 7 the influence of the age of an electrolyte, containing glycine as complexing agent, on the microstructure of a Ni-W electrodeposit is investigated. The microstructure of the electrodeposits was characterized with scanning electron microscopy (SEM), X-ray diffraction (XRD) analysis and glow discharge optical emission spectroscopy (GD-OES). It was observed that an anomalous Bragg peak at $2\theta \approx 41.5°$ occurs for layers deposited from the aged electrolyte and not for layers deposited from the fresh electrolyte; the intensity of the Bragg peak increases with the age of the electrolyte. Simultaneously, the presence of carbon is observed with GD-OES in layers deposited from the aged electrolyte. The carbon dissolution in the Ni-W alloy deposit is associated with the formation of a new phase in the electrodeposit, giving rise to the anomalous Bragg peak.

In Chapter 8 hardness, grain size and thermal stability of nickel and Ni-W alloy layers deposited from electrolytes containing equal amounts of citrate, glycine and triethanolamine are investigated. The hardness of the deposits was investigated in the as-deposited layer as well as after annealing for 1 hour at temperatures up to 550°C. The grain size and microstrains were determined for several crystal orientations by pseudo-Voigt single line analysis of the corresponding X-ray line profiles. The micro Vickers hardness of the nickel deposits depends on the thermal history of the sample. Depending on the microstructure and composition of the electrodeposit the hardness increases or decreases with annealing temperature (for 1 hour). The results are discussed in terms of the possible strengthening mechanisms for nano-crystalline electrodeposits.

In Chapter 9 the evolution of residual stress in Ni-W layers electrodeposited from electrolytes based on $NiSO_4$ and Na_2WO_4 upon storage at room temperature is investigated. An increase in tensile stress in the Ni-W electrodeposit upon storage at room temperature was observed; the increase in tensile residual stress is larger for higher the current densities during electrodeposition. For one current density the electrical resistivity of a Ni-W layer was measured as a function of storage time. The evolution of stress increase and reduction of electrical resistivity are equal for the first three hours.

Dansk resumé

Emnet for nærværende afhandling er udvikling af en ny elektrodeponeringsproces til Ni-W legeringerne som har høj hårdhed og termisk stabilitet. Kapitel 3 indeholder teoretiske overvejelser samt en litteraturoversigt, og forsyner dermed det videre arbejde med retningslinier for, hvordan problemstillingen skal håndteres. De eksperimentelle resultater fra det nærværende arbejde er beskrevet i kapitel 4 til 9. I kapitel 4 er udviklingen af en ny elektrolyte til Ni-W legeringerne behandlet. Kapitel 5 til 9 undersøger indre spændinger, mikrostrukturen, hårdheden og termisk stabilitet. Der er også en rapport om fremstilling af værktøjer til massivformning fremstillet af nikkellegeringer i appendiks til denne afhandling. Det er et eksempel på anvendelse af det udviklede materiale. Detaljer vedrørende specielle eksperimentelle tekniker såsom tværsnit fremstillet og observeret med Focused Ion Beam (FIB) mikroskopi, kompositionsanalyse ved Glow Discharge Optical Emission Spectroscopy (GD-OES) og linieforbredningsanalyse ved røntgendiffraktion er angivet i kapitel 3.

I kapitel 4 blever effekten af citrat, glycin og triethanolamin (TEA), anvendt som kompleksdannere, på elektrodeponering af Ni-W legeringerne fra elektrolyter basered på $NiWO_4$ og $NaWO_4$ undersøgt. Højt strømudbytte og passende W indhold blev virkeliggjort i elektrolytter indeholdende alle tre kompleksdannere. Mindre mængder af glycin i elektrolyter baseret på citrat og TEA indvirker positivt på den forholdsmæssige strøm der går til Ni og Ni-W elektrodeponering.

Kapitel 5 undersøger indre spændinger i Ni-W deponeret fra elektrolyter baseret på $NiWO_4$ og $NaWO_4$. Typen af kompleksdanner har indflydelse på spændingerne. Spændingerne forøges som funktion af tiden efter elektrodeponering i alle tilfælde. Forøgelsen med tiden er større ved høje strømtætheder.

Kapitel 6 undersøger Ni-W deponeret fra elektrolyter baseret på $NiWO_4$ og $NaWO_4$ ved GD-OES og røntgendiffraktion. Røntgendiffraktion viser dannelse af en afvigende fase i Ni-W legeringerne, som er forbundet med tilstedeværelsen af kulstof i de deponerede lag. Den afvigende fase viser lavt termisk stabilitet og forsvinder efter varmebehandling i en time ved temperaturer på 550 °C.

Kapitel 7 undersøger effekten af ældning af elektrolytter indeholdende citrat, glycin og TEA på mikrostrukturen af Ni-W legeringerne. Mikrostrukturen blev karakteriseret med scanning electron microscopy (SEM), røntgendiffraktion og GD-OES. Det blev observeret, at et afvigende Braggs peak ved $2\theta \approx 41.5°$ opstår ved Ni-W deponeret fra en brugt elektrolyt men ikke ved fra frisk elektrolyt. Intensiteten af Braggs peaken forøger med elektrolyttens alder. Tilstedeværelsen af kulstof i udfældninger fra en brugt elektrolyt blev observeret samtidigt med GD-OES analyse. Kulstof opløst i Ni-W legeringen er forbundet med dannelse af den nye fase.

Kapitel 8 undersøger mikrostrukturen, hårdheden og den termiske stabilitet af Ni og Ni-W deponeret fra elektrolytter indeholdende samme mængde af citrat, glycin og TEA. Denne elektrolyt resulterer i et vist kulstof indhold og nanokrystallinske Ni og Ni-W lag. Ni-W lag viser højere termisk stabilitet end Ni lag indeholdende kulstof. Ni lag udviser en mere homogen kornstørrelse end Ni-W lag. Hårdheden af Ni lagene forøges efter varmebehandling i en time ved temperature på 250 °C men aftager i

intervallet fra 250 °C til 550 °C. Hårdheden af Ni-W lagene fortsætter med at stige ved temperaturer op til 550 °C.

Kapitel 9 undersøger udviklingen af de indre spændinger i Ni-W deponeret fra elektrolytter baseret på $NiWO_4$ og $NaWO_4$ opbevaret ved stuetemperatur. Forøgelsen af spændingerne ved opbevaring ved stuetemperatur bliver større ved høje strømtæthed. Den elektriske modstand af Ni-W lag deponeret ved en udvalgt strømtæthed, som funktion af tiden, blev studeret. Forøgelsen i spændingerne er den samme som ændringen i den elektriske modstand i de første tre timer.

Content

1. Introduction

Micro-injection mouldin molding is foreseen to find wide future application for production of computer parts, microfluidic systems and polymer optical components. For the injection molding of high performance plastics, possessing high strength and chemical resistance, the molds must be able to withstand thermal exposure cycling at temperatures up to 350°C.
Fabrication of the mouldin molding tool is preferably performed by electroforming in order to be able to control the replication of microscale geometrical details. Nickel is a widely applied material for electroforming, but pure nanocrystalline nickel electrodeposits cannot withstand the relatively high temperature without loosing their hardness due to recrystallization. Among the metals and alloys which are expected to have a higher thermal stability than nickel, and which can be electrodeposited, Ni-W is a favorable candidate. Furthermore, a Ni-W alloy is an excellent material, because it has high corrosion resistance and mechanical strength.
Therefore, several authors have investigated on the electrodeposition of Ni-W alloys [1-13]. The formation of precipitates (probably $NiWO_4$)[13] in the electrolyte for the electrodeposition of Ni-W alloys can be overcome by adding a suitable complexing agent. The influence of such a complexing agent on the current efficiency, the composition of the deposit and mechanical properties, etc. is critical. Actually, citrate which forms a complex with both the nickel ion and tungstate and gives stability to the electrolyte is a common complexing agent for Ni-W electroplating. However, citrate is associated with low current efficiency. To overcome this disadvantage ammonia is often added, which raises the current efficiency, but ammonia enhances only the transport of nickel ions by complex formation and consequently reduces the tungsten content in the deposit[2]. Consequently, it is hard to obtain the combination of high current efficiency and high tungsten content with citrate as the main complexing agent in the electrolyte.

The purpose of this work is to develop a process for Ni-W alloy electrodeposition with high current efficiency, low residual stress, high hardness and high thermal stability.
Optimizing complexing agents contained in the electrolyte is a critical point of this work, because a complexing agent influences seriously the current efficiency, microstructure and mechanical properties such as hardness and strength of the deposit.

The result part in this thesis is composed of six chapters (Chapter 4-9). These are independent papers, nevertheless; actually those are associated with one another in several ways.
Chapter 4 is a paper on development of the process for Ni-W alloy deposition with high current density and reasonable tungsten content. Chapter 5 is a paper on investigation of residual stress in Ni-W electrodeposits which gives rise to a serious problem of crack occurrence in the deposit. Chapter 6 is a paper on identification of an anomalous phase which was found in the Chapter 4. Chapter 7 is a paper on influence of age of glycine based-electrolyte, which is actually associated with the formation of the anomalous phase investigated in Chapter 6. Chapter 8 is a paper on the crystallographic microstructure, hardness and thermal stability of Ni-W alloy layers electrodeposited from the electrolyte, which were optimized in the Chapter 4. Comparison with investigations of pure Ni layers from the electrolyte containing

same complexing agents is also given in the chapter. Chapter 9 is a paper on time-dependence of residual stress in the Ni-W alloy electrodeposits, which was recognized as a critical matter in the work described in the Chapter 5.

Furthermore, a paper on fabrication of forming tool by electroforming of nickel based alloys is added as an appendix in this thesis. The work was performed based on the fundamental work. This serves as an example of an application of the material developed in this work.

References

1. A. Brenner, "Electrodeposition of Alloys", Vol. 2, p. 347, Academic Press, New York (1963)
2. O. Younes & E. Gileadi, J. Electrochem. Soc., **149** (2) C100-C111 (2002)
3. O. Younes & E. Gileadi, Electrochemical Solid-State Letters, **3** (12) 543-545 (2000)
4. O. Younes, L Zhu, Y Rosenberg, Y. Shacham-Diamand & E. Gileadi, Langmuir, **17**, 8270-8275 (2001)
5. Y. Wu, Do-Y. Chang, Sik-C. Kwon & D. Kim, Plating and Surface Finishing, (2) 46-49 (2003)
6. M. Bratoeva & N. Atanasov, Russian Journal of Electrochemistry, **36** (1) 60-63 (2000)
7. H. Cesiulis, M. Donten, M.L. Donten & Z. Stojek, ISSN Material Science, (4) 230-234 (2001)
8. T. Yamasaki, P. Schloßmacher & Y. Ogino, Nanostructured Materials, Vol. 10, No. 3 (1998) 375-388
9. T. Yamasaki, Mater. Phys. Mech., Vol. 1 (2000) 127-132
10. P. Schloßmacher & T. Yamasaki, Mikrochim. Acta, 132 (2000) 309-313
11. K. Itoh, Feng Wang & T. Watanabe, J. Japan Inst. Metals, Vol. 65, No 11, 1023-1028 (2001)
12. L. Huang, J. X. Dong, F. Z. yang, S. K. Xu & S. M. Zhou, Trans. IMF, 77 (5) 185-187 (1999)
13. N. Eliaz, T. M. Sridhar, E. Gileadi, Electrochimica Acta, 50, 2893-2904 (2005)

2. Literature reviews

2.1 Electroplating of Ni-W alloys[1,2]

Electrodeposition of tungsten has been attempted numerous times, because of the interests in the unusual properties of the metal such as the high melting point of 3410°C, the tensile strength, the high isotropic Young's modulus of elasticity, and the low coefficient of linear thermal expansion.
Tungsten deposits electroplated from an electrolyte containing ammonium salts and ammonium hydroxide have so far been in poor condition and porous.[1] The failure of tungsten deposition was attributed to a low potential for hydrogen evolution on tungsten, so deposition of tungsten alone from aqueous solution could not be sustained.[1] Baths for alloy deposition of tungsten and iron group metals have been developed, using organic compounds of citrate and malate as complexing agents.[1]

Indeed, the potential of Ni-W alloy deposition is more positive than both for the pure nickel and tungsten depositions, indicating that both nickel and tungsten stimulate each other for deposition, as shown in Fig. 2.1. The current for an electrolyte containing Na_2WO_4 and citrate is mostly spent for hydrogen evolution. The voltammetric curve shows that tungsten promotes hydrogen evolution.

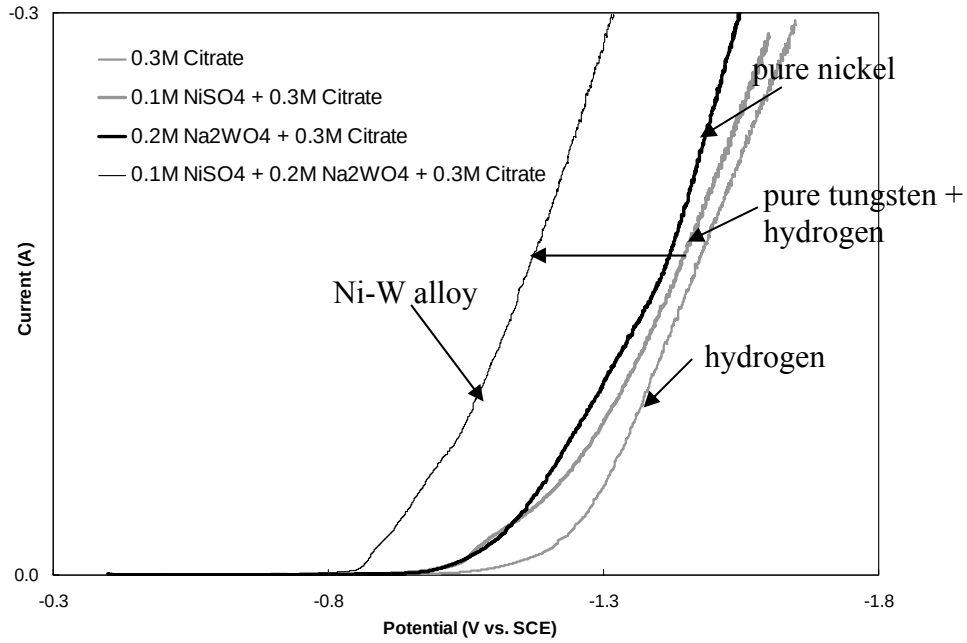

Fig.2.1: Voltammetric curves from electrolytes containing 0.3M citrate, 0.1M $NiSO_4$ and 0.3M citrate, 0.2M Na_2WO_4 and 0.3M citrate, and 0.1M $NiSO_4$, 0.2M Na_2WO_4 and 0.3M citrate

Younes et al. have studied the ammoniacal citrate bath for Ni-W alloy electrodeposition systematically [1]. They attempted to understand the mechanism of deposition of Ni-W alloys, taking into account the distribution of the different ions as a function of pH value and concentration of citric acid and ammonia (Fig.2.2).
The number of active hydrogen atoms on the carboxyl groups of citric acid decreases with increasing pH value. The predominant ion Cit^{3-} in the range of pH=6-10 is the main ligand in all the complexes in the electrolyte.

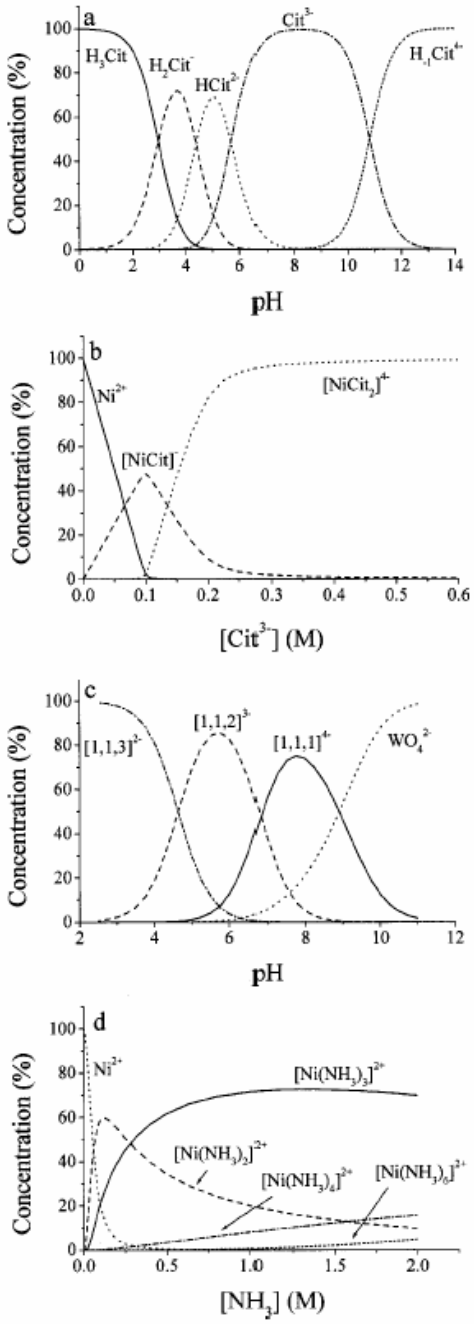

Fig.2.2: Concentration distributions of chemical species of citric acid as function of pH (a), complex of Ni-citrate as function of concentration of citric acid (b), tungstate as a function of pH (c) and complex of Ni-ammonium as a function of pH (d) [1]

Citrate forms a complex with the nickel ion as follows:

$$Ni^{2+} + xCit^{3-} \rightarrow (Ni)(Cit)_x^{2-3x} \qquad (2.1)$$

Citrate forms a complex also with the tungstate ion as following,

$$WO_4^{2-} + Cit^{3-} + xH^+ \rightarrow [(WO_4)(Cit)(H)_x]^{x-5} \qquad (2.2)$$

Hayashi et al. also confirmed [2] the complex formation with an increase in pH value in potentiometric titration method.

The number x decreases with increasing pH value, as shown in Fig. 2.3. The complex equilibrium constants are 10.2, 17.2 and 21.7 for $x = 1$, 2 and 3, respectively.[1]

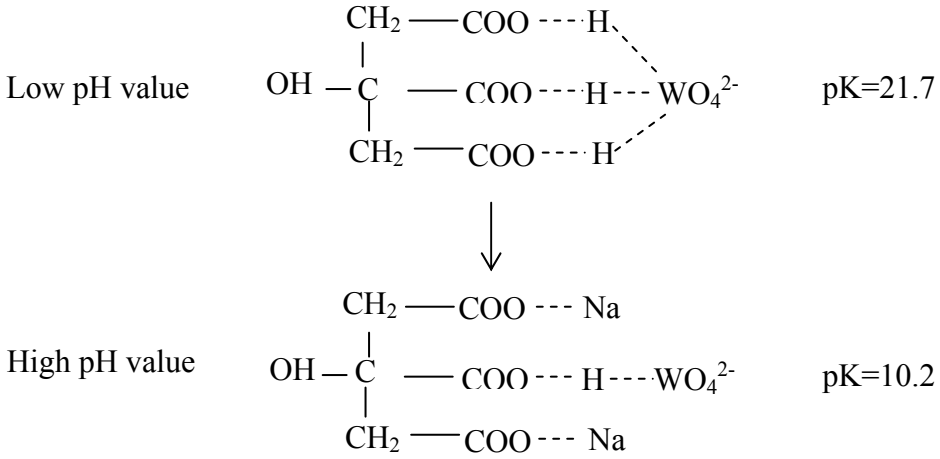

Fig.2.3: schematic drawing of complex formation between citrate and tungstate

The ternary complex of Ni, W and citrate can be formed, as shown in Fig. 2.4.

$$[(Ni)(Cit)]^- + [(WO_4)(Cit)(H)]^{4-} \rightarrow [(Ni)(WO_4)(Cit)(H)]^{2-} + Cit^{3-} \qquad (2.3)$$

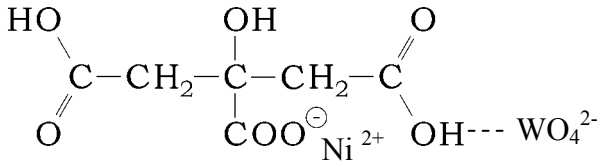

Fig.2.4: A schematic drawing of ternary complex formation of citrate, nickel ion and tungstate ion

Deposition of Ni-W alloy can be achieved through ternary complex formation.

$$[(Ni)(WO_4)(Cit)(H)]^{2-} + 8e^- + 3H_2O \rightarrow NiW + 7(OH)^- + Cit^{3-} \qquad (2.4)$$

In this system the depositions of nickel alone and Ni-W alloy take place.
Increasing concentration of $NiSO_4$ increases both the partial current for tungsten and nickel.
Ammonia concentration has also a substantial influence on the composition of the alloy deposit, since ammonia competes with citrate as a ligand for the nickel ion. With increasing ammonia concentration, the partial current for tungsten decreases, but the one for nickel increases. Increasing pH value also decreases the partial current for tungsten deposition.

2.2 Electrocrystallization of Ni-W alloys

2.2.1 Electrocrystallization[3]

Electrocrystallization involves distinct steps, such as the diffusion of ions in the solution to the electrode surface, electron transfer, partial or complete loss of the solvation sheath which results in the formation of adsorbed atoms, surface diffusion of ad-atoms, clustering of ad-atoms to form critical nuclei, incorporation of ad-atoms at lattice sites and development of crystallographic and morphological characteristics of the deposit, as shown in Fig. 2.5.

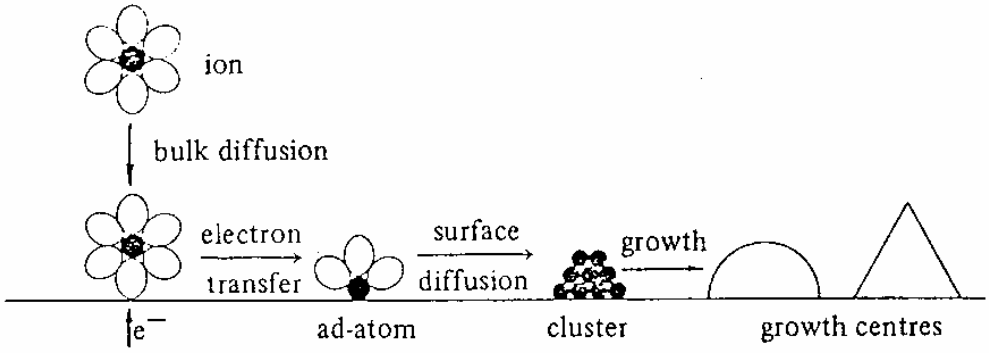

Fig.2.5: A schematic drawing of the process of electrocrystallization

For a complicated thermodynamic description of electrochemical phase formation taking into account the changes in energy and entropy associated with the process, it is useful to examine the process (2.5) of the growth of a solid phase M(s) from its supersaturated vapour M(g), which has many features in common with the electrocrystallisation.

$$M(g) \rightarrow M(s) \qquad (2.5)$$

When the solid M is in full thermodynamic equilibrium with its own vapour, the chemical potential of the gas is exactly equal to that of the solid.
The chemical potential of this component in the gas μ_M is related to its partial pressure p.

$$\mu_M = \mu_M^0 + RT \ln(p / p^*) \qquad (2.6)$$

where $p*$ is the equilibrium vapour pressure in the reference state μ_M^0, and R is the universal gas constant. If the vapour pressure exceeds $p*$, in which case the vapour is said to be supersaturated with M, and spontaneous growth of the solid phase can only occur.
The Gibbs energy change associated with growth of the solid phase in case of increasing the pressure is given by,

$$\Delta G_{\mathrm{v}} = -\frac{RT}{\overline{V}} \ln(p / p*) \qquad (2.7)$$

where $p / p*$ is referred to as the supersaturation ratio, and $\overline{V} = M / \rho$ is the molar volume of condensed phase.
The driving force for the formation of solid phase is determined by pressure and temperature.

In case of electrochemical phase formation, equilibrium is established by electron transfer. If the electrode process is of the general type the following to the equation applied,

$$M^{n+} + ne \leftrightarrow M \qquad (2.8)$$

The equilibrium electrode potential, E_e, is given by the Nernst equation.
Under the equilibrium conditions the surface activity of ad-atoms has its equilibrium value $a^*_{M_{ads}}$. If the electrode potential is charged to some value $E = E_e + \eta$, where η is the overpotential, the surface activity of ad-atoms is determined by the relationship.

$$E = E_e + \eta = E_e + \frac{RT}{nF} \ln \frac{a_{M_{ads}}}{a^*_{M_{ads}}} \qquad (2.9)$$

$$\frac{a_{M_{ads}}}{a^*_{M_{ads}}} = \exp(-nF\eta / RT) \qquad (2.10)$$

where n is the charge number of the reduction reaction, F is Faraday's constant, and T is temperature.
By pursuing the analogy with homogeneous nucleation from the vapour and replacing the supersaturated ratio of the vapour, p / p^* of the equation (2.7) with the surface activity, $a_{M_{ads}} / a^*_{M_{ads}}$, the volume Gibbs energy of formation of the condensed phase is given by,

$$\Delta G_V = nF\eta / \overline{V} \left(\Delta G = -RT \ln a / a^*\right) \qquad (2.11)$$

where $\overline{V}$ is the molar volume of the formed phase. The Gibbs energy change depends on the over-potential associated with the surface activity. (Fig. 2.6)

$$\eta > 0 \rightarrow 0 < \frac{a}{a*} < 1 \rightarrow \Delta G_V > 0 \qquad \eta < 0 \rightarrow \frac{a}{a*} > 1 \rightarrow \Delta G_V < 0$$

more positive potential than equilibrium electrode potential

more negative potential than equilibrium electrode potential (overpotential)

Fig.2.6: A schematic drawing of overpotential and supersaturation of ad-atoms

The electrochemical nucleation is considered to proceed via surface diffusion and incorporation of atoms or molecules into a pre-existing solid phase. The total Gibbs energy change during nucleation associated with the incorporation of atoms is a sum of changes of the Gibbs energy for the surface and the bulk formation.
If the nucleation process is homogeneous, the overall Gibbs energy change associated with the formation of a spherical nucleus has components of ΔG_{bulk} and $\Delta G_{surface}$, and is given by,

$$\Delta G = \Delta G_{bulk} + \Delta G_{surface} = \frac{4}{3}\pi r^3 \Delta G_V + 4\pi r^2 \gamma = -\frac{4\pi r^3 nF\eta}{3\overline{V}} + 4\pi r^2 \gamma \qquad (2.12)$$

where γ is the interfacial energy between nucleus and electrolyte.
As shown in Fig. 2.7, the growth of the new electrochemical phase occurs at the boundary between the electrode material and the solution. Therefore, the nucleation process must be heterogeneous, and the total change ΔG_{net} for a spherical nucleus at the electrode surface is

$$\Delta G_{net} = \Delta G_{bulk} + \Delta G_{surf} = \left\{ -\frac{4\pi r^3 nF\eta}{3\overline{V}} + 4\pi r^2 \gamma \right\} S(\theta) \qquad (2.13)$$

$$S(\theta) = (2 + \cos\theta)(1 - \cos\theta)^2 / 4 \qquad (2.14)$$

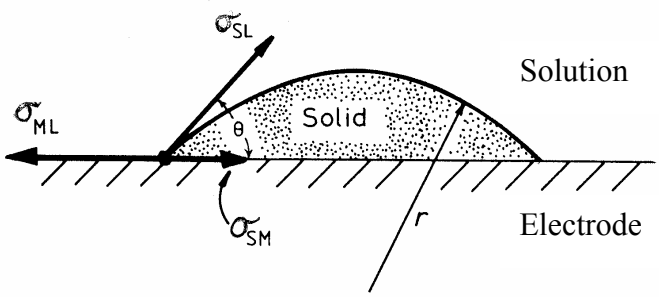

Fig.2.7: A schematic drawing of nucleation

The critical nucleus radius and the critical Gibbs energy decrease with increasing over potential, as shown in Fig. 2.8.

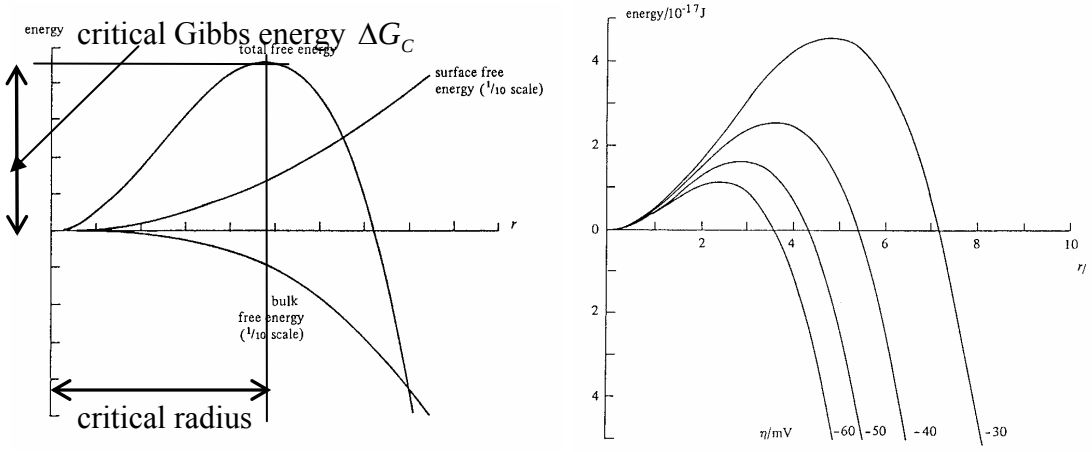

Fig.2.8: Gibbs energy for nucleation and the dependence on over- potential

The nucleation rate J is given by,

$$J = Z\alpha \exp\left(-\frac{\Delta G_C}{kT}\right) \qquad (2.15)$$

, where ΔG_C is the critical Gibbs energy, and Z is a dimensionless factor, α is the rate at which atoms are added to the critical cluster. The rate is faster for a higher over-potential.

The process of phase growth involves incorporation of atoms at lattice sites in the surface of the solid. The change of energy associated with the incorporation of atoms is related to the effective coordination number of the sites, as shown in Fig. 2.9. The most favourable sites for deposition are those high values of m.

(i) surface sites ($m = 1$)
(ii) edge sites ($m = 2$)
(iii) kink sites ($m = 3$)
(iv) edge vacancies ($m = 4$)
(v) surface vacancies ($m = 5$)

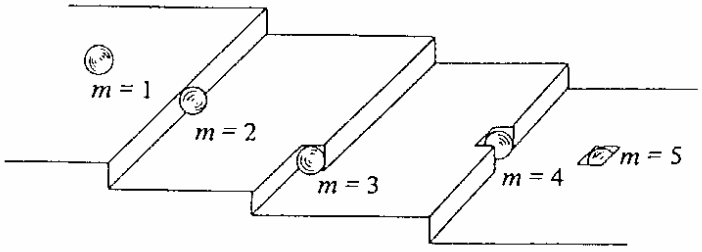

Fig.2.9: Sites characterized by coordination number

In the growth process the slowest step may involve the diffusion of ad-atoms to the sites at which they are incorporated into the crystal lattice. Distribution of ad-atoms concentration between two parallel steps depends on the over-potential η, as shown in Fig. 2.10. The atom concentration at the largest distance from the steps increases with the over-potential. The concentration of ad-atoms which diffuse to the steps increases with decreasing the over-potential. When the overpotential is high, the situation corresponds to diffusion control.

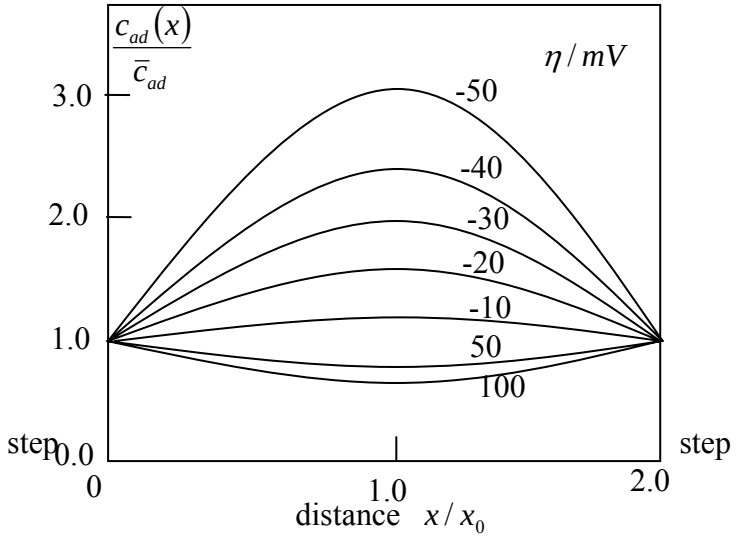

Fig. 2.10: Distribution of ad-atom concentration between two steps from each other for different values of the over-potential

2.2.2 Electrocrystallization of Ni-W alloy[3,4]

Nucleation of alloy electrodeposits is more complicated by the need to consider the change in energy and entropy associated with the mixing of several elements. As shown in Fig. 2.11, the Gibbs energies of the system after bringing together X_A mol of A and X_B mol of B and of the system after the formation of a new phase by mixing together the A and B atoms, G_1 and G_2, are given by,

$$G_1 = X_A G_A + X_B G_B \qquad (2.16)$$

$$G_2 = G_1 + \Delta G_{mix} \qquad (2.17)$$

where G_A and G_B are the molar Gibbs energies of pure A and pure B, respectively, and ΔG_{mix} is the change in Gibbs free energy involved in mixing.

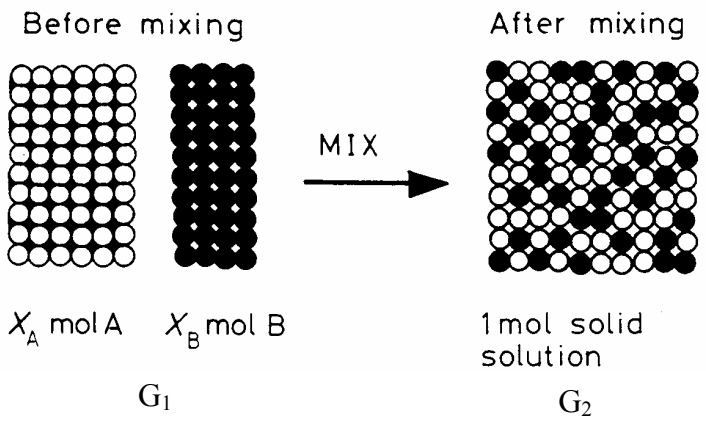

Fig.2.11: Free energy of mixing

As shown in Fig. 2.12, the Gibbs energy change ΔG_{mix} depends on the composition of the alloy and the combination of A and B atoms, in addition to temperature and pressure of the system (surface activity of ad-atoms α/α* for electrocrystallization). The Gibbs energy change has two components of the heat of solution ΔH_{mix} related to the difference between the A-B bond energy and the average of the A-A and B-B bond energies $\varepsilon = \varepsilon_{AB} - 1/2(\varepsilon_{AA} + \varepsilon_{BB})$ and the difference in entropy between the mixed and unmixed states ΔS_{mix}.

If $\varepsilon = 0$, $\Delta H_{mix} = 0$ and the resultant solution after mixing is ideal, the change in the entropy is given by,

$$\Delta S_{mix} = RT(X_A \ln X_A + X_B \ln X_B) \qquad (2.18)$$

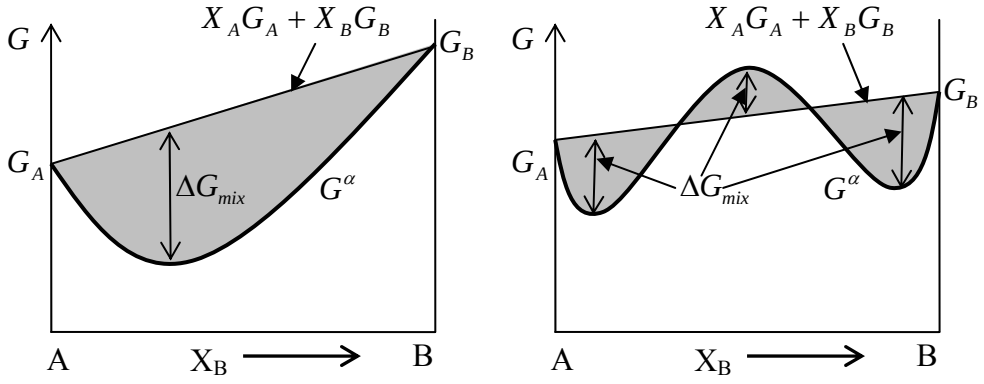

strong bond between A-B
$\varepsilon < 0 \rightarrow \Delta H_{mix} < 0$

weak bond between A-B
$\varepsilon > 0 \rightarrow \Delta H_{mix} > 0$

Fig.2.12: The molar free energy curve for the α phase

At equilibrium, alloy X_1 is a single phase α, whereas; alloy X_2 has a minimum free energy, when it is a mixture of α + β, as shown in Fig. 2. 13. The changes in Gibbs energy associated with formation of the bulk of alloys X_1 and X_2 are given by,

$$\Delta G_{net}{}^{X_1} = \left\{\frac{4}{3}\pi r^3 \Delta G_V{}^{L\to\alpha}{}_{X1} + 4\pi r^2\gamma\right\} S(\theta) \qquad (2.19)$$

$$\Delta G_{net}{}^{X_2} =$$

$$\left\{\frac{4}{3}\pi r_\alpha{}^3 \Delta G_V{}^{L\to\alpha+\beta}{}_{X\alpha}\right\} S(\theta_1) + \left\{\frac{4}{3}\pi r_\alpha{}^3 \Delta G_V{}^{L\to\alpha+\beta}{}_{(1-X_\alpha)}\right\} S(\theta_2) \qquad (2.20)$$

where θ_1 and θ_2 are contact angles of independently nucleated α and β, respectively.

Surface energy also depends on the kind of element in the crystal. The energy of Cu and W are 1720 mJ m^{-2} and 2650 mJ m^{-2}, respectively. Metals with high melting point tend to have high values for the surface energy. Change in surface energy after mixing should also be taken into account.
The free energy change is determined by alloy composition and combination of A and B atoms.

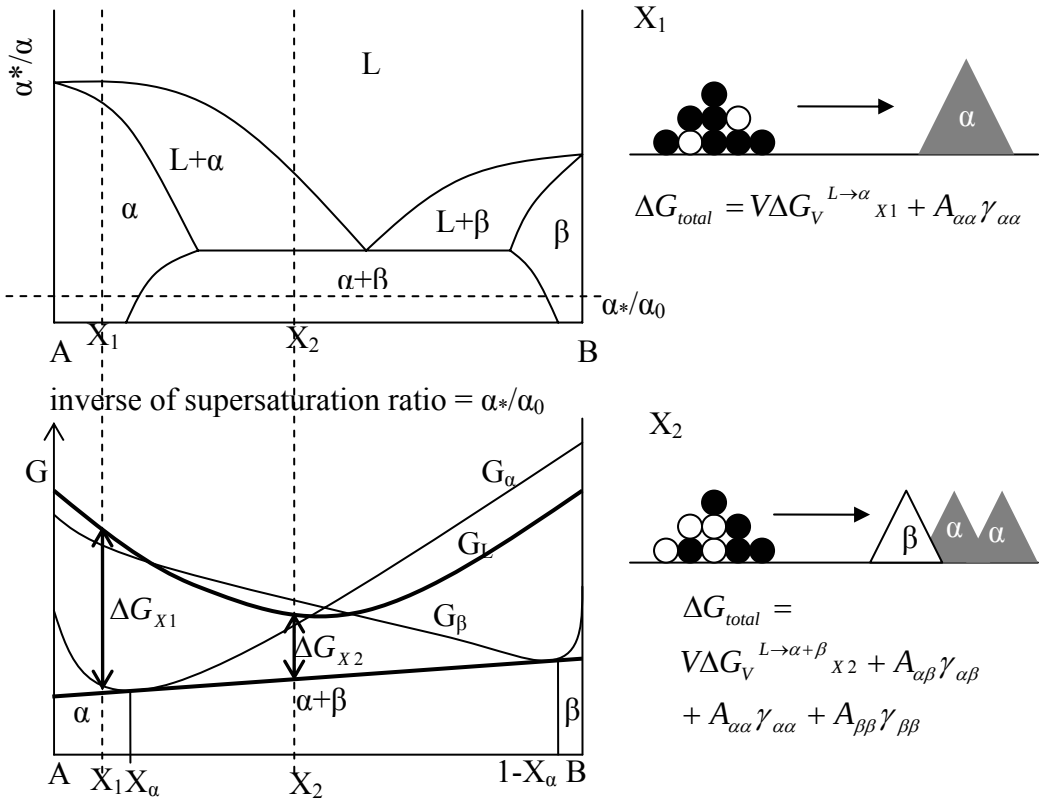

Fig.2.13: Phase diagrams and free energy variation of binary alloy and schematic drawing of nucleation of alloy

2.2.3 Microstructure of Ni-W alloy electrodeposit [5-8]

Several authors reported the structure of Ni-W alloy electrodeposits.

Ito et al. reported [4] that for Ni-W alloy electrodeposits with tungsten content ranging from 6at% to 35at% solid solution is formed and the grain size decreases for W contents above 24 at.% in the alloy. The Bragg reflections shift toward lower scattering angle with increasing tungsten content in the deposit, indicating that the f.c.c lattice expands with dissolution of tungsten in nickel. They also observed the crystallographic microstructure of the Ni-W alloy deposit with transmission electron microscope. Crystal lattices of grains in the deposits with W=0-24 at.% are observed, whereas the layers with W>28 at. % are completely amorphous.

Although in Ni-W alloy with compositions ranging 12-50at% the intermetallic phase of Ni_4W is thermodynamically stable at room temperature according to the phase diagram (Fig. 2.15), the phase could not be identified in Ni-W alloy electrodeposits with compositions ranging 12-35 at.% with X-ray diffraction phase analysis. However, Yamasaki et al. [4] suggested the presence of nano crystalline Ni_4W in Ni-W electrodeposits with W=24 at.%, taking interatomic distances determined by EXAFS as evidence. Therefore, eutectic solidification of solid solution phase and the intermetallic phase in alloy with W>14 at. % is considered to occur.

The change in Gibbs energy associated with the formation of the bulk of the alloy increases with tungsten content, as shown in Fig. 2.14. Consequently, the nucleation rate is faster and the critical radius is smaller for alloy with higher tungsten content. The supersaturation rate of ad-atoms associated with the Gibbs energy changes drastically at the liquid/solid interface. The nucleation occurs too rapid to allow solid state diffusion.

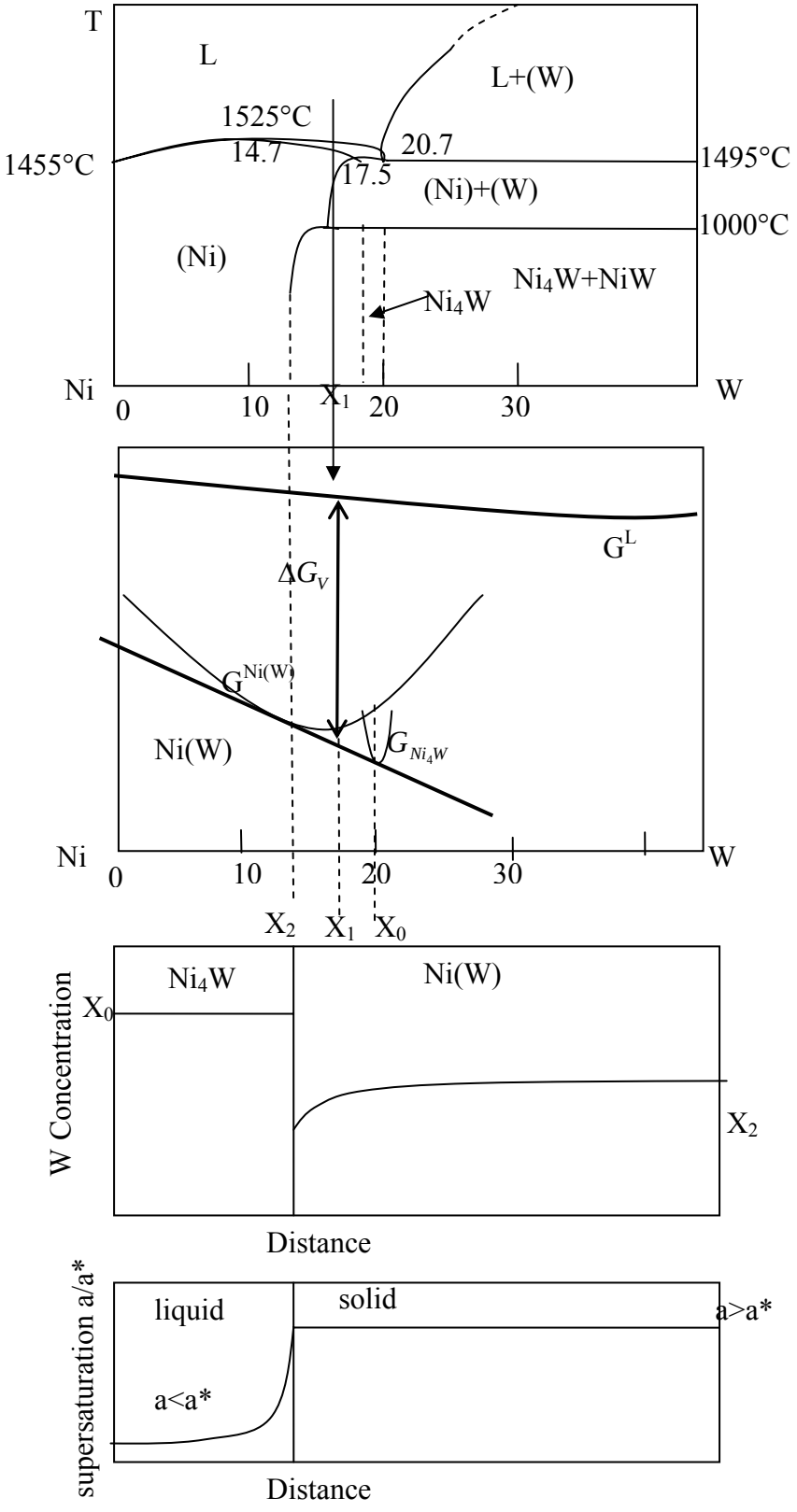

Fig.2.14: Equilibrium diagram and free energy diagram of Ni-W alloy and a concentration profile at interface Ni(W)/Ni_4W, and distribution of supersaturation of ad-atoms at interface liquid/solid

2.3 Thermal stability of Ni-W alloy electrodeposits [5-8]

There are also reports on thermal stability of structure and hardness of Ni-W electrodeposits.
Yamasaki et al. reported that a slight change in grain size of Ni-W electrodeposit with 25 at.%W with annealing for 24 hours up to 600°C and a substantial increase at 700°C, as shown in Fig. 2.15. The DTA thermogram shows crystallizations of the intermetallic compound of NiW and NiW_2 at high temperatures of 982K and 1100K, respectively. Recrystallization of the intermetallic phase Ni_4W with annealing is fairly slow. The grain growth rate is low due to the strong chemical bond between atoms in the phase, resulting in lower grain boundary mobility associated with driving force for boundary migration.

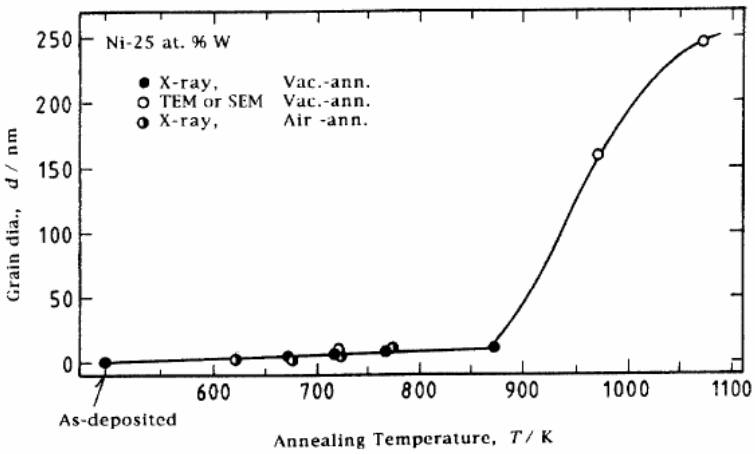

Fig.2.15: Change of grain size with annealing of Ni-W alloy electrodeposits [5]

As shown in Fig. 2.16, the hardness of the deposits increases up to 1400 MPa upon annealing at temperature up to 600 °C, and decreases above 700 °C. The hardness is still 700 MPa upon annealing at 800 °C.

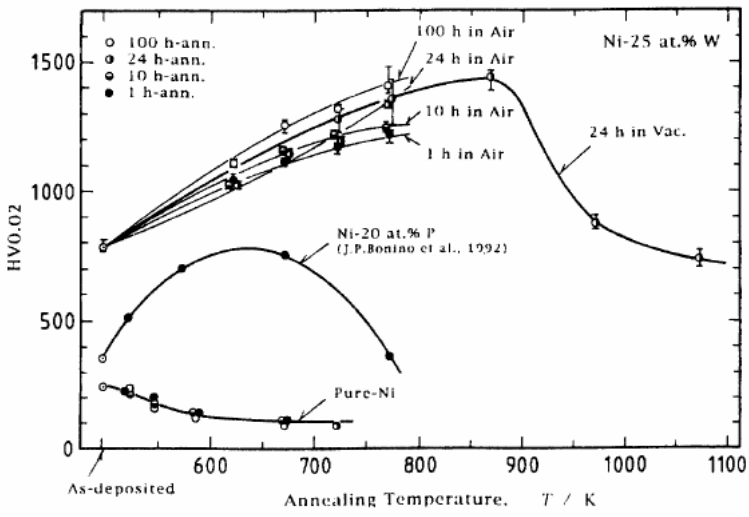

Fig.2.16: Change of grain size and hardness with annealing of Ni-W alloy electrodeposits [5]

The grain boundary hardening is well-known as the Hall-Petch relation, given by,

$$\sigma = \sigma_0 + kd^{-\frac{1}{2}} \qquad (2.21)$$

where d is particle size, σ is strength, σ_0 and k are material constants.[9,10]
For Ni-W, grain boundary strengthening has been reported to occur for grain sizes down to 12nm. For smaller grain sizes the hardness decreases with decreasing grain size, as shown in Fig. 2.17.

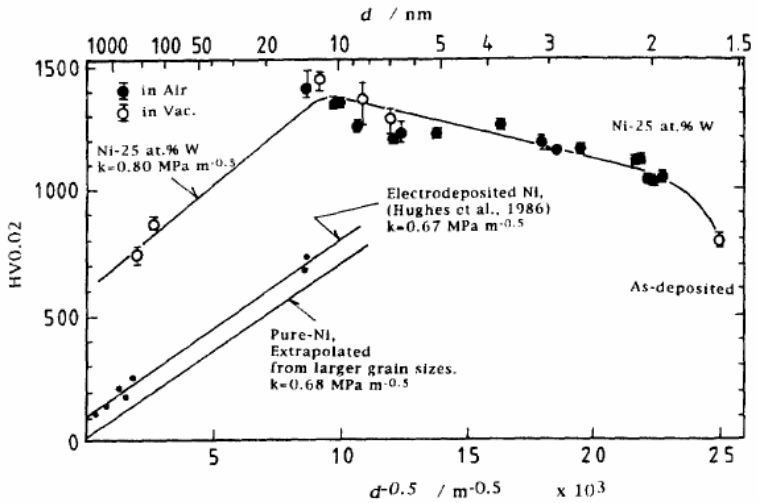

Fig.2.17: Hall-Petch relation of Ni-W alloy electrodeposits [5]

The decrease in hardness with grain size in the nanocrystalline material as compared to the Hall-Petch relation was attributed to a change of the deformation mechanism. Owing to high volume fraction of grain boundaries and triple junctions, which have a disordered structure in a gas-like manner, and possess lower Young's modulus. The volume fractions of total intercrystal V_f^{ic}, grain boundary V_f^{gb}, and triple junction V_f^{tj} are given by,

$$V_f^{ic} = 1 - \left[(d - D)/d\right]^3 \qquad (2.22)$$

$$V_f^{gb} = \left[3D(d - D)^2\right]/d^3 \qquad (2.23)$$

$$V_f^{tj} = V_f^{ic} - V_f^{gb} \qquad (2.24)$$

where d and D are the grain diameter and the grain boundary thickness, respectively. The thickness of the grain boundary was determined with high resolution transmission electron microscopy.
The calculated values of the volume fraction as a function of the square root of the grain diameter are shown in Fig. 2.18. As shown in the figure, intercrystalline fractional volume is approximately 80%, when grain boundary thickness and grain size are 1.5nm and 5nm, respectively.

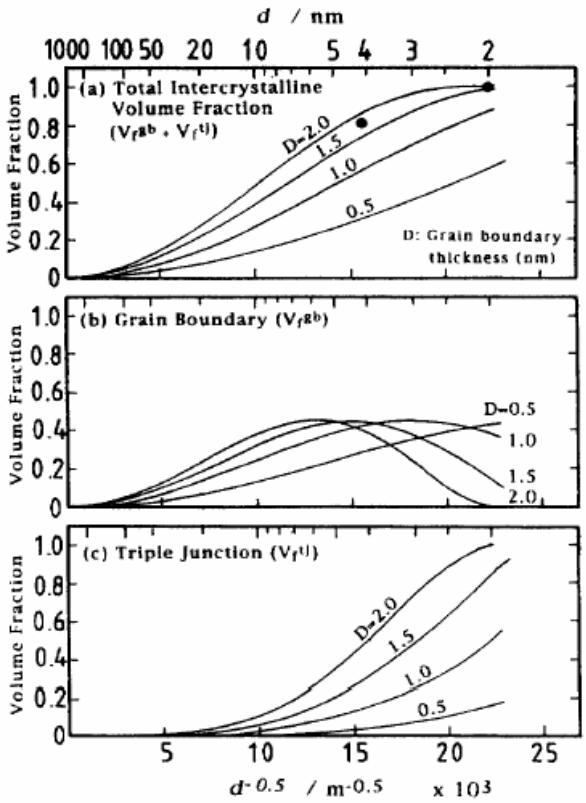

Fig.2.18: Caluculated volume fractions for total intercrystalline volume fraction, grain boundary volume fraction and triple junction volume fraction as function of the square root of the grain diameter [5]

The intercrystalline volume fraction increases remarkably with decreasing grain size. When the intercrystalline fractional volume is higher than a critical point, grain boundary sliding occurs along the suitable intercrystalline planes. The critical point is determined by the thickness of the sliding plane, as given by,

$$\Delta = \left(\frac{\sqrt{3}}{2} - 1 \right) d + D \qquad (2.25)$$

A schematic explanation of the deformation model of nanocrystalline material is given in Fig. 2. 19. As the thickness Δ decreases, grain boundary sliding is more difficult, leading to high hardness. When Δ is negative, competition between grain interior deformation and grain boundary sliding occurs. Hardness decreases with increasing grain size for materials where grain interior sliding is the predominant deformation mechanism.

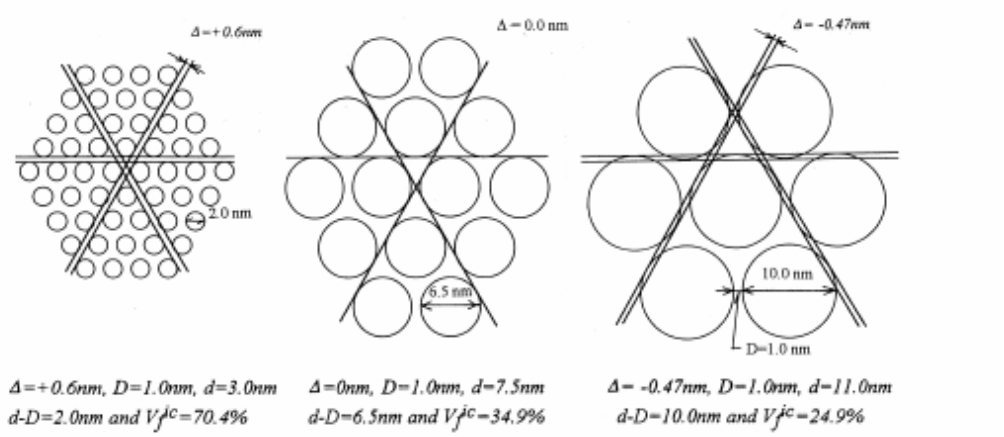

Fig.2.19: Schematic drawing of the modeling of deformation nanocrystalline materials by grain boundary sliding [6]

2.4 References

1. O. Younes & E. Gileadi, J. Electrochem. Soc., 149 (2) C100-C111 (2002)
2. H. Hayashi & M. Kasai, Hyoumen Gijutsu, Vol. 55, No. 1, 85-86 (2004)
3. Instrumental Methods in Electrochemistry, Southampton Electrochemistry Group, Ellis Horwood Ltd., (1990)
4. D.A. Porter and K.E. Easterling, Phase Transformations in Metals and Alloys, Nelson Thornes Ltd., (2001)
5. K. Itoh, Feng Wang & T. Watanabe, J. Japan Inst. Metals, Vol. 65, No 11, 1023-1028 (2001)
6. T. Nasu, M. sakurai, T. Kamiyama, T. Usuki, O. Uemura and T. Yamasaki, Journal of Non-Crystalline Solids 312-314 (2002) 319-322
7. T. Yamasaki, P. Schloßmacher & Y. Ogino, Nanostructured Materials, Vol. 10, No. 3 (1998) 375-388
8. T. Yamasaki, Mater. Phys. Mech., Vol. 1 (2000) 127-132
9. E.O. Hall, Proc. Ohys. Soc. London, 1951, vol. B64, 747-753
10. N.J. Petch, J. Iron Steel Inst., 1953, vol. 174, 25-28

3 Experimental procedures

As described in Chapter 2, Ni-W alloy has high mechanical strength and thermal stability. Yet, there is a serious problem of a difficulty in designing a proper electrolyte of Ni-W alloy possessing high current efficiency and reasonable tungsten content.

As shown in Fig. 3.1, firstly efforts were made toward the development of electroplating processes for Ni-W alloys. Especially, optimizing the complexing agents which can help for co-deposition of Ni and W was focused on. For the optimization, examination of complex formation in electrolyte with ultraviolet and visible spectrophotometry, measurement of deposition potential with voltammetry and estimation of fractional current for Ni and W depositions were performed, in order to know how the complexing agents affect the electrochemical process.

For the development of material for injection moulding tool examination of the internal stress which gives rise to crack occurrence in the deposit might be important. The mechanical stress in the deposits was estimated from the deflection of one side deposited test strips. The estimation using the test strip is a rapid method, and useful for the optimization of electroplating process.

The process parameters govern the obtained microstructure, and the microstructure determines the properties.
The surface topography was examined with scanning electron microscopy (SEM). The contents of Ni and W, in the electroplated layer, were determined semi-quantitatively with energy dispersive X-Ray spectrometry. Phase constitution of the electrodeposits was assessed with X-ray diffraction (XRD). Compositional depth profiling of the layers was obtained with glow discharge optical emission spectroscopy, in order to examine a presence of light elements as hydrogen, carbon and oxygen which might also influence the microstructure and mechanical properties. The values of grain size of the layers deposited from the electrolyte containing the complexing agents were assessed from the broadening of XRD line profiles .

For preparation of specimens for the hardness measurement and examination of the thermal stability, a 25L tank was used as the electrochemical cell, in order to obtain a batch of many specimens under identical conditions.

Details of the experimental procedures are given in the following sections, as well as a description of the principles of the less well-known experimental methods.

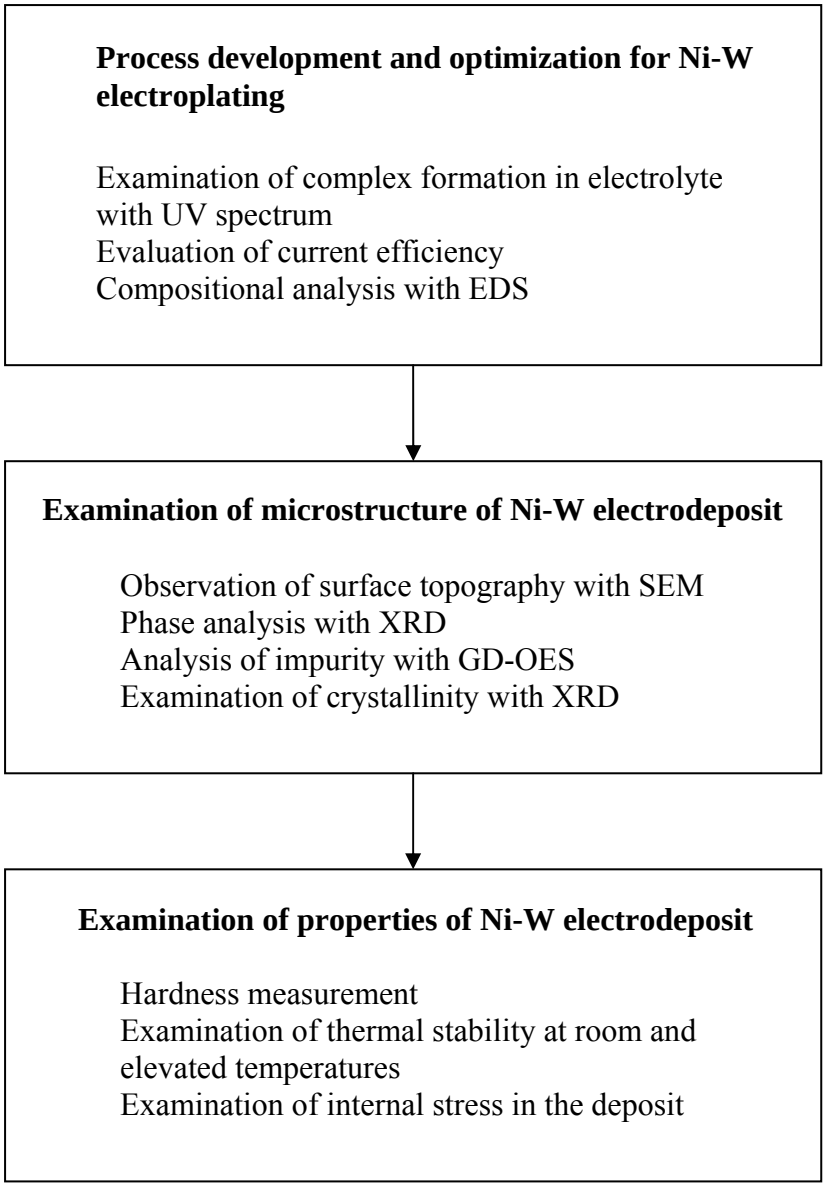

Fig.3.1: Flow of this study on Ni-W electrodeposits

3.1 Electrodeposition

3.1.1 Pre-examination of complexing agent useful for Ni-W alloy electrodeposition

For development of electroplating processes for Ni-W alloys, optimizing the complexing agents contained in the electrolyte is very important.
Citrate is known to form a complex with both the nickel and tungstate ions and gives stability to the electrolyte; citrate is the most common complexing agent for Ni-W electroplating. However, citrate is associated with a low current efficiency.
Therefore, the effect of adding other complexing agents, which possess high complex stability with both nickel and tungstate ions, into the electrolyte containing $NiSO_4$ and Na_2WO_4 was investigated. Data for the equilibrium constant of complex of tungstate

has not been found except citrate-tungstate complex. Tungstate coordinates to hydrogen atom of a group of complexing agent molecule. Tungstate is supposed to form complexes with molecules having a carboxyl or amino group. Complexing agents which satisfy such conditions are given in Table 3.1.

Table 3.1 Complex stability of nickel ion and tungstate

	Chemical formula	Equilibrium Constant K
Citric acid	$CH_2C(OH)CH_2(COOH)_3$	Ni: 4.38 WO_4:10.21
Tartaric acid	$CH(OH)CH(OH)(COOH)_2$	Ni: 5.42
Glycine	$CH_2(COOH)(NH_2)$	Ni: 6.44
Triethanolamine	$N(CH_2CH_2OH)_3$	Ni: 2.7
5-sulfosalicylic acid	$C_6H_3(SO_3)(OH)(COOH)$	Ni: 5.6

The equilibrium constant K is defined as follows,

$$\mathrm{M} + n\mathrm{L} \leftrightarrow \mathrm{ML}_n \qquad (3.1)$$

$$K = \frac{[\mathrm{ML}_n]}{[\mathrm{M}][\mathrm{L}]^n} \qquad (3.2)$$

Except for citrate, glycine and triethanolamine, precipitation occurred in the $NiSO_4$ and Na_2WO_4 based electrolyte containing the chosen complexing agents n Table 3.1. Therefore, citrate, glycine and triethanolamine were selected for further investigation.

3.1.2 Electrodeposition

A 1 dm^3 beaker was used as the electrochemical cell (Fig.3.2). A nickel rod was used as the anode in order to replenish nickel ions consumed by electrodeposition. Agitation was conducted with a magnetic stirrer. The temperature was kept at 70 °C by a hot plate and thermostat. A copper plate 0.5 mm in thickness was cut into samples of $30 \times 30 mm^2$ and prepared as substrates for deposition. A hole at the upper side of the plate was made and copper wire was fixed through the hole. The plate was masked with tape at the back and part of the front in order to avoid edge effects, thus reducing the effective deposition area to $20 \times 20 mm^2$.

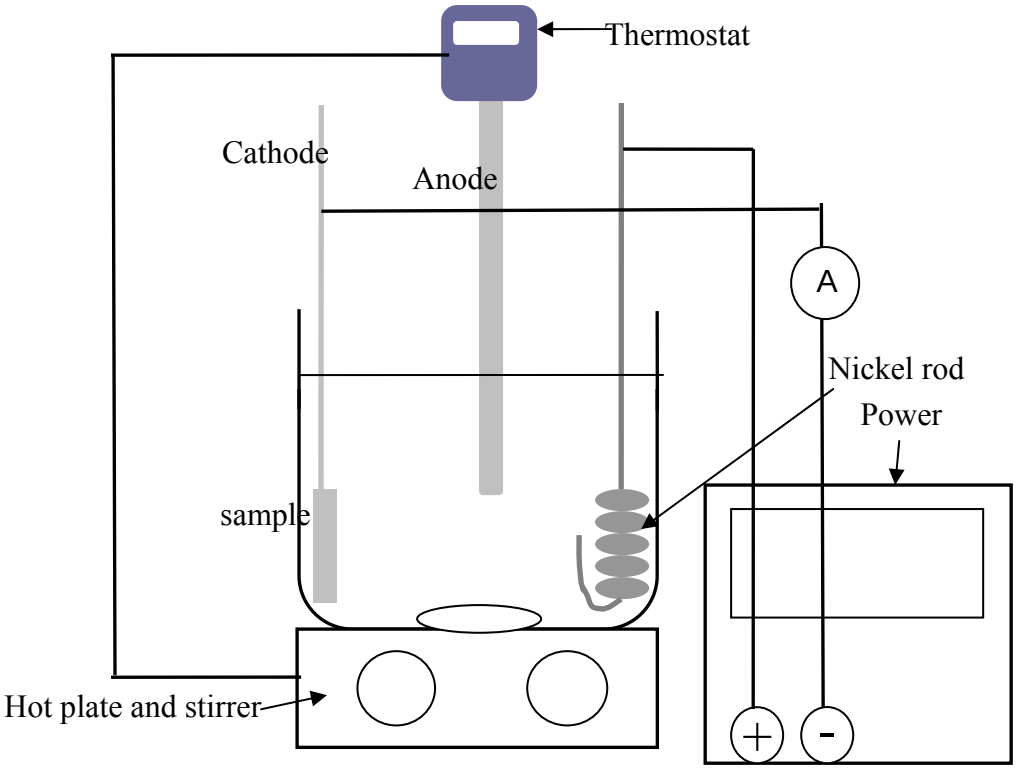

Fig.3.2 Schematic representation of the electrochemical cell for Ni-W electroplating

3.1.3 Calculation of current efficiency

The current efficiency (CE) is defined as the ratio between the theoretical and the actual amount of a deposit:

$$CE = \frac{Q_j}{Q_{total}} \qquad (3.3)$$

where Q_j and Q_{total} are the number of coulombs required for the reaction and the total number of coulombs passed, respectively.
Q is the product of the current I, in ampères, and the elapsed time t, in seconds:

$$Q = It \qquad (3.4)$$

One gram of Ni and W are equivalent to:

$$W_{\text{eq}}\left(\text{Ni}^{2+} + 2e \rightarrow \text{Ni}\right) = \frac{58.69}{2}(g) = 29.35(g) \qquad (3.5)$$

$$W_{\text{eq}}\left(WO_4^{2-} + 6e \rightarrow \text{W}\right) = \frac{183.85}{6}(g) = 30.64(g) \qquad (3.6)$$

According to the Faraday's law, the production of one gramequivalent of a product at the electrode, W_{eq}, in a cell, requires 96,487 coulombs.

Then, from (3.5) and (3.6) the weight of a product of electricity quantity in one coulomb, w, can be given by,

$$w_{\mathrm{Ni}} = \frac{W_{eq}(Ni^{2+} + 2e \rightarrow Ni)}{F} = \frac{29.35(g)}{96487(C)} = 3.04 \times 10^{-4}\, g \text{ coulomb}^{-1} \qquad (3.7)$$

$$w_{\mathrm{NiW}} = \frac{W_{eq}\left(WO_4^{2-} + 6e \rightarrow W\right)}{F} = \frac{30.64(g)}{96487(C)} = 3.18 \times 10^{-4}\, g \text{ coulomb}^{-1} \qquad (3.8)$$

From the formula of weight of a product (3.10) and (3.11), the number of coulombs required for the reaction, Q_j, and current efficiency, CE, are given by,

$$Q_j = \frac{\Delta w}{w_j} = \frac{\Delta w}{X_{Ni} w_{Ni} + X_{NiW} w_{NiW}} = \frac{\Delta w}{\left[3.04 \times 10^{-4} X_{Ni} + 3.18 \times 10^{-4} X_W\right]} \qquad (3.9)$$

$$CE = \frac{Q_j}{Q_{\text{total}}} = \frac{Q_j}{It} = \frac{\Delta w}{\left[3.04 \times 10^{-4} X_{Ni} + 3.18 \times 10^{-4} X_w\right] \times It} \qquad (3.10)$$

where X_{Ni} and X_W are compositions of nickel and tungsten, respectively, and Δw is the weight amount of the deposit.

3.1.4 Examination of complex formation in electrolyte with ultraviolet and visible (UV) spectrophotometer

Adsorption of visible radiation in the wavelength range 300 to 800 nm results from electron transfer in the molecule. The photon energy with the wave length, λ, $E = h/\lambda$ (h: Planck's constant), changes electronic state of the metal d-orbital, associated with colour of solution of metal ion as green and blue etc. A ligand, coordinating to a metal ion acts upon the electron. The change in the electronic state with complex formation of the metal ion influences the photo energy for the electron transfer of the metal. The spectrum of the radiation adsorption obtained with visible spectrophotometer gives information on condition of complex formation of metal ions in an electrolyte.

Usually metal possesses two electron energy level of e_g and t_{2g}. An electron in the level of t_{2g} is excited to another one of e_g with the photon energy. The energy level is affected by the ligand strength around the metal, because the ligand charge changes distribution of metal electron in a direction due to repulsion. The ligand strength influences the visible spectrum. The ligand strength depends on the type of complexing agent which the metal ion coordinates.

The peak position shifts to lower wave length with increase of ligand field strength, as shown in Fig. 3.3. The UV spectra indicate the field strength of ligand coordinating to nickel ion depends on type of complexing agent.

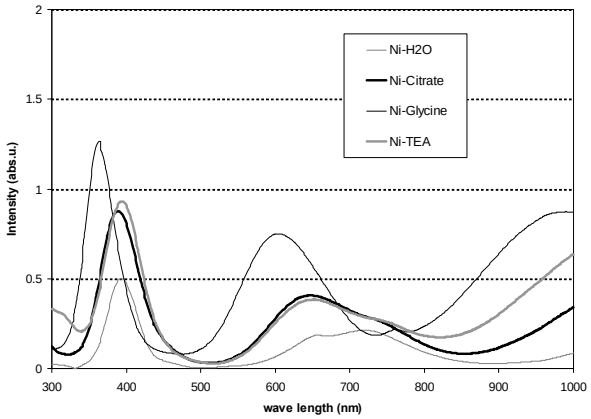

Fig.3.3: Visible spectrum of a solution containing $NiSO_4$ with H_2O (Ni-H_2O), citrate (Ni-citrate), glycine (Ni-glycine) and triethanolamine (Ni-TEA)

Complex formation with tungstate changes the electron energy level due to a difference in coordination number around the Ni ion. A change of the field strength due to mixing the complexing agents is visible near the UV range (Fig. 3.4). This indicates that tungstate is also involved in complex formation of nickel ion and the complexing agents.

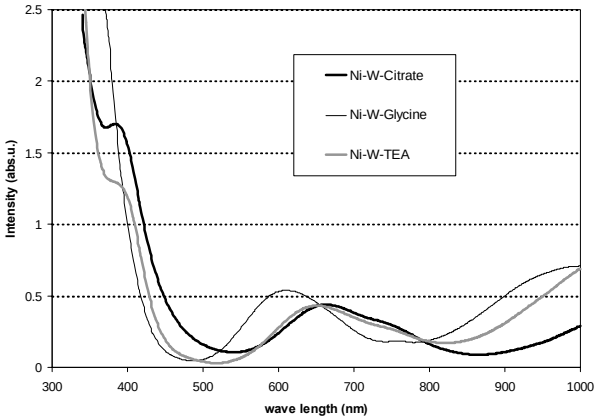

Fig.3.4: Visible spectrum of solution containing $NiSO_4$, tungstate, and complexing agents of citrate, glycine and triethanolamine,

3.1.5 Voltammetry measurement

Voltammetry measurement provides the cell current as a function of the applied potential for a potential sweep. The current depends on the electrochemical reaction rate, which could be the diffusion of species in electrolyte to or away from the working electrode.
Voltammetry was carried out using a potentiostat/galvanostat (PGP201 Radiometer Copenhagen). A 500mL beaker was used as the electrochemical cell (Fig.3.8). A saturated calomel electrode (SCE) was used as the reference electrode. The temperature was kept at 70°C by circulating hot water around the electrolyte cell. A copper disk was used as working electrode, whereas a titan basket was used as

counter electrode. The working electrode was located in the centre of the cell. The potential sweep rate was 50mV/min.

3.2 Microstructure investigations

3.2.1 Focused ion beam (FIB) microscopy

Cross-section observation can be performed with focused ion beam (FIB) microscope. A gallium ion beam is produced by applying a suitable electric field to the molten gallium under vacuum. The energy of the ions is very well defined, so an ion beam with a width of only a few nm can be obtained by using an aperture and a demagnifying lens. The controlled ion beam can manufacture precise microscope sections.
By scanning the ion beam an image of the sample can be obtained with secondary electrons emitted from the location of incidenceof the ions on the sample. The intensity of the secondary electron emission depends on atomic number (Z), crystal orientation and surface roughness. The crystallographic and compositional contrasts of the image formed with scanning the ion beam are generally higher than with SEM.
As shown in Fig. 3.5, the FIB instrument manufactures a cross-section by removal of material through scanning the ion beam, decreasing the width of the beam with increasing the depth of the sample. The image of the section is obtained after tilting the sample and exposing the cross section towards the secondary electron detector.

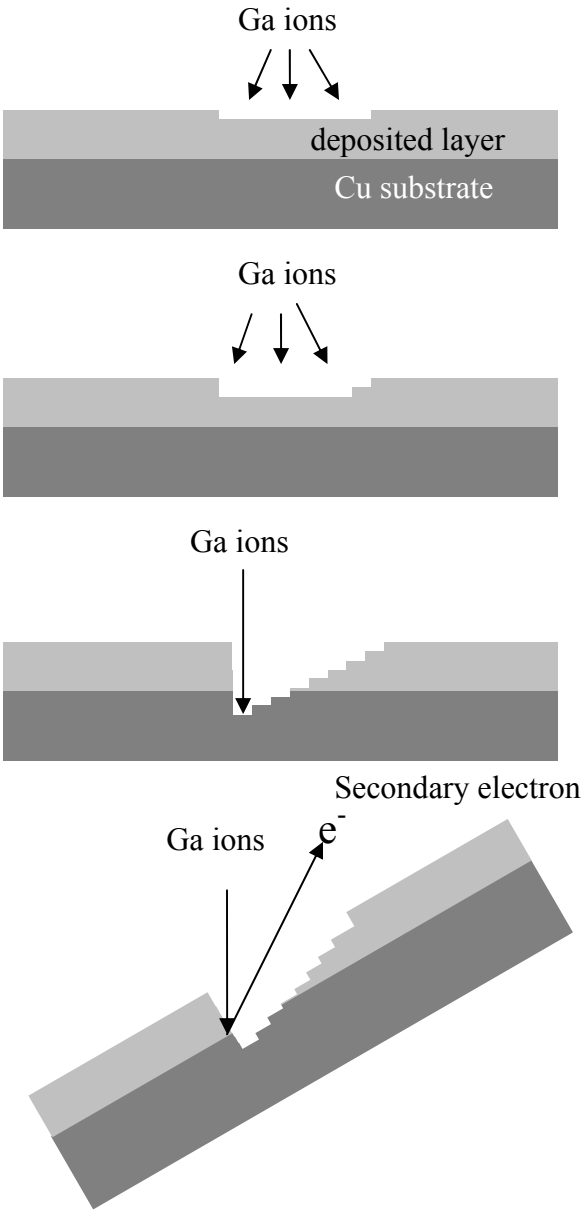

Fig.3.5: A schematic drawing of preparation of cross-section and obtaining the image with the FB-2000A

Fig. 3.6 shows a three-dimensional schematic drawing of the cross-section manufactured by the instrument. The scanning ion microscope (SIM) image of the section of an electrodeposited Ni-W alloy layer, which corresponds to the part of the gray circle in the drawing, is shown in Fig. 3.7. Coarse grains of the copper substrate and columnar grains of the Ni-W alloy can be observed. The contrast from different crystallographic orientation in the copper substrate is clearly seen.

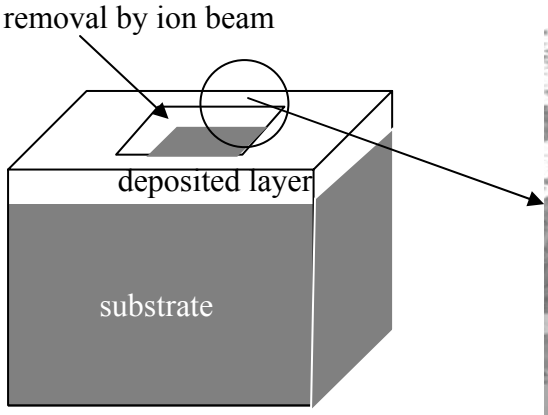

Fig.3.6: Schematic representation of cross-section prepared with FIB

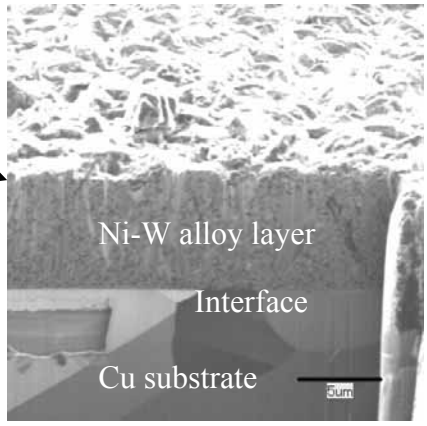

Fig.3.7: Scanning ion macroscope image of electrodeposited Ni-W alloy on Cu

3.2.2 Glow Discharge-Optical Emission Spectroscopy (GD-OES)

Compositional analysis can be performed by Glow Discharge-Optical Emission Spectroscopy (GD-OES).

With GD-OES a composition profile is obtained through measuring the intensity of a chosen wavelength in the emission spectrum as a function of sputtering time (Fig. 3.8). This analysis is also available for layers as thin as 5nm.
The process of the GD-OES analysis is composed of sputtering atoms by glow discharge, exciting the atoms by an argon plasma, emission of the atoms, and identification of the emission spectrum.
Fig. 3.9 shows a schematic drawing of the system of GD-OES. A specimen is attached with the cathode. The diameter of the anode is variable and can be determined depending on size and position of the specimen. Gas atoms are ionized by high voltage and the ions sputter atoms away from the specimen as cathode. The sputtered atoms are excited by an argon plasma leading to emission. (Fig. 3.10) Spectrometry of the emission is performed by a diffraction grating. A photomultiplier increases the intensity of the diffracted wavelength of the spectrum.

GD-OES also allows the analysis of element down to hydrogen. The spectroscope is available for the wavelength range 110nm to 800nm.
In order to avoid interference with other elements in the spectrum, a monochoromater can be used to analyse a fixed wavelength.

Quantitative analysis of GD-OES intensity-depth profiles is difficult (but not impossible) and requires calibration of the sputter rate as well as the intensity-composition relation for similar matrices as the sample to be investigated.

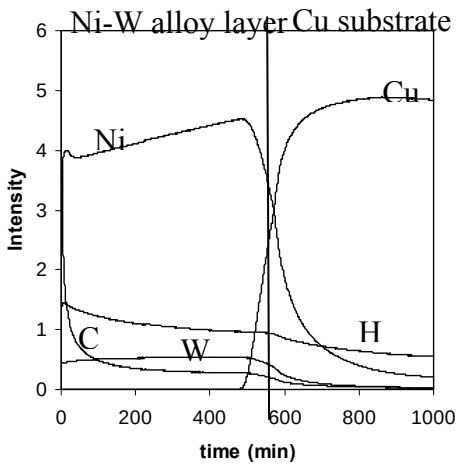

Fig. 3.8: GD-OES depth profile of Ni-W electrodeposited layer on copper substrate

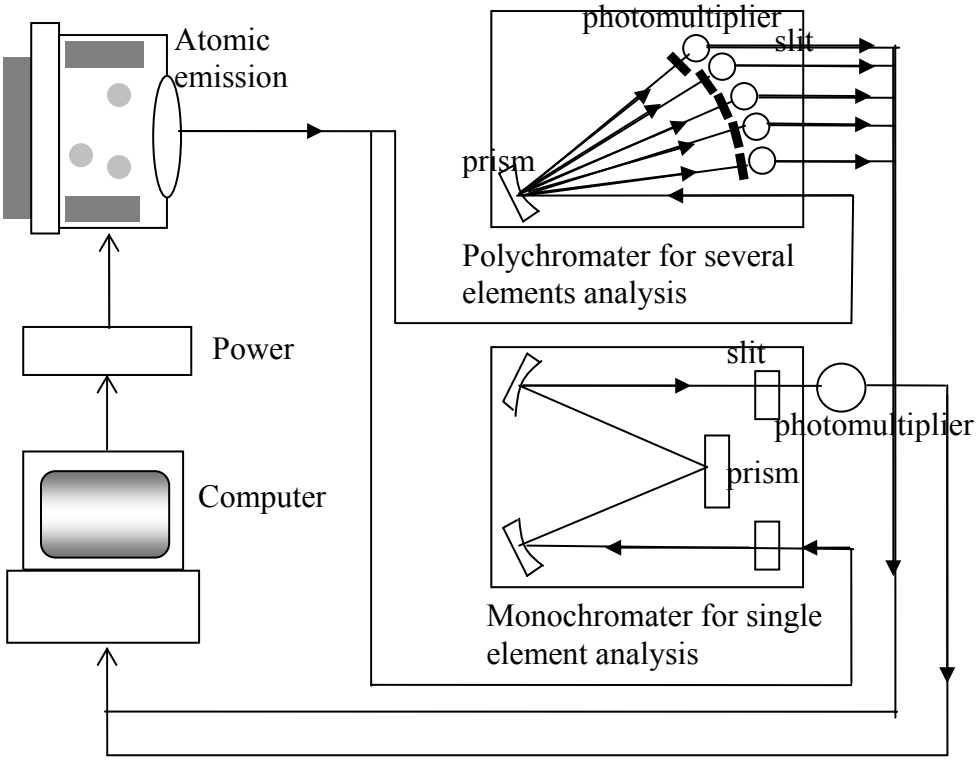

Fig. 3.9: A schematic drawing of system of the whole instrument of GD-OES

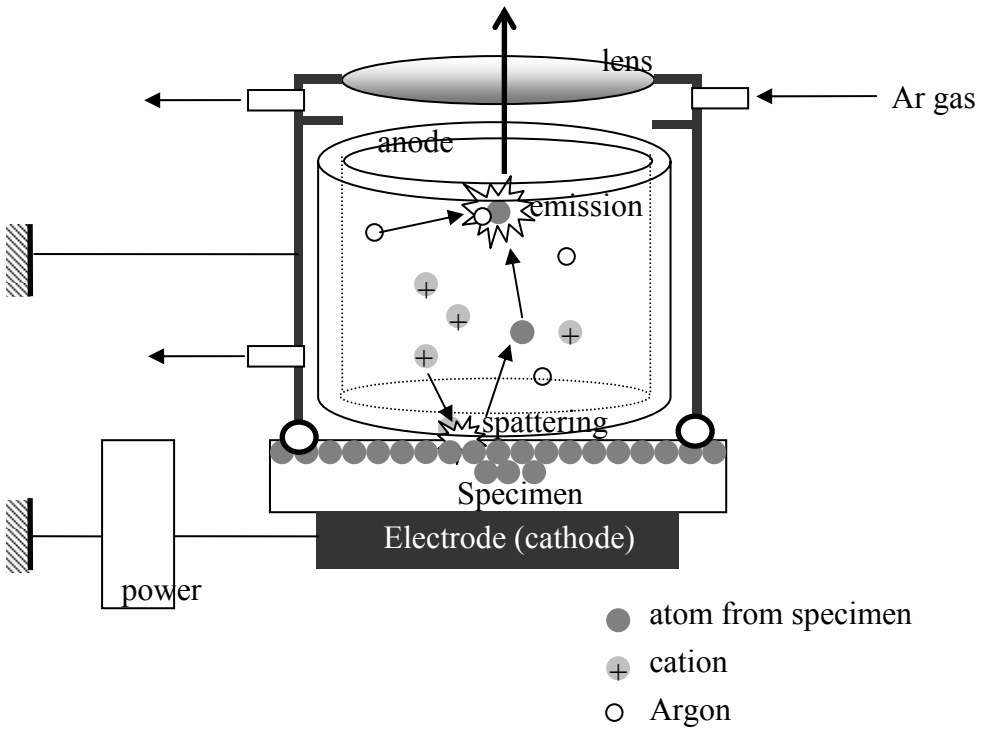

Fig. 3.10: A schematic drawing of the emission part in the GD-OES instrument

3.2.3 Method for estimation of the grain size from broadening of X-ray line profiles

3.2.3.1 A survey of the method

In this study, a method of line broadening of X-ray diffraction patterns given by literatures [I-5] was applied to estimate the size of the crystallites in the electrodeposited layers in the direction perpendicular to the surface..

Scherrer proposed the following equation for the calculation of the grain size from the line width:

$$t = \frac{0.9\lambda}{B\cos\theta_B} \qquad (3.11)$$

where t is average crystallite size, B is the angular width at half maximumof intensity (FWHM), and θ_B is the incident angle at maximum intensity. It is used to estimate the particle size of very small crystals from the measured width of their diffraction curves.

Later, various methods were proposed for eliminating the instrumental influence on the width of the profile, and for separating the contributions of size and strain components to the line broadening.

For separation of instrumental and physical (particle size and strain) broadening, there are two methods: “Fourier-space-Method” and “Real-space Method”.

The Real-space method, which is a more rapid technique, based on the assumption that the line profiles can be described by symmetrical Voigt functions which represent the mathematical convolution of Cauchy (Lorentzian) and Gaussian functions, was applied in this study. Particle size broadening is described approximately by a Cauchy distribution, whereas the profile arising from lattice strains is closer to a Gaussian distribution.
Langford et al. developed the rapid method for the deconvolution of the Voigt function consisting of Cauchy and Gaussian functions using several parameters of a line profile. These are the peak height, $I(0)$, the area, A, the full width at half the maximum intensity, $2w$, and the integral breadth, β, defined by,

$$\beta = A / I(0) \qquad (3.12)$$

The ratio $2w/\beta$ characterizes any symmetrical profile, and can be applied for the deconvolution of Cauchy and Gaussian functions.

The Cauchy function, $I_c(x)$, is given by,

$$I_c(x) = I_c(0)\frac{w_c^2}{w_c^2 + x^2} \qquad (3.13)$$

, where

$$\beta_c = \pi w_c \qquad (3.14)$$

Then, the form factor $2w/\beta$ for a Cauchy function is $2/\pi$ (=0.63662).
The Gaussian function, $I_G(x)$, is given by,

$$I_G(x) = I_G(0)\exp\left(-\pi x^2 / \beta_G^2\right) \qquad (3.15)$$

The half width is,

$$\beta_G^2 = \frac{\pi}{4\log_e 2}(2w_G)^2 \qquad (3.16)$$

The form factor, $2w/\beta$, for a Gaussian function is $2(\log_e 2)^{1/2} / \pi^{1/2}$ (=0.93949).
The Fourier transforms of $I_c(x)$ and $I_G(x)$ given by equations (3.13) and (3.15) are

$$F_c(t) = \beta_c I_c(0)\exp(-2\beta_c t) \qquad (3.17)$$

$$F_G(t) = \beta_G I_G(0)\exp\left(-\pi\beta_G^2 t^2\right) \qquad (3.18)$$

The Voigt function, $I(x)$, can be obtained by the inverse transform of the functions given by equations (3.17) and (3.18).

$$I(x) = \mathrm{Re}\{F_c(x)F_G(x)\} = \mathrm{Re}\left\{\beta_c I_c(0) I_G(0)\omega\left[\frac{\pi^{1/2}x}{\beta_G} + ik\right]\right\} \qquad (3.19)$$

where

$$k = \beta_c / \pi^{1/2}\beta_G \qquad (3.20)$$

From the equations (3.17) and (3.18),

$$A = \mathrm{Re}\{I_c(0)I_g(0)\} = F(0) = \beta_c\beta_g I_c(0)I_g(0) = I(0)\beta \qquad (3.21)$$

Then, from the equations (3.19) and (3.21)

$$I(0) = \beta_c I_c(0) I_G(0)\exp(k^2)erfc(k) = \beta_c\beta_G I_c(0)I_G(0)/\beta \qquad (3.22)$$

Then,

$$\frac{\beta}{\beta_G} = \frac{\exp(-k^2)}{1 - erfc(k)} \qquad (3.23)$$

and also the relationship between the full width at half height and the ratio k is given by the following formula.

$$2w^2 \approx \frac{4\beta_G^2}{\pi}(1 + k^2) \qquad (3.24)$$

Then $2w/\beta$ and β_G/β can be plotted as a function of the ratio k by using formulas of (3.23) and (3.24), as shown in Fig.3.11.

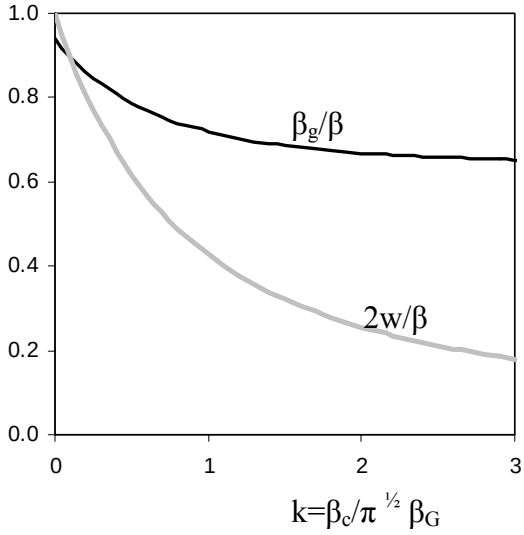

Fig. 3.11: Analysis of Voigt functions: graphical separation of β_c and β_G

From the plot shown in Fig. 3.11, plots of the ratios of integral breadth β_C / β , β_G / β against the ratio $2w/\beta$ can be obtained, as shown in Fig.3.12.

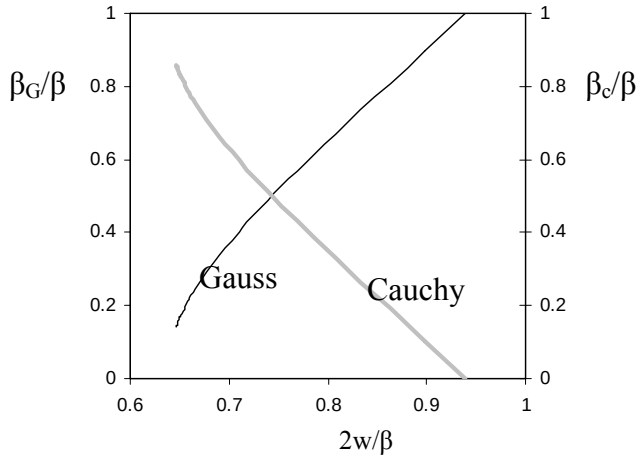

Fig. 3.12: The ratio of integral breadth as a function of the ratio of

The ratios of integral breadth of the Cauchy and Gaussian components β_c/β, β_g/β are obtained from the plot in Fig. 3.12, as following,

$$\beta_c / \beta = 2.0207 - 0.4803\left(\frac{2w}{\beta}\right) - 1.7756\left(\frac{2w}{\beta}\right)^2 \qquad (3.25)$$

$$\beta_G / \beta = 0.642 + 1.4187\left(\frac{2w}{\beta} - \frac{2}{\pi}\right)^{1/2} - 2.2043\left(\frac{2w}{\beta}\right) + 1.8706\left(\frac{2w}{\beta}\right)^2 \qquad (3.26)$$

The measured line h is the convolution of the standard profile g with the structurally broadened profile. Then, the structurally broadened profile f is given by

$$h_c = g_c * f_c \qquad (3.27)$$

$$h_G = g_G * f_G \qquad (3.28)$$

From (3.27) and (3.28) the integral breadths of β_C^f and β_G^f are given by

$$\beta_c^f = \beta_c^h - \beta_c^g \qquad (3.29)$$

$$\left(\beta_G^f\right)^2 = \left(\beta_G^h\right)^2 - \left(\beta_G^g\right)^2 \qquad (3.30)$$

It is assumed that grain size and strain can be estimated by the integral breadths β_C^f and β_G^f , respectively, from (3.25), (3.26), (3.27) and (3.28). There is some theoretical justification for this assumption and experimental evidence. Grain size D and strain e are given by

$$D = \lambda / \beta_C^f \cos\theta \qquad (3.31)$$

$$(3.32)$$

$$e = \beta_G^f / 4\tan\theta$$

3.2.3.2. Fitting a curve to a function

It is necessary to take into account the radiation composed of several waves for obtaining function I(θ).
In this study, CuKα radiation composed of two rays α_1 (λ=1.540596Å) and α_2 (λ=1.544493Å) was used for XRD measurement. Curve is separated into two functions $f_1(\theta)$, $f_2(\theta)$ of intensity as an incident angle which satisfy the following condition.

$$\lambda_1 = d\sin\theta_1 = 1.540596 \qquad (3.33)$$

$$\lambda_2 = d\sin\theta_2 = 1.544493 \qquad (3.34)$$

$$\sin\theta_2 = \frac{1.544493}{1.540596}\sin\theta_1 \qquad (3.35)$$

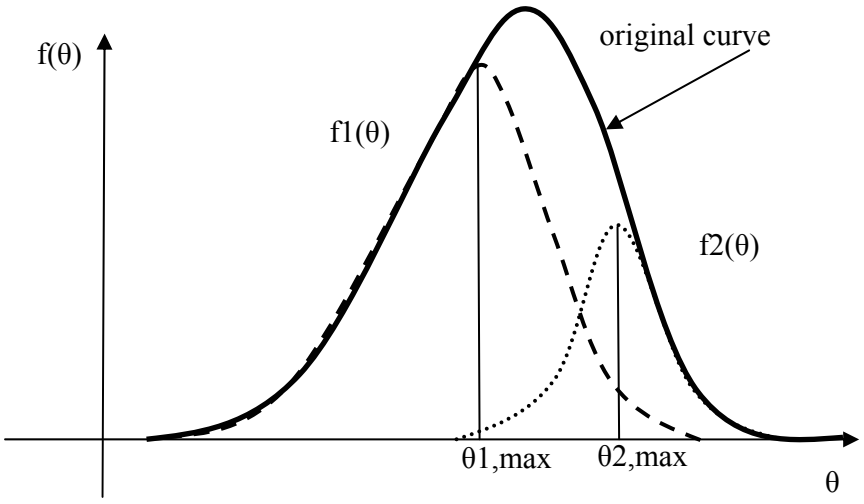

Fig.3.13: Separation into two functions of an incident angle of θ_1 and θ_2

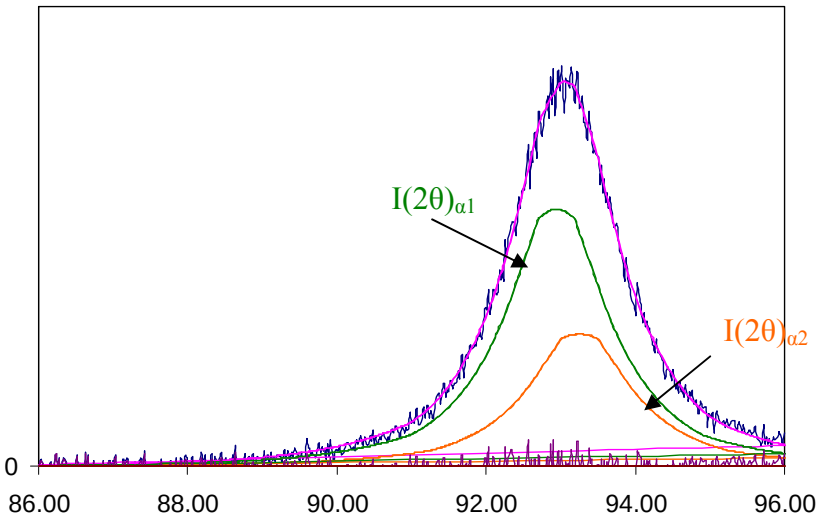

Fig.3.14: Fitting a curve to a function of $I(2\theta)_{\alpha 1}$ and $I(2\theta)_{\alpha 2}$

3.2.3.3 Practical problem with the Real-space method

In case of large broadening peak, fitting function should be conducted in large range of angle, with taking the extended angular distribution into consideration. Actually, the particle size contribution to broadening increased up to 0.67 from 0.46 with changing angular range from 90-96°/2θ to 86-100°/2θ for the calculation. The tail part of the distribution in the large range cannot be neglected.
Actual fitting to the function is performed in angular range from 86°/2θ to 96°/2θ due to the existence of other peak, so the function ranging from 96°/2θ to 100°/2θ could be obtained by the estimation from the function ranging from 86°/2θ to 90°/2θ due to the symmetry curve.

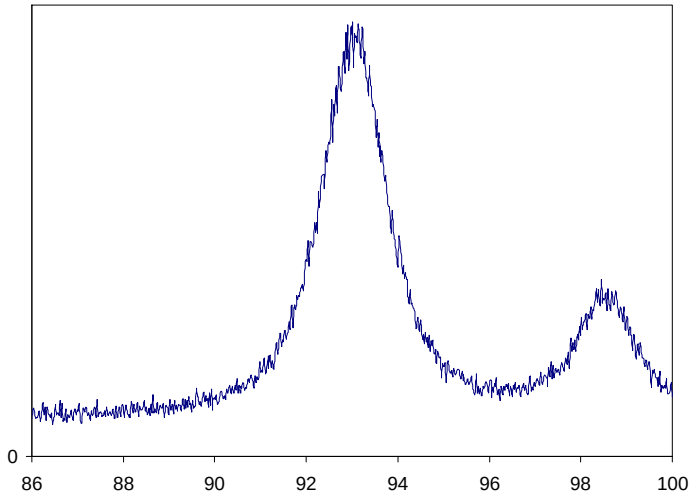

Fig. 3.15: XRD pattern at about 2θ=93°

For a large crystal it is hard to calculate precisely the grain size from the broadening of the peak at about 44°/2θ, because the peak width is too small due to large plane space. The factor of 2w/β is too sensible to the figure of the peak width to estimate contributions of grain size and strain to peak broadening precisely. Actually, the contributions to peak broadening at 44°/2θ are significantly different from the ones at 93°/2θ.

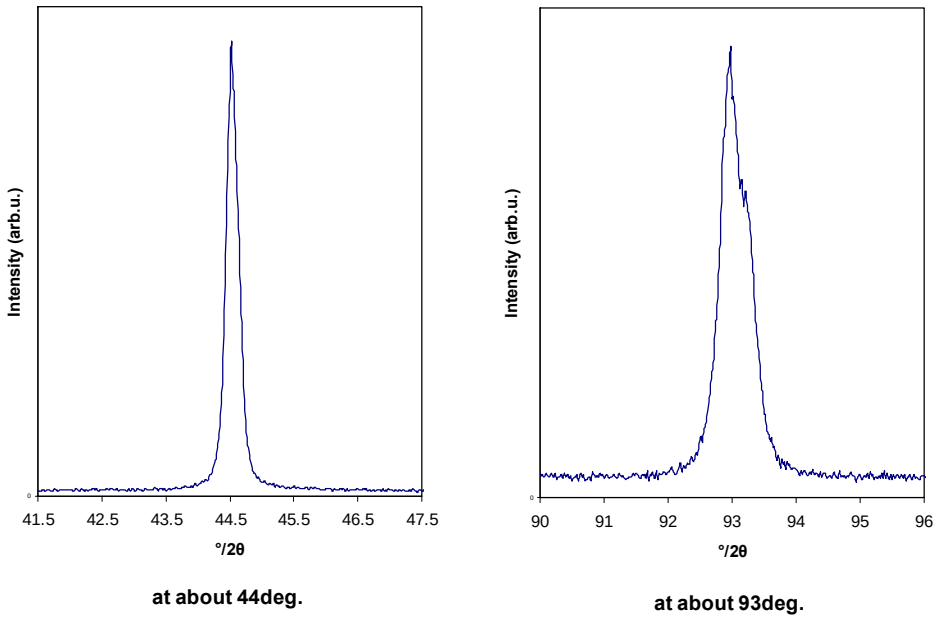

Fig.3.16: XRD profile at scattering angle of 44°/2θ and 93°/2θ of Ni deposit

Table3.2 Separation into contributions of particle size and strain to broadening of peak at about 44°/2θ and 93°/2θ by means of Voigt deconvolution

	Area	I_{max}	2w	2w/β	β_C/β	β_G/β	β	β_C	β_G
44°/2θ	1291	5551	0.20	0.86	0.29	0.71	0.23	0.07	0.16
93°/2θ	739	1605	0.32	0.70	0.83	0.17	0.46	0.38	0.08

3.3 Property investigations

3.3.1 Mechanical stress measurement

The mechanical stress in the deposits was estimated from the deflection of one side coated test strips (Specialty Testing & Development Co.) with known elastic constants, as shown in Fig. 3.21. The test strip is made from a CuBe foil and is approximately 60 μm in thickness, consists of a 15 mm wide base and has two "legs" that are 76 mm long and 5 mm wide. The base and legs of the strip are covered with a deposition preventing resist layer, but on facing sides of the legs.

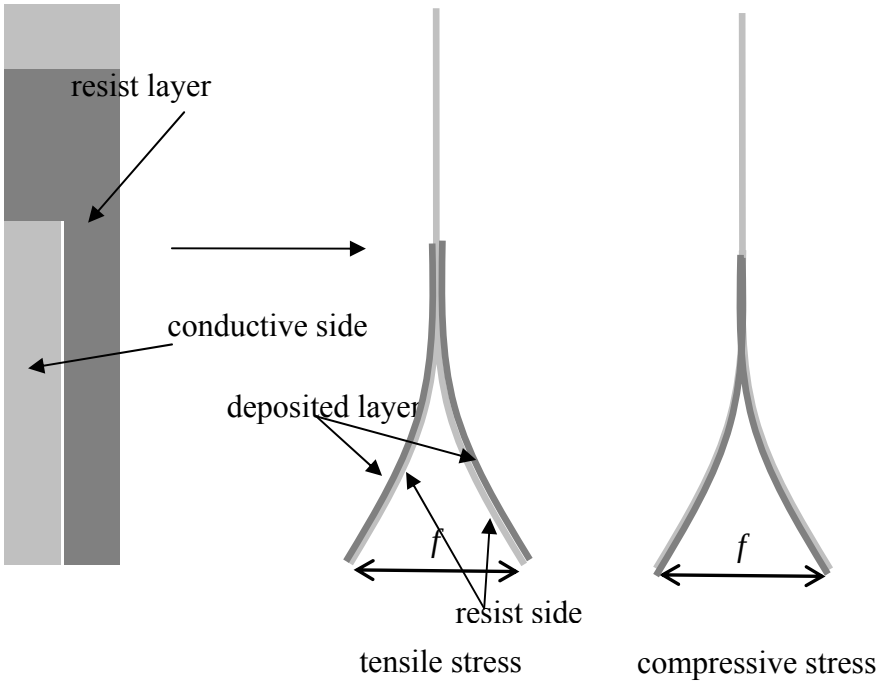

Fig.3.17: Deflection of test strip resulted from mechanical stress

A 1 dm^3 beaker was used as the electrochemical cell. The cell for preparing specimens for stress measurement has two anodes and one cathode (the test strip) which is located centrally between the anodes, such that the opposite sides of the test strip experience identical deposition conditions.

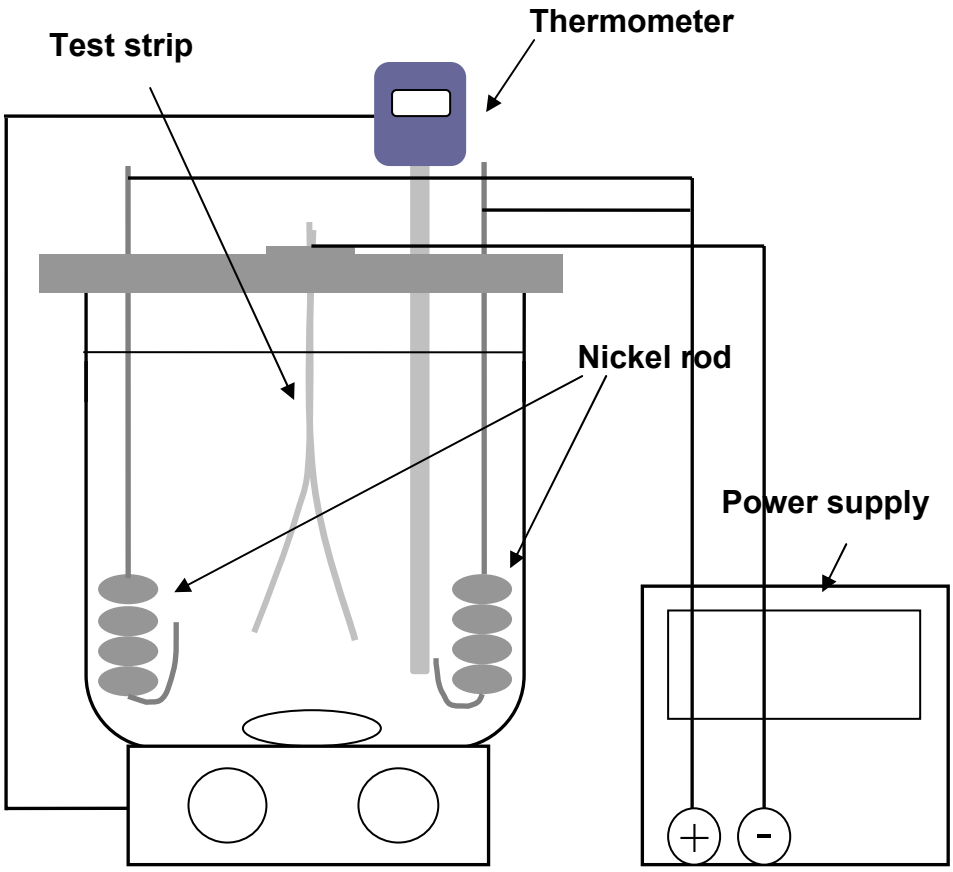

Fig.3.18: A schematic drawing of the cell for stress measurement

Fig.3.19: The cell for stress measurement

Internal stress in the deposits makes the two legs of the strip bend in opposite directions. The value of the distance between the deflected beams of the test strip was

converted into mechanical stress using Perakh's equation for a deflection on the free end of a cantilever substrate as follows [6];

$$\sigma = \frac{E_0 d^2 (1 + 4\tilde{\gamma}\theta + 6\tilde{\gamma}\theta^2 + 4\tilde{\gamma}\theta^3 + \tilde{\gamma}^2\theta^4)}{6l^2(1-\upsilon_0)(1 + 2\theta + \tilde{r}\theta^2)} \frac{df}{dt} \qquad (3.36)$$

where d and t are values of thickness of substrate and deposit, respectively, and l and f are given by Fig. 3.20, E_0 and E_1 are Young's modulus of substrate and deposit respectively (E_{CuBe}=130 GPa, E_{Ni}=199 GPa, E_W=345 GPa), and $\tilde{\gamma}$ and θ are given by

$$\tilde{\gamma} = \frac{E_1(1-\upsilon_0)}{E_0(1-\upsilon_1)} \qquad (3.37)$$

$$\theta = \frac{t}{d} \qquad (3.38)$$

where υ_0 and υ_1 are Poisson ratios of substrate and deposit, respectively (υ_{CuBe}=0.350, υ_{Ni}=0.312, υ_W=0.284), d is the thickness of substrate, t is the thickness of the deposit, f is spread distance between the legs of the strip.
Then, when $\theta \le 0.1$ is, the stress is given by

$$\sigma = \frac{E_0 d^2 (1 + 4\tilde{\gamma}\theta)}{6l^2(1-\upsilon_0)(1+2\theta)} \frac{df}{dt} \qquad (3.39)$$

Furthermore, when $\theta \le 0.01$ is, the stress is as follows obeys

$$\sigma = \frac{E_0 d^2}{6l^2(1-\upsilon_0)} \frac{df}{dt} \qquad (3.40)$$

which is equivalent to Stoney's equation.

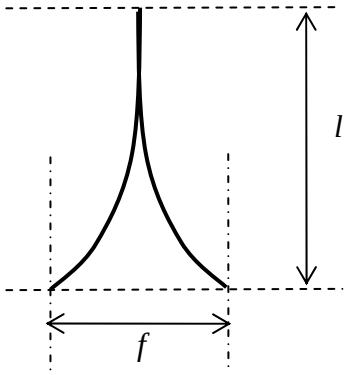

Fig.3.20: A schematic drawing of strip deflection

3.3.2 Hardness measurement

For preparing specimens for the investigation of hardness and thermal stability, a bigger scale system was used. A 25 dm^3 plastic container was used as the electrochemical cell, shown in Fig. 3.21. The temperature was kept at 60 °C with heater and thermostat, and agitated with air bubbling. Nickel rounds were used as the anode electrode, and the blocks were put in a titanium basket. The electrolyte circulated through a filter with pump. A bigger copper plate as substrate was prepared, as shown in Fig. 3.22.
After electrodeposition the specimen was cut in 30 mm wide pieces, which annealed at 100 °C , 250 °C, 400°C or 550 °C. The as-deposited and annealed samples, prepared under identical electrodeposition conditions, were examined with hardness testing to evaluate their thermal stability.

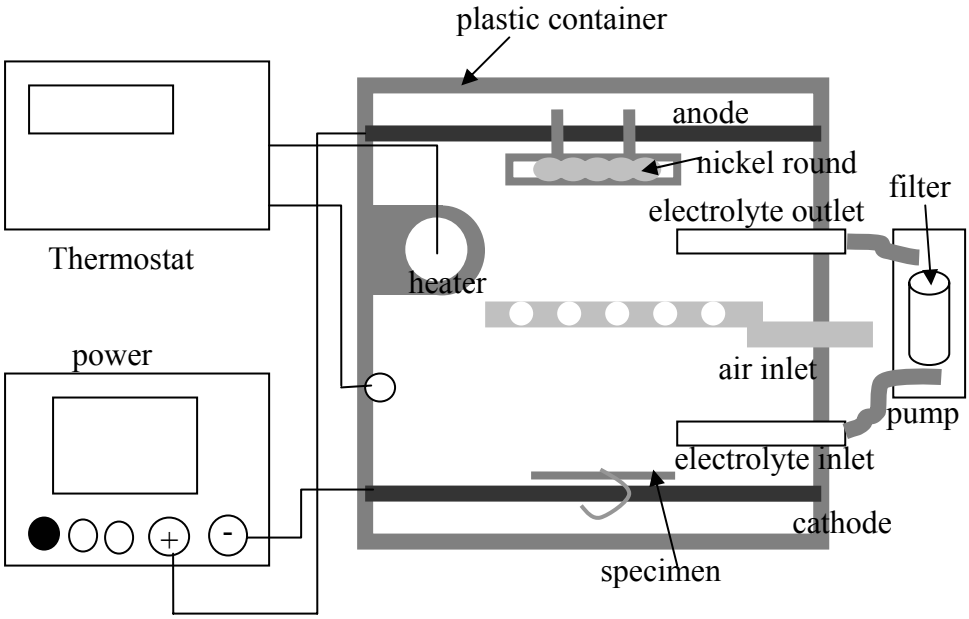

Fig.3.21: Schematic representation of specimen for hardness measurement

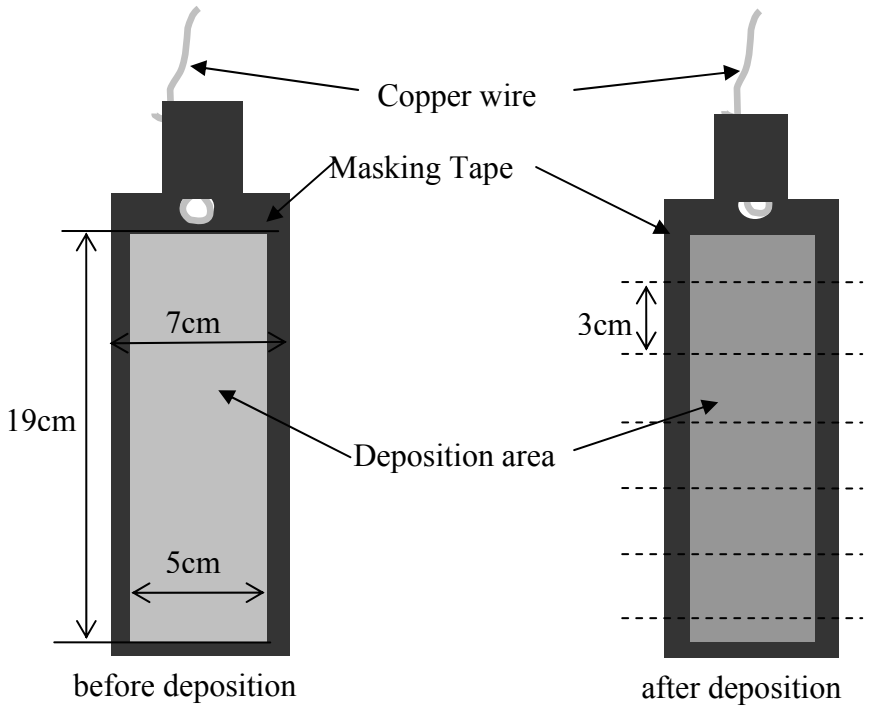

Fig.3.22: Schematic representation of specimen for hardness measurement

Microhardness was measured with a load of 25g. The cross-sections of the specimens for measurement were polished in order to avoid the influence of surface roughnesst. For preparation the specimens were mounted in epoxy resin (Seriefix 20), and polished as described in Tables 3.3 and.3.4. Each hardness value presented is the average of 10 independent indentations on the cross-section.

Table3.3 Polishing conditions

Grid	RPM	Force, N	Time, min
320	150	100	2
500	150	100	2
1000	150	100	3
4000	150	70	3

Table 3.4 Fine polishing conditions

Plate cloth	diamond particle size, µm	RPM	Force, N	Time, min	Lubricant
Dur	3	150	70	3	Blue
Nap	1	150	70	3	Blue

3.4 References

1. B. D. Cullity; Elements of X-Ray Diffraction, Addison-Wesley Publishing Company, INC (1967)
2. Viktor Hauk; Structural and Residual Stress Analysis by Non-destructive Method, Elsevier (1997)
3. TH. H. De Keijser, J. I. Langford, E. J. Mittemeijer and A. B. Vogels, J. Appl. Cryst. (1982) 15, 308-314
4. J. I. Langford, J. Appl. Cryst. (1978) 11, 10-14
5. P. Scardi, M. Leoni and R. Delhez, J. Appl. Cryst. (2004) 37, 381-390
6. M. Perakh, Surface Technology, 8 (1979) 265-309

Chapter 4

Development of A New Electroplating Process for Ni-W Alloy Deposits

Available online at www.sciencedirect.com
SCIENCE DIRECT®
Electrochimica Acta 51 (2005) 888–896
ELECTROCHIMICA Acta
www.elsevier.com/locate/electacta

Development of a new electroplating process for Ni–W alloy deposits

Io Mizushima *, Peter T. Tang, Hans N. Hansen, Marcel A.J. Somers

Department of Manufacturing Engineering and Management, Technical University of Denmark, DTU, DK-2800 Kgs. Lyngby, Denmark

Received 20 October 2004; received in revised form 12 April 2005; accepted 25 April 2005
Available online 9 August 2005

Abstract

In the present work, the effect of the complexing agents citrate, glycine and triethanolamine (TEA) on the electrodeposition of Ni–W layers from electrolytes based on $NiSO_4$ and Na_2WO_4, is investigated. The investigations include measurement of the current efficiencies, determination of the tungsten content in the electrodeposits (by energy dispersive X-ray analysis), voltammetry studies and characterization of complex formation by UV-spectrometry. High W content and current efficiency could be realized by using electrolytes containing all of the three complexing agents. The results show that small amounts of glycine in a citrate–triethanolamine based electrolyte positively influences both the mass-transfer and the deposition potential.

Keywords: Nickel–tungsten; Electrodeposition; Complexing agent; Microstructure; XRD patterns

1. Introduction

Micro-injection molding is foreseen to find wide future application for production of computer parts, microfluidic systems and polymer optical components. For the injection molding of high performance plastics, possessing high strength and chemical resistance, the molds must be able to withstand repeated thermal cycling at temperatures up to 350 °C.

Fabrication of the molding tool is preferably performed by electroforming in order to be able to control the reproduction of microscale geometrical details. Nickel is a widely applied material for electroforming, but pure nanocrystalline nickel electrodeposits cannot withstand the relatively high temperature without loosing their hardness and form stability. Among the metals and alloys which are expected to have a higher thermal stability than nickel, and which can be electrodeposited, Ni–W is a favorable candidate. Furthermore, a Ni–W alloy is an excellent material because it has high corrosion resistance and mechanical strength. Several authors have investigated electrodeposition of Ni–W alloys [1–12]. Unfortunately, the traditional bath for Ni–W plating, containing citrate and ammonia as complexing agents, is characterized by a low current efficiency and poor stability of the pH value. Citrate is mainly responsible for the low current efficiency. Ammonia contributes to improving the current efficiency, but reduces the bath stability owing to its rapid evaporation. Therefore, in the present research project other complexing agents with a high complex stability towards the nickel ion were investigated. Initially, tartaric acid, glycine, triethanolamine and 5-sulfosalicylic acid were selected. It was found that tartaric acid and 5-sulfosalicylic acid gave rise to precipitation in the nickel sulfate and sodium tungstate based electrolyte. Therefore, we only report on the results obtained with citrate, glycine and triethanolamine (TEA) in the present contribution.

2. Experimental procedure

A 1 dm^3 beaker was used as electrochemical cell. The electrolytes consisted of 0.1 mol dm^{-3} $NiSO_4 \cdot 6H_2O$, 0.2 mol dm^{-3} $Na_2WO_4 \cdot 2H_2O$, 0.3 mol dm^{-3} complexing agent (citrate, glycine and/or TEA) and 0.44 mol dm^{-3} H_3BO_3. Agitation was conducted with a magnetic stirrer. A copper plate cathodically degreased with an alkaline

* Corresponding author. Fax: +45 45 93 62 13.
E-mail address: tanaka@ipl.dtu.dk (I. Mizushima).

0013-4686/$ – see front matter © 2005 Elsevier Ltd. All rights reserved.
doi:10.1016/j.electacta.2005.04.050

solution and pickled in a commercial HCl solution was used as substrate.

Voltammetry was carried out using a potentiostat/galvanostat (PGP201 Radiometer Copenhagen) with a saturated calomel electrode (SCE) as the reference electrode. Complex formation was investigated with a UV-spectrophotometer (UV1240 Shimadzu Ltd.). The composition in the electroplated layer was determined semi-quantitatively with energy dispersive X-ray spectrometry (Oxford Scientific). The surface topography was examined with scanning electron microscopy (JSM-5900, JEOL) and cross-sections were investigated with scanning ion microscopy (FIB-2000A, Hitachi Ltd.). Phase characterization was conducted with X-ray diffraction (M21X TXJ-FO88, Mac Science Co. Ltd.) using Cu Kα radiation.

3. Results and discussion

In order to examine the properties of glycine and TEA, as compared to citrate, electrolytes containing a single complexing agent were examined first.

3.1. Electrolytes containing a single complexing agent

The current efficiencies and layer compositions obtained from electrolytes containing either citrate, glycine or TEA are given in Table 1.

For the glycine and TEA-based electrolytes, the current efficiencies are markedly higher than for the citrate-based electrolyte, but the W contents of the deposits are lower. In order to investigate the co-deposition of Ni and W in more detail, and evaluate both current efficiency and layer composition simultaneously, the partial current densities for reduction of hydrogen and metal deposition were estimated for the various current densities applied. We assumed that the alloy deposition is performed by simultaneous depositions of Ni and NiW, according to the literatures [2–4,13]. Therefore, the partial current densities for Ni, NiW and H_2 were estimated from the total charge passed during deposition, the W content as determined with EDS and total weight increase of the sample upon deposition.

Table 1
Current efficiencies of electrodeposition and tungsten contents in the layer electrodeposited from electrolytes containing 0.1 mol dm^{-3} $NiSO_4$, 0.2 mol dm^{-3} Na_2WO_4 and 0.3 mol dm^{-3} complexing agent (citrate, glycine or triethanolamine)

Complexing agent	Current density (A cm^{-2})	Tungsten content (at.%)	Current efficiency (%)
Citrate	0.01	17	37
	0.1	25	6
Glycine	0.01	10	65
	0.1	2	35
Triethanolamine (TEA)	0.01	9	79
	0.1	15	50

The tungsten contents were calculated from the following equation W (at.%) = W/(W + Ni) × 100.

It was found that for citrate-based electrolytes the partial current density for Ni–W deposition is significantly lower than that for TEA-based electrolytes and similar to that for glycine baths (Fig. 1). Ni–W deposition from citrate baths already reaches the limiting current at 0.05 A cm^{-2}. For both the citrate bath and the glycine bath mass-transfer of NiW species is poor. However, the partial current density for nickel deposition in the glycine bath is high, even at 0.15 A cm^{-2}. Correspondingly, a low tungsten content results in layers electroplated at high current density. In contrast to these observations, the partial current densities for both of Ni and NiW species for TEA bath are relatively high.

Voltammetric measurements from citrate, glycine and TEA-based electrolytes, with and without nickel sulfate, were conducted in order to distinguish between metal depositions of Ni and NiW species and hydrogen evolution, shown in Fig. 2. In the electrolytes without $NiSO_4$ neither of the metal depositions is possible.

The potential for hydrogen evolution from all the electrolytes is predicted to be −1.0 V versus SCE from the substantial increase in current density observed in all the curves from the electrolytes containing $NiSO_4$ and from the electrolytes without $NiSO_4$. The potential at which metal deposition occurs depends on the electrolyte. Particularly, metal deposition from the citrate bath starts at a more negative potential, i.e. closer to the potential for hydrogen evolution. This is consistent with the low current efficiency even at low current density. In glycine and TEA-based baths higher currents are shown at positive potentials where hydrogen evolution does not occur. Therefore, high partial current densities for Ni and NiW depositions are obtained at relatively low current density.

Fig. 3 shows scanning electron microscopy (SEM) micrographs of the surface morphology and scanning ion microscopy (SIM) micrographs of cross-sections of Ni–W alloys electroplated at 0.01 or 0.1 A cm^{-2}.

Cracks are observed in the layers deposited from the citrate bath, even at 0.01 A cm^{-2}. The cracks are caused by relaxation of internal tensile stress in the deposits. Presumably, massive hydrogen dissolution into the deposit occurs during plating. A subsequent release of hydrogen leads to high tensile stress, which promotes cracking in the direction of the thickness of the Ni–W layer. Compared with layers from the citrate bath, deposits from glycine and TEA baths are rougher and seem to have larger grains. Although the compositions of the deposit electroplated at 0.01 A cm^{-2} from the citrate bath (17 at.% W) and at 0.1 A cm^{-2} from the TEA bath (15 at.% W) are close to each other, SIM images show a substantial difference in structure and grain size. Furthermore, the deposits plated at 0.1 A cm^{-2} from glycine and TEA baths possess a similar nodular morphology shown in the SEM micrographs, although tungsten contents in the deposits are as different as 2 and 15 at.%, respectively. Cracks occur at the boundaries between the nodules.

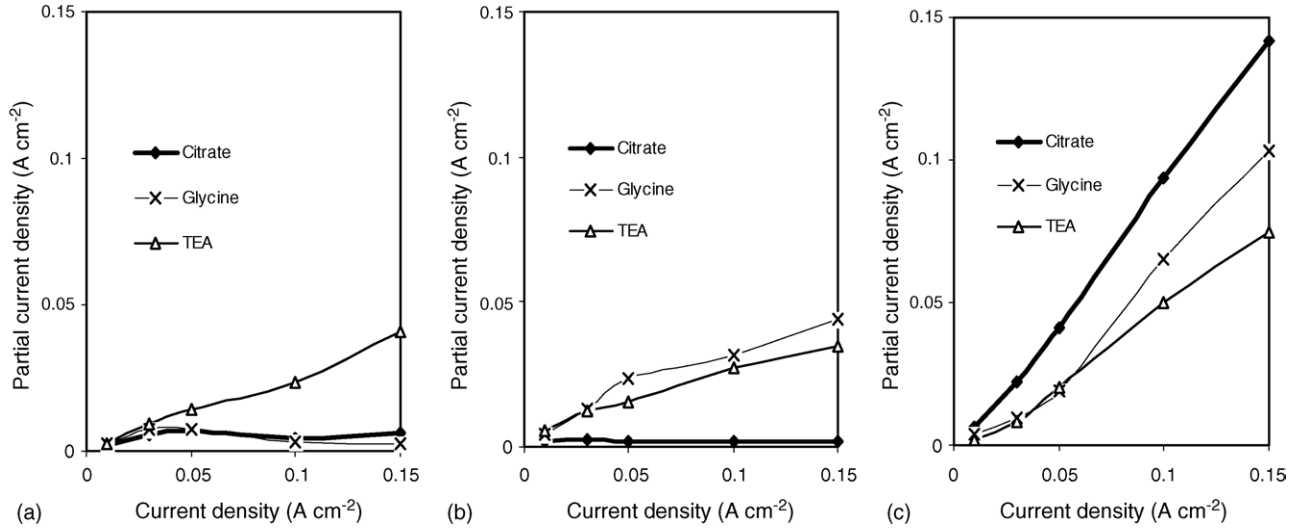

Fig. 1. Partial current density for NiW deposition (a), Ni deposition (b) and hydrogen evolution (c) as a function of current density from electrolytes containing 0.1 mol dm^{-3} $NiSO_4$, 0.2 mol dm^{-3} Na_2WO_4 and 0.3 mol dm^{-3} complexing agent (citrate, glycine or triethanolamine).

The complexing agents clearly influence the surface morphology as well as the structure of the electroplated layers. Other authors have proposed that electrolytes containing ammonium and glycine cause a nodular morphology [5]. The present investigations show that TEA also yields a similar nodular morphology.

It is obvious that electrolytes containing a single complexing agent, each have their specific problems; either with high hydrogen evolution, crack development due to stress relaxation or low tungsten content. Therefore, complexing agents were combined.

3.2. Electrolytes containing two complexing agents

Combinations of equal amounts of complexing agents of citrate and glycine or TEA were examined, while keeping the total concentration of complexing agents at 0.3 mol dm^{-3}.

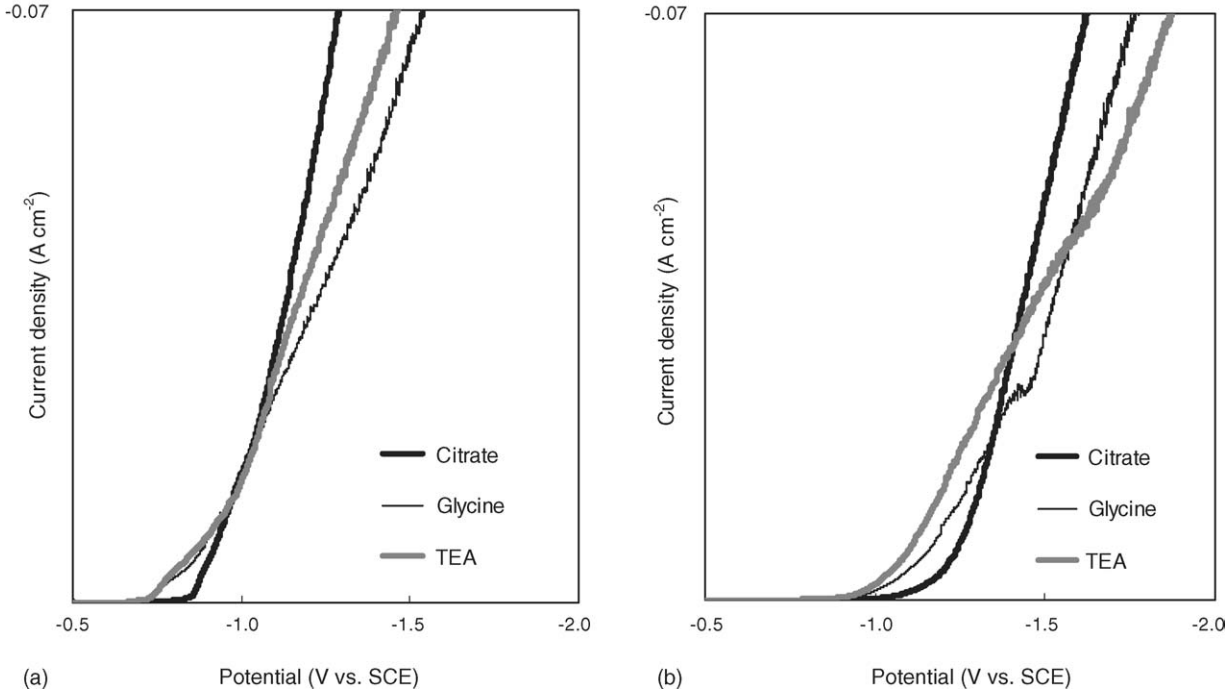

Fig. 2. Voltammetric curves from electrolytes containing 0.1 mol dm^{-3} $NiSO_4$, 0.2 mol dm^{-3} Na_2WO_4 and 0.3 mol dm^{-3} complexing agent (citrate, glycine or triethanolamine) (a) and from electrolytes 0.2 mol dm^{-3} Na_2WO_4 and 0.3 mol dm^{-3} complexing agent (citrate, glycine or triethanolamine) (b).

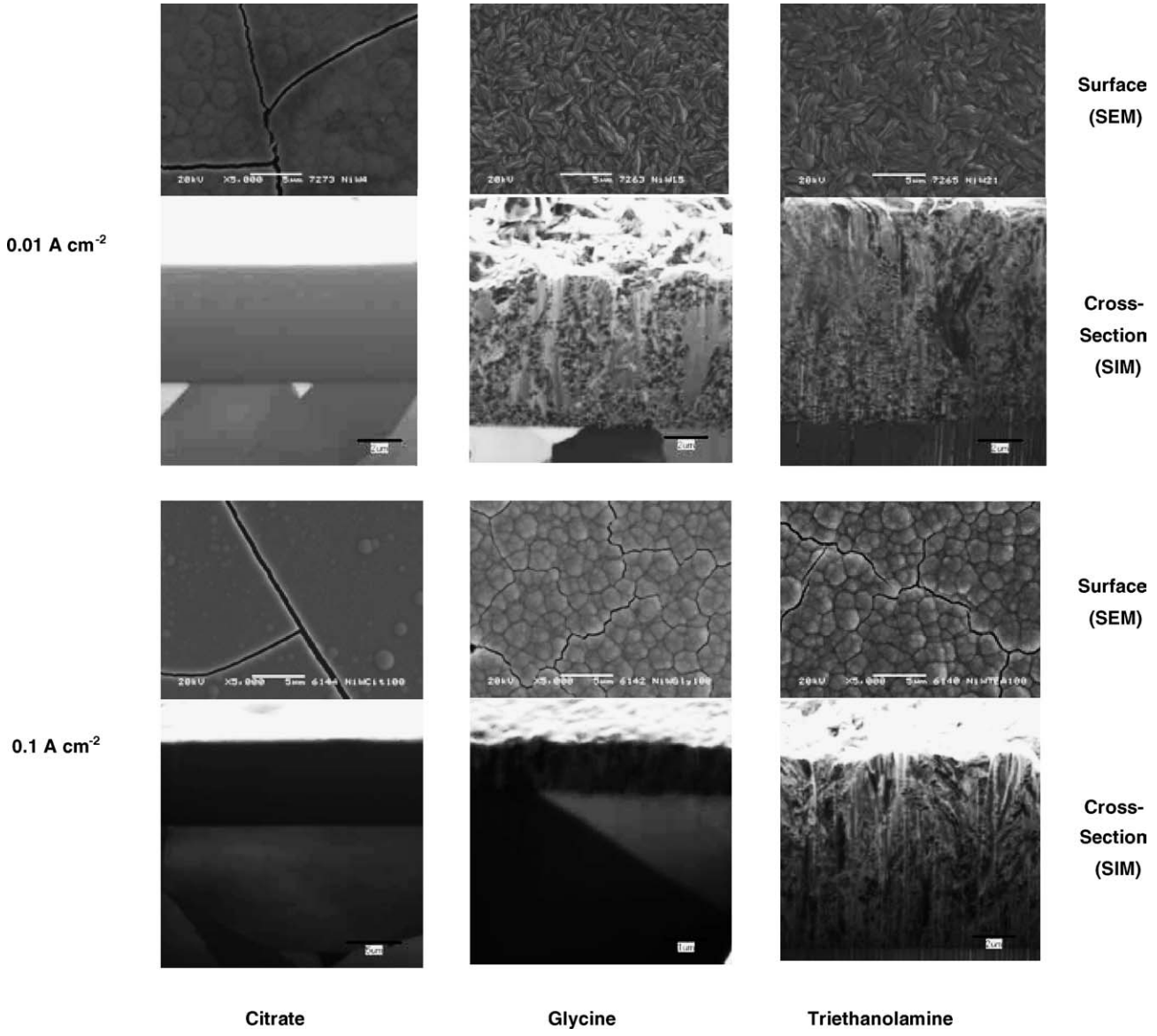

Fig. 3. SEM and SIM images of Ni–W alloy electroplated at 0.01 and 0.1 A cm^{-2} from electrolytes containing 0.1 mol dm^{-3} $NiSO_4$, 0.2 mol dm^{-3} Na_2WO_4 and 0.3 mol dm^{-3} complexing agent (citrate, glycine or triethanolamine).

For electrolytes mixing citrate with glycine or TEA the current efficiency was improved, but the tungsten contents decreased, as compared to the electrolyte containing a single complexing agent of citrate (Table 2). However, for the electrolyte containing mixtures of citrate and TEA a current efficiency of 29% and a tungsten content of 26 at.% was realized at 0.1 A cm^{-2}.

Figs. 4 and 5 give more detailed information about the effect of the combination of complexing agents on current efficiency and W content. In the figures, the fractional current density for Ni–W, Ni and H_2, respectively, are given, for the purpose of the examination on the effect of the electrolytes on Ni–W alloy deposition precisely. Voltammetry and UV-photometry were used to investigate the change in current density for metal depositions and complex formation on complexing agents, respectively.

Table 2
Current efficiencies of electrodeposition and tungsten contents in the layer electrodeposited from electrolytes containing 0.1 mol dm^{-3} $NiSO_4$, 0.2 mol dm^{-3} Na_2WO_4 and 0.3 mol dm^{-3} complexing agent (0.15 mol dm^{-3} citrate and 0.15 mol dm^{-3} glycine, and 0.15 mol dm^{-3} citrate and 0.15 mol dm^{-3} triethanolamine)

Complexing agent	Current density (A cm^{-2})	Tungsten content (at.%)	Current efficiency (%)
Citrate–glycine (1:1)	0.01	10	78
	0.1	13	48
Citrate–TEA (1:1)	0.01	9	73
	0.1	26	29

The tungsten contents were calculated from the following equation W (at.%) = W/(W + Ni) × 100.

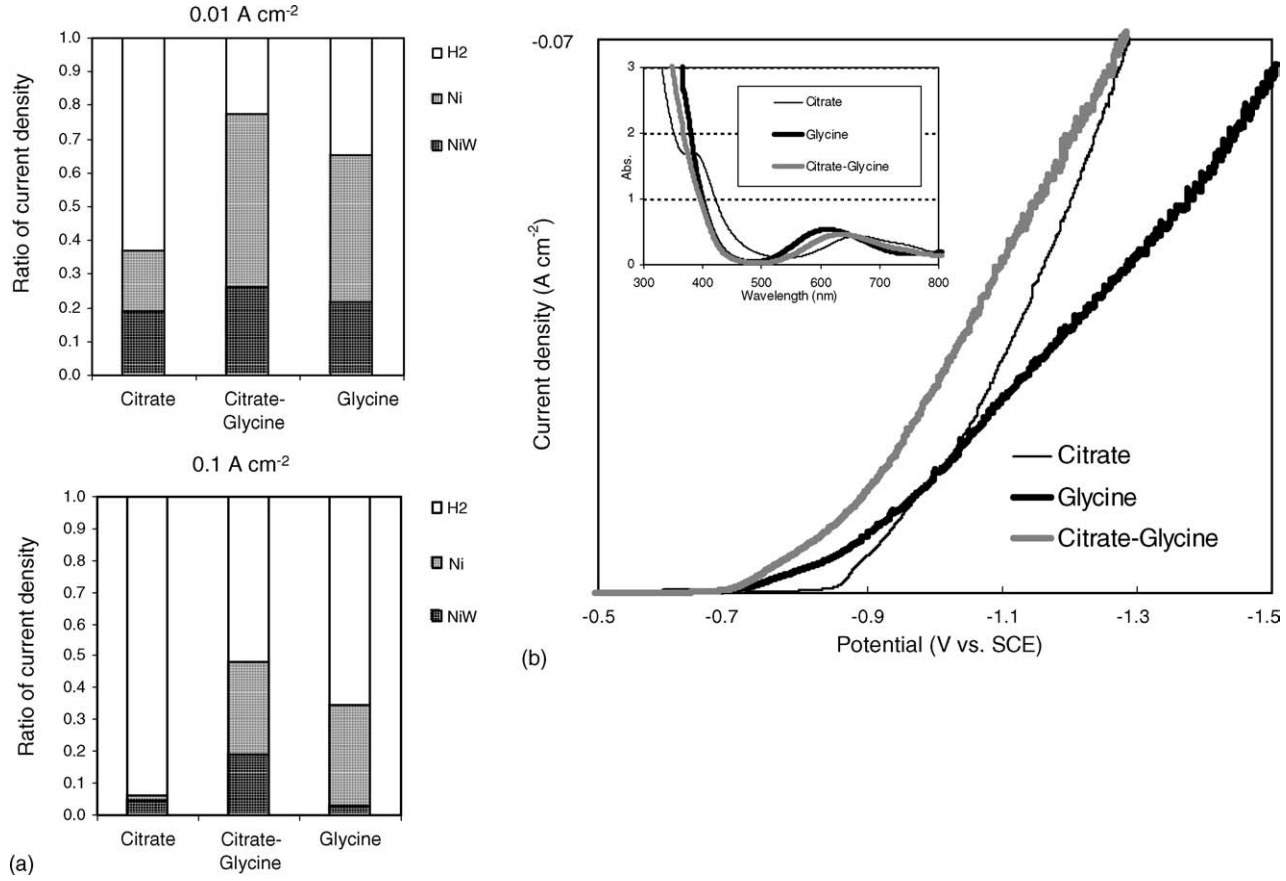

Fig. 4. Ratio of partial current density for NiW and Ni depositions and hydrogen evolution at 0.01 and 0.1 A cm^{-2} (a) and voltammetric curves and UV spectra (b) from electrolytes containing 0.1 mol dm^{-3} $NiSO_4$, 0.2 mol dm^{-3} Na_2WO_4 and 0.3 mol dm^{-3} complexing agent (0.3 mol dm^{-3} citrate and 0.3 mol dm^{-3} glycine or 0.15 mol dm^{-3} citrate and 0.15 mol dm^{-3} glycine).

In practice, though the effect of the combination with glycine on NiW deposition is unclear in Table 2, the electrolyte improves fractional current density for deposition of the NiW species in Fig. 4. And also, the voltammetric curves show an increase in current density at positive potential ranging from −0.7 to −1.0 V versus SCE where hydrogen evolution is expected not to occur, indicating that the mixture of citrate and glycine enhanced current density for metal depositions. Furthermore, even at more negative potential an increase in current density was shown, and fractional current density for deposition of the NiW species even at relatively high current density of 0.1 A cm^{-2} was improved. Thus, the mixture of citrate and glycine enhances mass-transfer of the NiW species.

Looking at the UV spectra, the significant adsorption below 400 nm which is assigned to electron transfer of tungsten and the peak at about 600 nm, which is assigned to electron transfer of nickel, a competition to form complexes with tungstate is expected to occur between citrate and glycine.

In contrast, the effect of the combination with TEA was not substantial. The voltammetric curve corresponds to the curve from the TEA-based bath at lower potential, leading to similar fractional current densities at 0.01 A cm^{-2}. The fractional current density for hydrogen evolution in the citrate–TEA bath is between the current densities for the citrate and the TEA based electrolytes (Fig. 5).

The reason for the positive effect of mixing citrate with glycine must be found in the problem with poor mass-transfer of the NiW–glycine complex. Probably, the competition between citrate and glycine to form complexes with tungstate may prevent complex formation between glycine and tungstate, leading to the improvement of the mass-transport of the complex.

Glycine and TEA also raise the partial current density for Ni–W deposition owing to complex formation with tungstate, while ammonium does not promote Ni–W deposition in citrate-based electrolyte [1,2].

3.3. Electrolytes containing three complexing agents

In a quest for a higher current efficiency, and higher tungsten content in deposits and encouraged by the findings for two complexing agents, the effect of adding glycine to an electrolyte with equal amounts of citrate and TEA was investigated. Also in these experiments the total concentration of

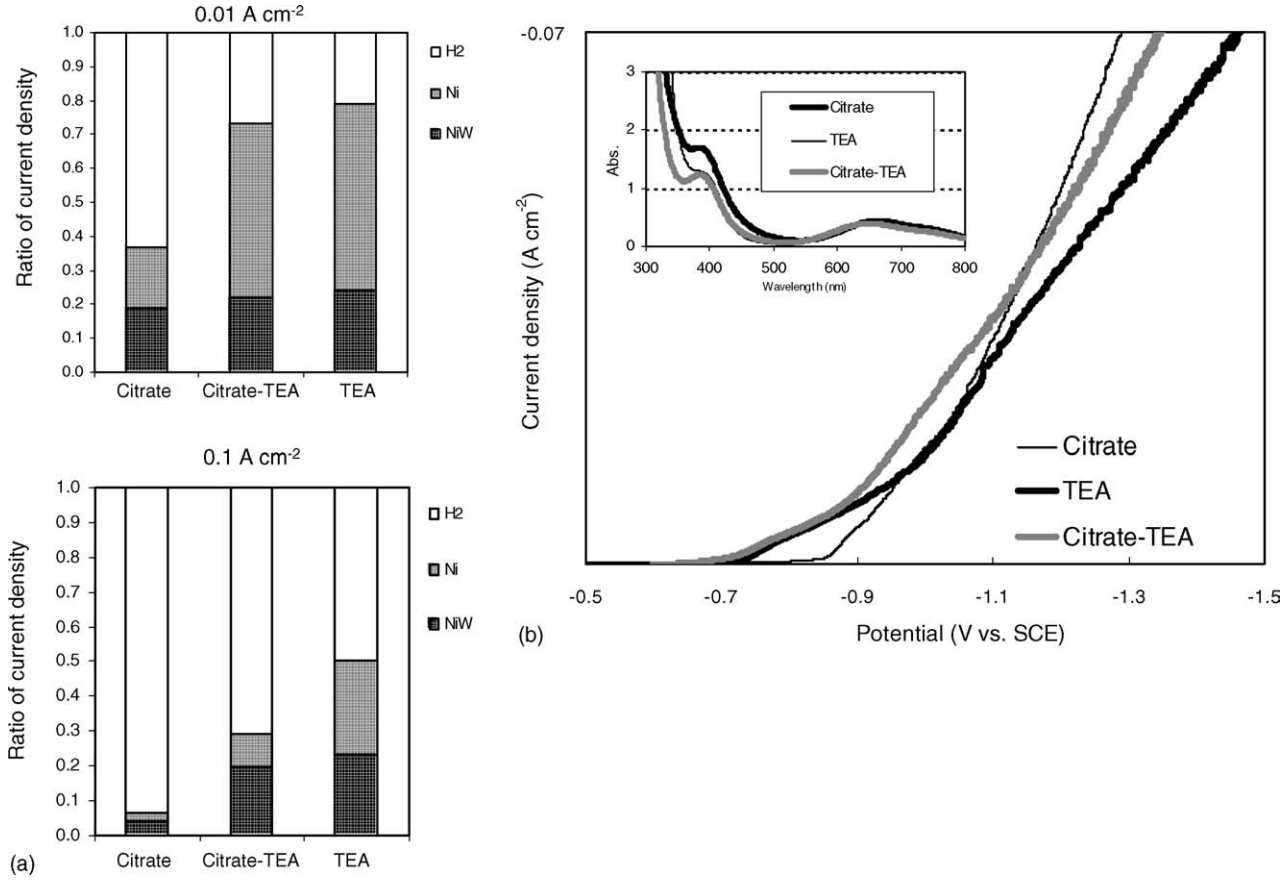

Fig. 5. Ratio of partial current density for NiW and Ni depositions and hydrogen evolution at 0.01 and 0.1 A cm^{-2} (a) and voltammetric curves and UV spectra (b) from electrolytes containing 0.1 mol dm^{-3} $NiSO_4$, 0.2 mol dm^{-3} Na_2WO_4 and 0.3 mol dm^{-3} complexing agent (0.3 mol dm^{-3} citrate and 0.3 mol dm^{-3} triethanolamine or 0.15 mol dm^{-3} citrate and 0.15 mol dm^{-3} triethanolamine).

complexing agents was kept constant at 0.3 mol dm^{-3}. The ratio of glycine compared to citrate–TEA was investigated at three levels: 0.14:1:1 (6.7%), 0.4:1:1 (16.7%) and 1:1:1 (33.3%).

Although the tungsten content in the electrodeposits decreases with increasing the content of glycine in the electrolyte, the current efficiency is markedly improved even for the smallest addition of glycine (Table 3).

Actually, the fractional current density for deposition of the NiW species increases by adding glycine, and the increase in the amount of current used for metal plating is shown in the voltammetric curve (Fig. 6). While a glycine concentration of 0.1 mol dm^{-3} (33.3% of the total concentration of complexing agents) has a substantial influence on complex formation between nickel and tungstate, the effect for 6.7% glycine is negligible, according to the UV-spectrum. It is suggested that glycine works as a support salt for the promotion of metal ion mass-transport.

Fig. 7 shows SEM micrographs of Ni–W alloys electrodeposited from electrolytes containing all three complexing agents. The surface morphology changes considerably by adding glycine. For a total current density of 0.01 A cm^{-2}, the deposit becomes more needle shaped. For 0.1 A cm^{-2}, the nodular appearance becomes finer with increasing

Table 3
Current efficiencies of electrodeposition and tungsten contents in the layer electrodeposited from electrolytes containing 0.1 mol dm^{-3} $NiSO_4$, 0.2 mol dm^{-3} Na_2WO_4 and 0.3 mol dm^{-3} complexing agent (0.15 mol dm^{-3} citrate and 0.15 mol dm^{-3} triethanolamine (glycine 0%), or 0.14 mol dm^{-3} citrate and 0.14 mol dm^{-3} triethanolamine and 0.02 mol dm^{-3} glycine (glycine 6.7%), or 0.125 mol dm^{-3} citrate, 0.125 mol dm^{-3} triethanolamine and 0.05 mol dm^{-3} glycine (glycine 16.7%) or 0.1 mol dm^{-3} citrate, 0.1 mol dm^{-3} triethanolamine and 0.1 mol dm^{-3} glycine (glycine 33.3%))

Ratio of glycine to total amount of complexing agents (%)	Current density (A cm^{-2})	Tungsten content (at.%)	Current efficiency (%)
0	0.01	9	73
	0.1	26	29
6.7	0.01	8	81
	0.1	19	56
16.7	0.01	6	85
	0.1	15	65
33.3	0.01	7	86
	0.1	13	58

The tungsten contents were calculated from the following equation W (at.%) = W/(W + Ni) × 100.

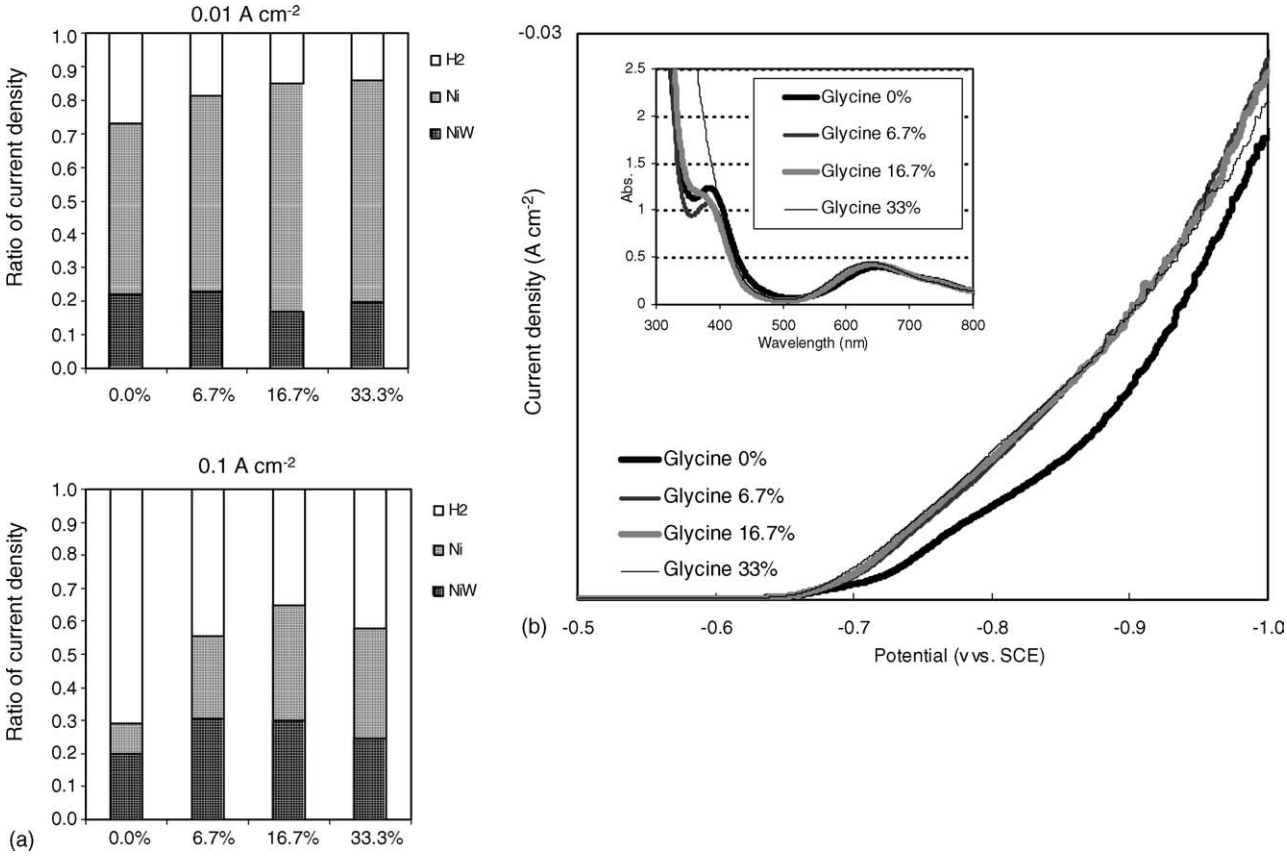

Fig. 6. Ratio of partial current density for NiW and Ni depositions and hydrogen evolution at 0.01 and 0.1 A cm^{-2} (a) and voltammetric curves and UV spectra (b) from electrolytes containing 0.1 mol dm^{-3} $NiSO_4$, 0.2 mol dm^{-3} Na_2WO_4 and 0.3 mol dm^{-3} complexing agent (0.15 mol dm^{-3} citrate and 0.15 mol dm^{-3} triethanolamine (glycine 0%), or 0.14 mol dm^{-3} citrate and 0.14 mol dm^{-3} triethanolamine and 0.02 mol dm^{-3} glycine (glycine 6.7%), or 0.125 mol dm^{-3} citrate, 0.125 mol dm^{-3} triethanolamine and 0.05 mol dm^{-3} glycine (glycine 16.7%) or 0.1 mol dm^{-3} citrate, 0.1 mol dm^{-3} triethanolamine and 0.1 mol dm^{-3} glycine (glycine 33.3%)).

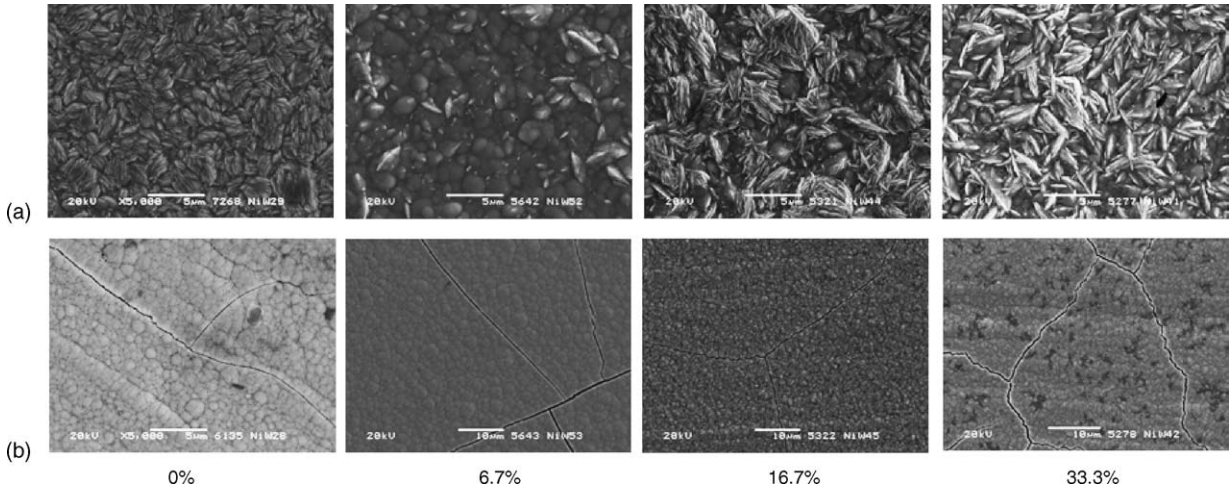

Fig. 7. SEM images of Ni–W alloy electroplated at 0.01 and 0.1 A cm^{-2} from electrolytes containing 0.1 mol dm^{-3} $NiSO_4$, 0.2 mol dm^{-3} Na_2WO_4 and 0.3 mol dm^{-3} complexing agent (0.15 mol dm^{-3} citrate and 0.15 mol dm^{-3} triethanolamine (glycine 0%), or 0.14 mol dm^{-3} citrate and 0.14 mol dm^{-3} triethanolamine and 0.02 mol dm^{-3} glycine (glycine 6.7%), or 0.125 mol dm^{-3} citrate, 0.125 mol dm^{-3} triethanolamine and 0.05 mol dm^{-3} glycine (glycine 16.7%) or 0.1 mol dm^{-3} citrate, 0.1 mol dm^{-3} triethanolamine and 0.1 mol dm^{-3} glycine (glycine 33.3%)).

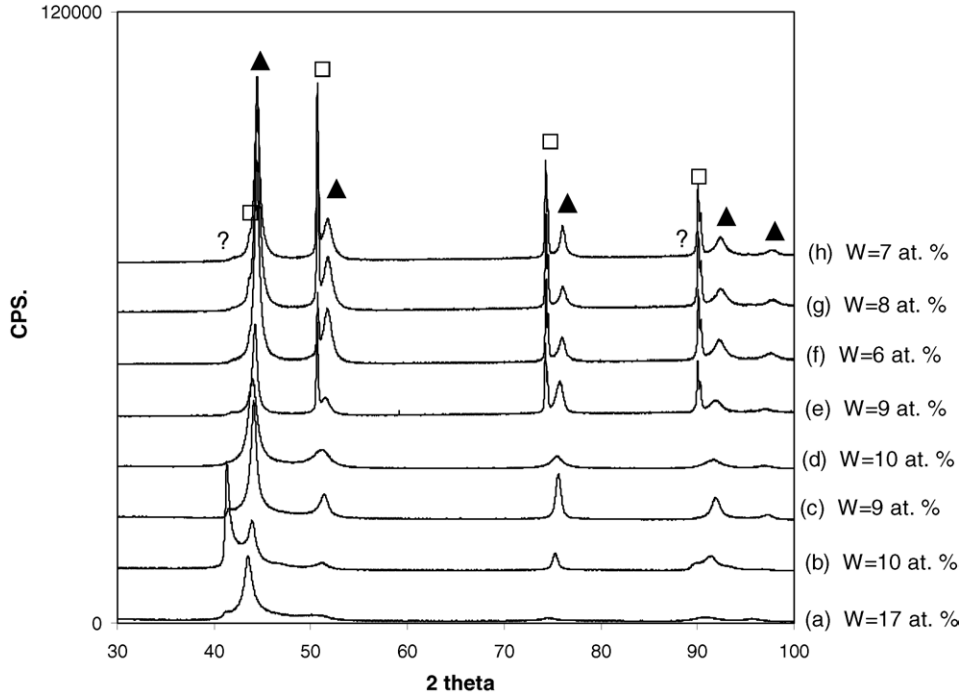

Fig. 8. X-ray diffraction patterns of Ni–W alloy electroplated at 0.01 A cm^{-2} from electrolytes containing 0.1 mol dm^{-3} $NiSO_4$, 0.2 mol dm^{-3} Na_2WO_4 and 0.3 mol dm^{-3} complexing agent constituted of: (a) 0.3 mol dm^{-3} citrate, (b) 0.3 mol dm^{-3} glycine, (c) 0.3 mol dm^{-3} triethanolamine, (d) 0.15 mol dm^{-3} citrate and 0.15 mol dm^{-3} glycine, (e) 0.15 mol dm^{-3} citrate and 0.15 mol dm^{-3} triethanolamine, (f) 0.14 mol dm^{-3} citrate, 0.14 mol dm^{-3} triethanolamine and 0.02 mol dm^{-3} glycine (glycine 6.7%), (g) 0.125 mol dm^{-3} citrate, 0.125 mol dm^{-3} triethanolamine and 0.05 mol dm^{-3} glycine (glycine 16.7%) and (h) 0.1 mol dm^{-3} citrate, 0.1 mol dm^{-3} triethanolamine and 0.1 mol dm^{-3} glycine (glycine 33.3%): (▲) solid solution of Ni(W); (□) Cu substrate and (?) unknown diffraction peaks.

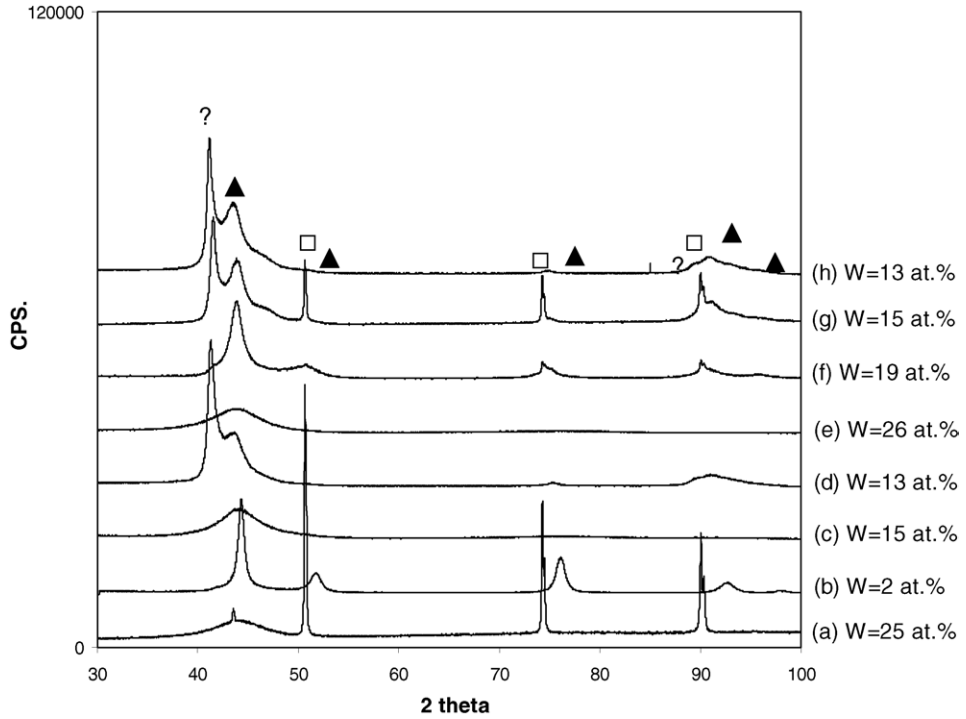

Fig. 9. X-ray diffraction patterns of Ni–W alloy electroplated at 0.1 A cm^{-2} from electrolytes containing 0.1 M $NiSO_4$, 0.2M Na_2WO_4 and 0.3 M complexing agent constituted of: (a) 0.3 mol dm^{-3} citrate, (b) 0.3 mol dm^{-3} glycine, (c) 0.3 mol dm^{-3} triethanolamine, (d) 0.15 mol dm^{-3} citrate and 0.15 mol dm^{-3} glycine, (e) 0.15 mol dm^{-3} citrate and 0.15 mol dm^{-3} triethanolamine, (f) 0.14 mol dm^{-3} citrate, 0.14 mol dm^{-3} triethanolamine and 0.02 mol dm^{-3} glycine (glycine 6.7%), (g) 0.125 mol dm^{-3} citrate, 0.125 mol dm^{-3} triethanolamine and 0.05 mol dm^{-3} glycine (glycine 16.7%) and (h) 0.1 mol dm^{-3} citrate, 0.1 mol dm^{-3} triethanolamine and 0.1 mol dm^{-3} glycine (glycine 33.3%): (▲) solid solution of Ni(W); (□) Cu substrate and (?) unknown diffraction peaks.

glycine content. Nevertheless, the mechanism of stress relaxation leading to cracks in the deposits demands further investigation.

3.4. Phase characterization of electroplated Ni–W alloy deposits

The phase constitutions of the electroplated Ni–W alloy layers were examined using X-ray diffraction (Figs. 8 and 9). Almost all of the peaks in the diffractograms are presumed to be assigned to solid solution of tungsten in nickel; as compared to W-free nickel, the peaks shifted to lower angles as a function of increased tungsten contents in layers. The dissolution of W atom in Ni leads to lattice expansion of Ni because there is a difference in atom size between Ni and W (Ni: 2.492 Å, W: 2.741 Å) The peak intensity decreases and peak width increases with increasing tungsten content, indicating a reduction of grain size, in accordance to the literature [4,8–12]. However, the peak shifts in the diffractograms from the layer, which possess high tungsten content, are relatively low. Besides, the low peak intensities accompanied by an increase in the peak width is remarkable. It was mentioned that the layer containing 25 at.% W forms nano-crystalline Ni_4W and amorphous phase which is transformed to NiW during annealing [8,10]. According to the literature, the peak position in the diffractograms of the layers with about 25 at.% W may indicate phase formation different from the solid solution in the layer. Furthermore, there are unknown peaks at about 41° (2θ) and 90° (2θ) in some of the patterns. Especially, the diffractograms of the layers deposited from electrolytes containing glycine in large amounts have substantial unknown peaks. Similar peaks were also found by other authors for XRD patterns of Ni–W layer [5,11]. The complex of NiW–glycine may influence the structure of the layer, but further in depth phase analysis must be conducted to identify the origin of these peaks.

Along the same lines, it should be noted that impurities in the layers are a very important issue. According to the literature, the complex formation between nickel and tungstate in citrate baths is achieved by coordination of the HWO_4^{2-} ion to a site in the complexing agent molecule next to a site occupied by a nickel ion [1,2,13]. Therefore, it is possible that the deposition of Ni–W from this type of complexes causes co-deposition of the complexing agent. The mechanisms leading to co-deposition of unexpected species, or impurities, will be the topic of future investigations.

4. Conclusion

Electrolytes containing a single complexing agent, such as citrate, glycine or TEA, are characterized by substantial hydrogen evolution, cracks in the deposits and low tungsten content.

High tungsten contents combined with high current efficiencies could be realized by applying electrolytes containing a combination of three complexing agents of citrate, glycine and triethanolamine.

A small amount of glycine in a citrate–TEA-based electrolyte has a positive effect on the current efficiency and the partial current density of Ni–W alloy deposition.

The predominant phase of the deposits is a solid solution of tungsten in nickel.

Acknowledgement

The authors wish to thank Professor T. Watanabe (Tokyo Metropolitan University) for providing scanning ion microscope and X-ray diffraction measurement facilities.

References

[1] A. Brenner, Electrodeposition of Alloys, vol. 2, Academic Press, New York, 1963, p. 347.
[2] O. Younes, E. Gileadi, J. Electrochem. Soc. 149 (2) (2002) C100.
[3] O. Younes, E. Gileadi, Electrochem. Solid-State Lett. 3 (12) (2000) 543.
[4] O. Younes, L. Zhu, Y. Rosenberg, Y. Shacham-Diamand, E. Gileadi, Langmuir 17 (2001) 8270.
[5] Y. Wu, D.-Y. Chang, S.-C. Kwon, D. Kim, Plat. Surf. Finish. 2 (2003) 46.
[6] M. Bratoeva, N. Atanasov, Russ. J. Electrochem. 36 (1) (2000) 60.
[7] H. Cesiulis, M. Donten, M.L. Donten, Z. Stojek, ISSN Mater. Sci. 4 (2001) 230.
[8] T. Yamasaki, P. Schloßmacher, Y. Ogino, Nanostruct. Mater. 10 (3) (1998) 375.
[9] T. Yamasaki, Mater. Phys. Mech. 1 (2000) 127.
[10] P. Schloßmacher, T. Yamasaki, Mikrochim. Acta 132 (2000) 309.
[11] K. Itoh, F. Wang, T. Watanabe, J. Jpn. Inst. Met. 65 (11) (2001) 1023.
[12] L. Huang, J.X. Dong, F.Z. yang, S.K. Xu, S.M. Zhou, Trans. IMF 77 (5) (1999) 185.
[13] H. Hayashi, M. Kasai, Hyoumen Gijutsu 55 (1) (2004) 85.

Chapter 5

Residual Stress in Ni-W Electrodeposits

Available online at www.sciencedirect.com
ScienceDirect
Electrochimica Acta 51 (2006) 6128–6134
ELECTROCHIMICA Acta
www.elsevier.com/locate/electacta

Residual stress in Ni–W electrodeposits

Io Mizushima*, Peter T. Tang, Hans N. Hansen, Marcel A.J. Somers

Department of Manufacturing Engineering and Management, Technical University of Denmark, DTU, DK-2800 Kgs. Lyngby, Denmark

Received 29 July 2005; received in revised form 15 November 2005; accepted 21 November 2005
Available online 12 May 2006

Abstract

In the present work, the residual stress in Ni–W layers electrodeposited from electrolytes based on $NiSO_4$ and Na_2WO_4, is investigated. Citrate, glycine and triethanolamine were used as complexing agents, enabling complex formation between the nickel ion and tungstate. The results show that the type of complexing agent and the current efficiency have an influence on the residual stress. In all cases, an increase in tensile stress in the deposit with time after deposition was observed. Pulse plating could improve the stress level for the electrolyte containing equal amounts of citrate, glycine and triethanolamine (TEA) as complexing agent. An additive as 1,3,6 naphthalene trisulphonic acid which has a grain refining effect, and chloride, which enables dissolution of metal during the anodic cycle, reduced crack occurrence in the electrodeposits.

Keywords: Nickel–tungsten; Electrodeposition; Residual stress; Hydrogen evolution; Pulse plating

1. Introduction

Microinjection molding is foreseen to find wide future application for production of computer parts, microfluidic systems and polymer optical components. For the injection molding of high performance plastics, possessing high strength and chemical resistance, the molds must be able to withstand repeated thermal cycling at temperatures up to 350 °C.

Fabrication of the molding tool is preferably performed by electroforming in order to be able to control the replication of microscale geometrical details. Nickel is a widely applied material for electroforming, but pure nanocrystalline nickel electrodeposits cannot withstand the relatively high temperature without loosing their hardness due to recrystallization. Among the metals and alloys which are expected to have a higher thermal stability than nickel, and which can be electrodeposited, Ni–W is a favorable candidate. Furthermore, a Ni–W alloy is an excellent material, because it has high corrosion resistance and mechanical strength.

Several authors have investigated electrodeposition of Ni–W alloys [1–13]. There is a major problem of the formation of participates (probably $NiWO_4$) in the electrolyte for the electrodeposition of Ni–W alloys [13]. This can be overcome by adding a suitable complexing agent. The influence of such a complexing agent on the current efficiency, the composition of the deposit and mechanical properties, etc., is critical. Actually, citrate which forms a complex with both the nickel ion and tungstate and gives stability to the electrolyte is a common complexing agent for Ni–W electroplating. However, citrate is associated with a low current efficiency. To overcome this disadvantage often ammonia is added, which raises the current efficiency, but ammonia enhances only the transport of nickel ions by complex formation and consequently reduces the tungsten content in the deposit [2]. Consequently, it is hard to obtain a combination of high current efficiency and high tungsten content with citrate as the main complexing agent in the electrolyte. The development of a new electrolyte containing citrate, glycine and triethanolamine (TEA) as complexing agents was conducted in our previous work [14].

Another problem with Ni–W deposits is that they suffer from relatively high tensile stress, which can give rise to crack occurrence in the electrodeposit. There are some reports on residual stress of Ni–W electrodeposits with using stress reducers [15–17]. Hydrogen dissolution in the deposit and its subsequent release is assumed to be the origin of the occurrence of tensile stress [15]. The release of hydrogen from solid solution in the deposit may result in a time-dependent residual stress. So far little attention has been denoted to the evolution of residual stress with time. Reduction of residual stress is the subject of the present contribution, taking into account the

* Corresponding author. Fax: +45 45 93 62 13.
E-mail address: tanaka@ipl.dtu.dk (I. Mizushima).

0013-4686/$ – see front matter © 2006 Elsevier Ltd. All rights reserved.
doi:10.1016/j.electacta.2005.11.053

influence of the complexing agents and time-dependence of stress.

Possibly pulse plating can affect properties such as internal stress, hardness, microstructure, texture and so on. Kim and Weil reported that pulse plating reduced the level of residual stress of Ni electrodeposit [18]. Moreover, pulse plating can provide useful conditions by charging and discharging of the electric double layer at the cathode/solution interface [19]. If a co-deposition process is controlled by mass transport, the low metallic concentration at the interface can be compensated during the off-time of pulse plating corresponding to no charge transfer of metallic ion. Marlot et al. reported the pulse plating increase Mo content in Ni–Mo alloy deposit, while maintaining current efficiency, in a co-deposition process controlled by mass transport [20]. Lee et al. that mentioned hydrogen could diffuse out of the surface of Ni–W deposits during off-period of pulse plating and pulse plating might change behavior of inhibitors such as SO_4^{2-} and Na^+ on the surface and interrupt growth of a coarsened nodule-crystal surface [21]. In the present manuscript, the contribution of pulse plating to modifying the level of residual stresses in Ni–W is investigated.

2. Experimental procedure

A 1 dm^3 beaker was used as the electrochemical cell. The electrolytes consisted of 0.1 mol dm^{-3} $NiSO_4{\cdot}6H_2O$, 0.2 mol dm^{-3} $Na_2WO_4{\cdot}2H_2O$, 0.3 mol dm^{-3} complexing agent (citrate, glycine and/or triethanolamine) and 0.44 mol dm^{-3} H_3BO_3. Agitation was conducted with a magnetic stirrer. The bath was kept at 70 °C during deposition. A copper plate treated with an alkaline solution and a 1 M HCl solution for removing contamination and passive layer was used as a substrate.

Pulse plating was conducted with a cathodic current density of 0.01 or 0.1 A cm^{-2} for 60 ms and an anodic current density of 0, 0.0075 or 0.075 and 0.015 or 0.15 A cm^{-2} for 20 ms. The charge ratios of anodic current to cathodic current, Q_a/Q_c, were 0, 0.25 and 0.5, respectively.

The mechanical stress in the deposits was estimated from the deflection of one side deposited test strips (Specialty Testing & Development Co.) with known elastic constants. The test strip is made from a CuBe foil and is approximately 60 μm in thickness, consists of a 15 mm wide base and has two "legs" that are 76 mm long and 5 mm wide. The base and legs of the strip are covered with a deposition preventing resist layer, but on facing sides of the legs. The cell for stress measurement has two anodes and one cathode (the test strip) which is located centrally between the anodes, such that the opposite sides of the test strip experience identical deposition conditions. Internal stress in the deposits makes the two legs of the strip bend in opposite directions. The distance between the deflected beams of the test strip, equaling twice the deflection of a single beam, gives an average value of deflection due to stress in the electrodeposit. The average value was converted into mechanical stress using Stoney's equation [22]. Mechanical stress values were determined immediately after deposition while the strips are still wet, immediately after drying in air at room temperature and 24 h after finished deposition. Voltammetry was carried out using a potentiostat/galvanostat (PGP201 Radiometer, Copenhagen) with a saturated calomel electrode (SCE) as the reference electrode. The composition in the electroplated layer was determined semi-quantitatively with energy dispersive X-ray spectroscopy (Oxford Scientific). The surface topography was examined with scanning electron microscopy (JSM-5900, JEOL).

3. Results and discussion

3.1. Mechanical stress in Ni–W electrodeposits from various electrolytes

The tungsten contents and current efficiencies of the Ni–W deposits obtained in various electrolytes at a current density of 0.01 A cm^{-2} are collected in Table 1. Except for the citrate-based electrolyte, deposits for all the electrolytes contain about 8 at.% W and the current efficiency is about 80%.

The mechanical stress values in the electrodeposits are given as a function of thickness for the electrolytes containing either citrate, glycine or TEA (Fig. 1). For all electrolytes the layers show a time-dependence of the stress; the stress also changed upon drying. For the deposits obtained in the glycine and TEA-based electrolytes the mechanical stress is initially much lower than for the citrate-based electrolyte, but in contrast to the deposits obtained in the citrate-based electrolyte, the stress increases rather than decreases, during storage for 24 h. Severe cracking had occurred in the citrate deposits; no cracks were observed with SEM in the glycine and TEA deposits (Fig. 2).

Table 1
Current efficiencies of electrodeposition and tungsten contents in the layer electrodeposited at 0.01 A cm^{-2} from electrolytes containing 0.1 mol dm^{-3} $NiSO_4$, 0.2 mol dm^{-3} Na_2WO_4 and 0.3 mol dm^{-3} complexing agent (citrate, glycine or triethanolamine)

Complexing agent	pH value	Tungsten content (at.%)	Current efficiency (%)
Citrate	8.0	17	37
Glycine	7.0	10	65
Triethanolamine (TEA)	7.6	9	79
Citrate–glycine (1:1)	7.5	10	78
Citrate–TEA (1:1)	7.8	9	73
Citrate–TEA–glycine (1:1:1) (glycine 33.3%)	7.5	7	86
Citrate–TEA–glycine (1:1:0.4) (glycine 16.7%)	7.5	6	85
Citrate–TEA–glycine (1:1:0.14) (glycine 6.7%)	7.6	8	81

The tungsten contents were caluculated from the following equation: $W\,(at.\%) = \frac{W}{W+Ni} \times 100$.

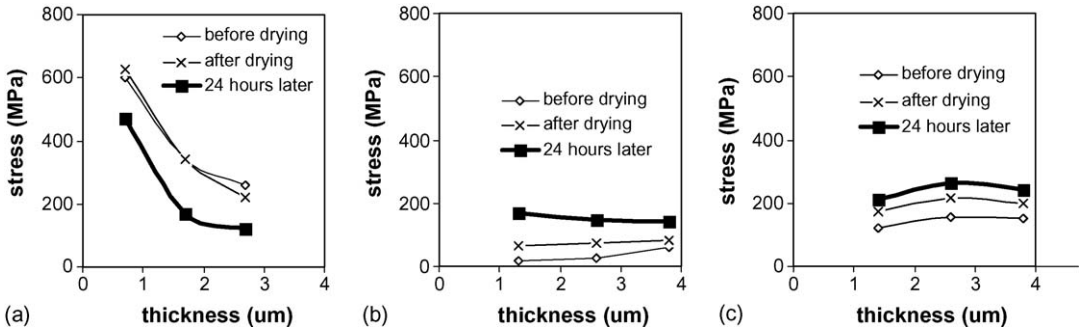

Fig. 1. Residual stress as a function of layer thickness in Ni–W deposits electroplated at 0.01 A cm^{-2} from electrolyte containing 0.1 mol dm^{-3} $NiSO_4$, 0.2 mol dm^{-3} Na_2WO_4 and 0.3 mol dm^{-3} complexing agent as citrate (a), glycine (b) and triethanolamine (c).

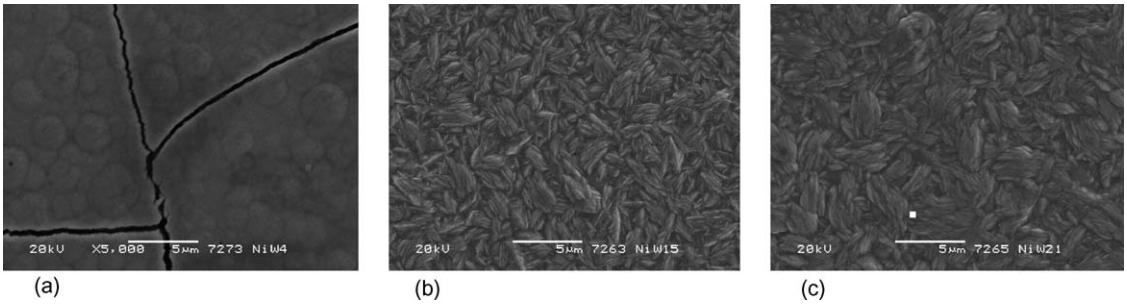

Fig. 2. SEM images of Ni–W deposits with thickness of 5 μm electroplated at 0.01 A cm^{-2} from electrolytes containing 0.1 mol dm^{-3} $NiSO_4$, 0.2 mol dm^{-3} Na_2WO_4 and 0.3 mol dm^{-3} complexing agent as citrate (a), glycine (b) and triethanolamine (c).

The stress values determined in the layers electrodeposited from citrate-based electrolytes, containing glycine or TEA, while keeping the total concentration of complexing agents at 0.3 mol dm^{-3}, are presented in Fig. 3. For the electrolyte containing mixtures of citrate and glycine mechanical stress in the electrodeposit is lower than for the citrate–TEA-based electrolyte; however, the increase in stress upon storage for 24 h is much larger. The current efficiencies for the citrate–glycine and citrate–TEA-based electrolytes are 78 and 73%, respectively. Even though the current efficiencies are close to each other, the kind of additional complexing agent contained in the citrate-based electrolyte is accompanied by a substantial influence on the stress level.

The stress values determined in the layers deposited from electrolytes containing all three complexing agents are given in Fig. 4. Also in these experiments the total concentration of complexing agents was kept constant at 0.3 mol dm^{-3}. The ratio of citrate:TEA:glycine was investigated at three levels: 1:1:0.14 (glycine 6.7%), 1:1:0.4 (glycine 16.7%) and 1:1:1 (glycine 33.3%). Although all the current efficiencies and W contents are similar, the stress decreases with increasing the content of glycine in the electrolyte.

3.2. Origin of stress in electrodeposited Ni–W layers

The thermal expansion coefficients of Cu, Ni and W are 15.4×10^{-6}, 12.5×10^{-6} and 4.5×10^{-6} K^{-1}, respectively. Hence, the difference in thermal shrinkage between the copper substrate and the Ni–W deposit after deposition is expected to result in a compressive stress in the deposit, as imposed by

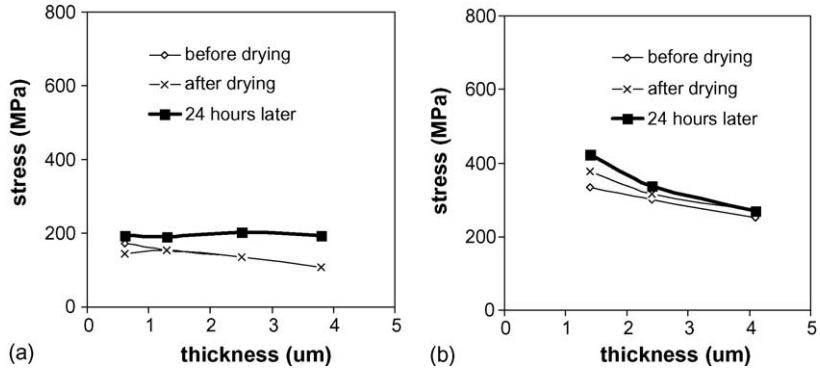

Fig. 3. Residual stress as a function of layer thickness in Ni–W deposits electroplated at 0.01 A cm^{-2} from electrolyte containing 0.1 mol dm^{-3} $NiSO_4$, 0.2 mol dm^{-3} Na_2WO_4 and 0.3 mol dm^{-3} complexing agent (0.15 mol dm^{-3} citrate and 0.15 mol dm^{-3} glycine (a) or 0.15 mol dm^{-3} citrate and 0.15 mol dm^{-3} triethanolamine (b)).

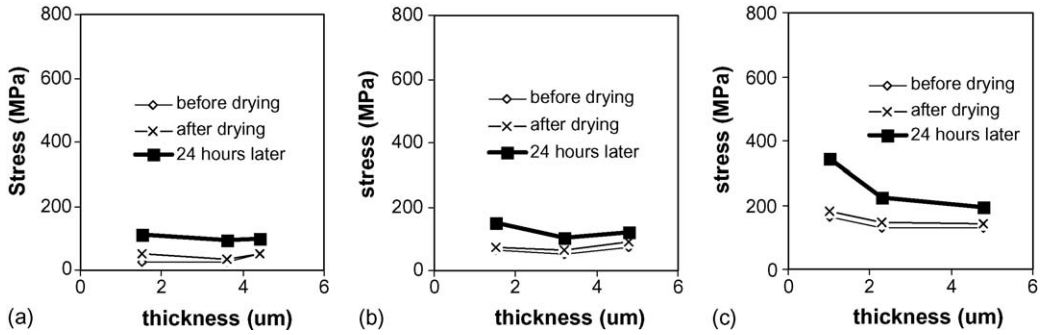

Fig. 4. Residual stress as a function of layer thickness in Ni–W deposits electroplated at 0.01 A cm^{-2} from electrolyte containing 0.1 mol dm^{-3} $NiSO_4$, 0.2 mol dm^{-3} Na_2WO_4 and 0.3 mol dm^{-3} complexing agent (0.1 mol dm^{-3} citrate, 0.1 mol dm^{-3} triethanolamine and 0.1 mol dm^{-3} glycine (glycine 33.3%) (a) or 0.125 mol dm^{-3} citrate, 0.125 mol dm^{-3} triethanolamine and 0.05 mol dm^{-3} glycine (glycine 16.7%) (b) or 0.14 mol dm^{-3} citrate, 0.14 mol dm^{-3} triethanolamine and 0.02 mol dm^{-3} glycine (glycine 6.7%) (c)).

the substrate. Nevertheless, all electrolytes yield tensile stress, indicating that the growth stress at the deposition temperature has been higher (more tensile) than the measured value.

For the citrate-based electrolyte the stress decreases with increasing thickness, and is reduced upon storage for 24 h at room temperature. Cracks were observed in the SEM micrograph of the deposit from citrate-based electrolyte taken about one week after deposition (Fig. 2). It is suggested that the decrease of the tensile stress value with increasing thickness of the deposit is a consequence of cracking during and upon deposition. Evidently, on storage at room temperature additional cracking occurs.

Armyyanov and Sotirova-Chakarova [23] described hydrogen dissolution into an iron deposit, leading to an expansion of the lattice; subsequent release of hydrogen from the deposit, was proposed as the main cause for the occurrence of tensile stress. This interpretation associated with lattice shrinkage would be consistent with the low current efficiency for the deposition from the citrate-based electrolyte (Table 1), which leads to a high tensile stress. In fact, Tsuru and Kawamoto [24] identified the dissolution and release of hydrogen on iron electroplating by measurement of buoyancy effects caused by hydrogen gas release with an electromagnetic balance. On Ni electroplating, Gerischer and Stambach studied the influence of hydrogen charging and discharging on mechanical stress [25] and Monev et al. studied the decomposition of NiH by X-ray analysis [26]. Raub explained [27] a time-dependent decrease of the hydrogen concentration in Ni electrodeposits from formation of an unstable compound between Ni and H. Also in the present case of a Ni–W deposit, the current efficiency below about 80% is considered enough to cause hydrogen dissolution during deposition; subsequent hydrogen release from the deposit yields the development of tensile stress.

In previous work, it was shown that, irrespective of the electrolyte used, electroplating at a high current density of 0.1 A cm^{-2} resulted in crack occurrence in all deposits. In contrast, at 0.01 A cm^{-2} cracks were only observed for the citrate-based electrolyte, corresponding with the lowest current efficiency. Thus, the development of the residual stress level in the deposit depends on the applied current density. Even though the current efficiency is almost constant at about 80%, the stress level changes with current density in the electrolyte (pH 7.5), containing equal amounts of citrate, glycine and triethanolamine (Fig. 5). While the initial stress decreases with increasing current density, the stress gains upon storage for 24 h increases with current density. As an outcome, the tensile stress of the deposit electroplated at 0.01 A cm^{-2} is the lowest.

Huang et al. reported that tensile stress in Ni–W deposits increased with current density, even though the current efficiency increased [15–17]. Possibly, the tensile stress level caused

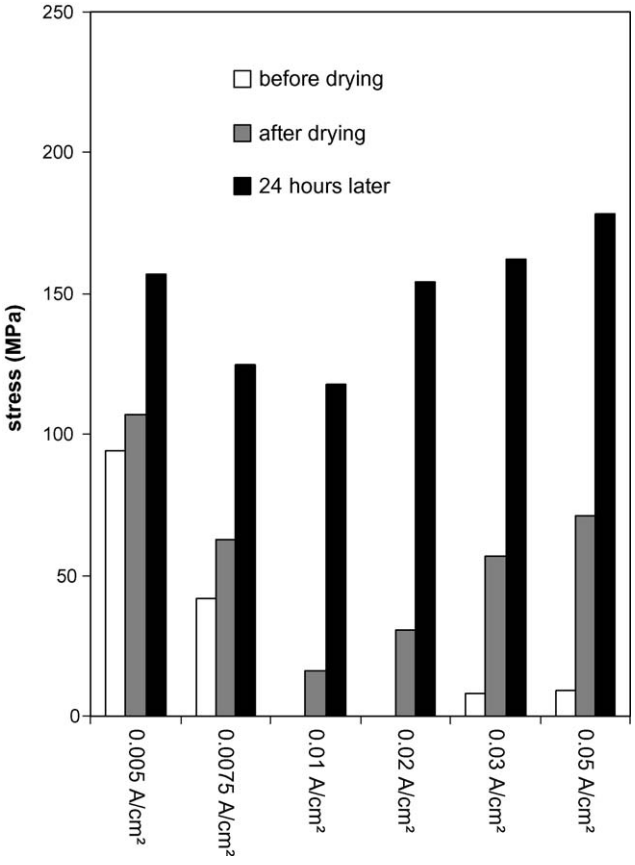

Fig. 5. Residual stress and current efficiency depending on current density for electrolytes (pH 7.5) containing 0.1 mol dm^{-3} $NiSO_4$, 0.2 mol dm^{-3} Na_2WO_4 and 0.3 mol dm^{-3} complexing agent (0.1 mol dm^{-3} citrate, 0.1 mol dm^{-3} triethanolamine and 0.1 mol dm^{-3} glycine (glycine 33.3%)).

by hydrogen dissolution and the subsequent release depends on current density. Fukai estimated gas pressure that would correspond to the hydrogen activity at the surface of the electrode as a function of the over potential. Then, since the over potential increases with current density, amount of dissolved hydrogen in the deposit is expected to increase with current density as well [28]. Thus, with increasing applied current density the grain size of the deposit decreases and in concentration of hydrogen in the deposit increases. The hydrogen solubility is likely to be larger in the intercrystalline regions than in the bulk of the grains, which is consistent with a higher driving force for dissolution of H and the smaller grain size. The subsequent release of the hydrogen results in shrinkage of the deposit and the introduction of tensile stress in the deposit. The substantial increase of the tensile stress after electroplating at high current density might be ascribed to an anticipated high hydrogen concentration in the deposit. Consequently, for layers deposited at high current density cracking occur readily owing to high tensile stress value.

In contrast, the layer deposited at 0.005 A cm^{-2} is characterized by an initial high tensile stress, rather than a large increase in stress upon storage. On increasing the current density up to 0.01 A cm^{-2} the initial tensile stress decreases and the stress increase during storage increases. It is suggested that the initial high tensile stress for low current densities is a consequence of the slow growth rate of the deposit interfering with the adsorption of complexing agents and hydrogen release already during growth of the deposit.

3.3. Effect of pulse plating technique on mechanical stress and crack occurrence

The evolution of tensile stress can qualitatively be explained from hydrogen dissolution into the deposit and its subsequent release as H_2. Next, it was verified whether the pulse plating technique can be applied to improve the current efficiency.

The stress values in the layers electrodeposited at 0.01 A cm^{-2} from the electrolyte (pH 7.5) containing equal amounts of citrate, glycine and triethanolamine were improved by applying pulse plating, while maintaining the tungsten content at 7 at.% (Fig. 6a). Simultaneously, crack occurrence in the deposit obtained at 0.1 A cm^{-2} was improved, and the tungsten content in the deposits plated with Q_a/Q_c ratio of 0 and 0.2 increase to 12 and 13 at.% W, respectively, which is higher than the 11 at.% W in the deposit obtained by applying direct current. However, for charge ratio of $Q_a/Q_c = 0.5$ the tungsten content was reduced to 9 at.%.

In order to investigate the reactions occurring in the anodic cyclic during pulse plating, cyclic voltammetry for the electrolyte (pH 7.5) was performed (Fig. 7). The curves performed by going to a reverse potential of −1.0 V versus SCE without involvement of hydrogen evolution was compared with one of −1.5 V versus SCE, in order to distinguish between hydrogen oxidation and metal oxidation. For the curve with sweep reversal point −1.5 V versus SCE the starting of an anodic current at approximately −0.5 V versus SCE is interpreted as associated with the oxidation of hydrogen atoms. For the curve with sweep reversal point of −1.0 V versus SCE an anodic current is first observed at a higher potential and attributed to anodic dissolution of part of the electrodeposit. However, further increase of the potential leads to passivation of the deposit and the anodic current virtually vanishes. Consequently, it is difficult to realize metal dissolution and rearrangement of atoms in the anodic cycle of pulse plating for the particular electrolyte. Hydrogen in the deposit can be removed partly by the pulse plating technique, but merely hydrogen release from the deposit, without metal dissolution, could cause an increase in the tensile stress during electroplating. Actually, pulse plating reduces the stress

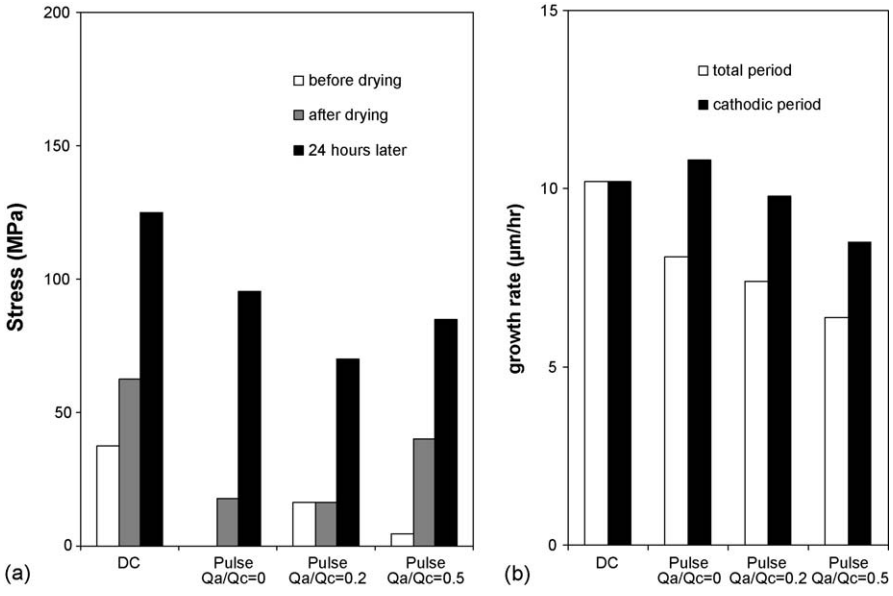

Fig. 6. Residual stress in Ni–W deposits (a) and growth rate (b) of layer as electroplated at 0.01 A cm^{-2} with direct current and pulse plating at charge ratio of $Q_a/Q_c = 0$, 0.2 and 0.5 for electrolyte (pH 7.5) containing 0.1 mol dm^{-3} $NiSO_4$, 0.2 mol dm^{-3} Na_2WO_4 and 0.3 mol dm^{-3} complexing agent (0.1 mol dm^{-3} citrate, 0.1 mol dm^{-3} triethanolamine and 0.1 mol dm^{-3} glycine (glycine 33.3%)).

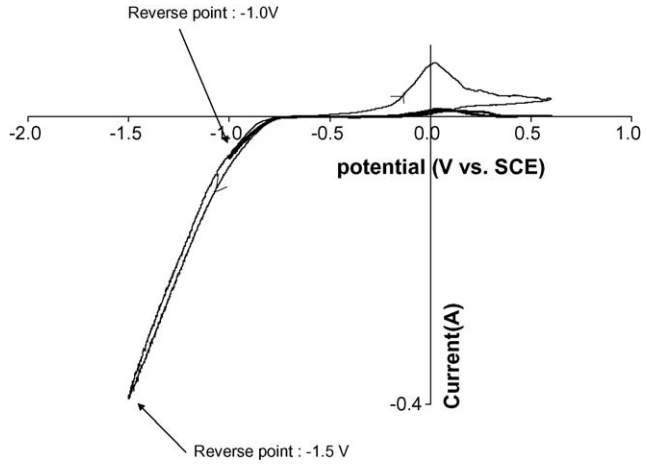

Fig. 7. Voltammetric curves with sweep reversal points −1.5 V vs. SCE (a) and −1.0 V vs. SCE (b) from electrolyte (pH 7.5) containing 0.1 mol dm^{-3} $NiSO_4$, 0.2 mol dm^{-3} Na_2WO_4 and 0.3 mol dm^{-3} complexing agent (0.1 mol dm^{-3} citrate, 0.1 mol dm^{-3} triethanolamine and 0.1 mol dm^{-3} glycine (glycine 33.3%)).

before drying. Evidently, the effect of pulse plating cannot be ascribed to an oxidation reaction during the anodic cycle.

Pulse plating may compensate partly for the decrease in the concentration of metal ion in the vicinity of the cathodic electrode, which might reduce the amount of hydrogen evolution. The growth rate estimated from the charge transfer in the cathodic period during pulse plating is higher than for plating in direct current mode, which indeed indicates an improvement of the current efficiency with pulse plating (Fig. 6b).

Even though pulse plating improved the level of tensile stress, further improvement is necessary for a successful application of Ni–W layers. Addition of 1,3,6 naphthalene trisulphonic acid (NTS) is often used for reducing the crystal size and results in smoothing of the surface. Tang et al. succeeded in reducing the residual stress level in Ni, Ni–Co and Ni–Fe deposits by combining this particular additive with the pulse plating technique [29]. Stress reducing additives as saccharine are more widely applied, but they bring about a high content of impurity in the deposit, which is not the case for NTS. Furthermore, chloride may help metal dissolution and rearrangement in the anodic cycle of pulse plating leading to removing hydrogen from the deposits.

Looking at pulse plating, the addition of 0.01 mol dm^{-3} NTS and replacement of nickel sulphate with nickel chloride ($NiSO_4$:$NiCl_2$ = 2:1) did not provide an improvement at 0.01 A cm^{-2} (Table 2). The level of tensile stress in the deposit before drying is higher with direct current plating. However, at 0.1 A cm^{-2} no cracks were observed in the deposit with pulse plating at a current ratio of $Q_a/Q_c = 0.5$ (Fig. 8). The voltammet-

Table 2
Residual stress and crack development in deposit with direct current or pulse plating for electrolyte (pH 7.5) containing 0.1 mol dm^{-3} $NiSO_4$, 0.2 mol dm^{-3} Na_2WO_4 and 0.3 mol dm^{-3} complexing agent (0.1 mol dm^{-3} citrate, 0.1 mol dm^{-3} triethanolamine and 0.1 mol dm^{-3} glycine) (standard), 0.1 mol dm^{-3} $NiSO_4$, 0.2 mol dm^{-3} Na_2WO_4 and 0.3 mol dm^{-3} complexing agent (0.1 mol dm^{-3} citrate, 0.1 mol dm^{-3} triethanolamine and 0.1 mol dm^{-3} glycine), 0.01 mol dm^{-3} 1,3,6 naphthalene trisulphonic acid (standard + additive), 0.067 mol dm^{-3} $NiSO_4$, 0.033 mol dm^{-3} $NiCl_2$, 0.2 mol dm^{-3} Na_2WO_4 and 0.3 mol dm^{-3} complexing agent (0.1 mol dm^{-3} citrate, 0.1 mol dm^{-3} triethanolamine and 0.1 mol dm^{-3} glycine) and 0.01 mol dm^{-3} 1,3,6 naphthalene trisulphonic acid (standard + additive + chloride)

Electrolyte	DC/PC	Stress at 0.01 A cm^{-2} (MPa)		Crack at 0.1 A cm^{-2}
		Initial	24 h later	
Standard	DC	38	125	Crack
	PC	0	70	Crack
Standard + additive	DC	41	130	Crack
	PC	11	96	Crack
Standard + additive + chloride	DC	58	153	Crack
	PC	5	89	No crack

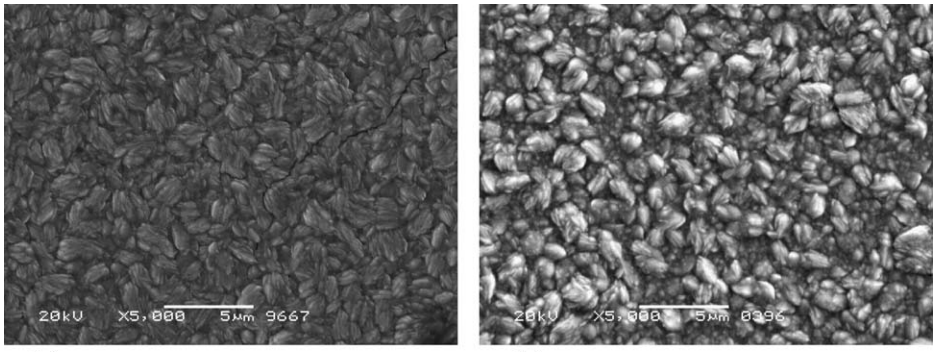

(a) (b)

Fig. 8. SEM images of Ni–W deposits with thickness of 5 μm as electroplated at 0.1 A cm^{-2} with pulse plating at charge ratio of $Q_a/Q_c = 0.5$ for electrolyte (pH 7.5) containing 0.1 mol dm^{-3} $NiSO_4$, 0.2 mol dm^{-3} Na_2WO_4 and 0.3 mol dm^{-3} complexing agent (0.1 mol dm^{-3} citrate, 0.1 mol dm^{-3} triethanolamine and 0.1 mol dm^{-3} glycine (glycine 33.3%)) (a) and for electrolyte (pH 7.5) containing 0.1 mol dm^{-3} $NiSO_4$, 0.135 mol dm^{-3} $NiCl_2$, 0.065 mol dm^{-3} Na_2WO_4 and 0.3 mol dm^{-3} complexing agent (0.1 mol dm^{-3} citrate, 0.1 mol dm^{-3} triethanolamine and 0.1 mol dm^{-3} glycine (glycine 33.3%)) and 1,3,6 naphthalene trisulphonic acid (b).

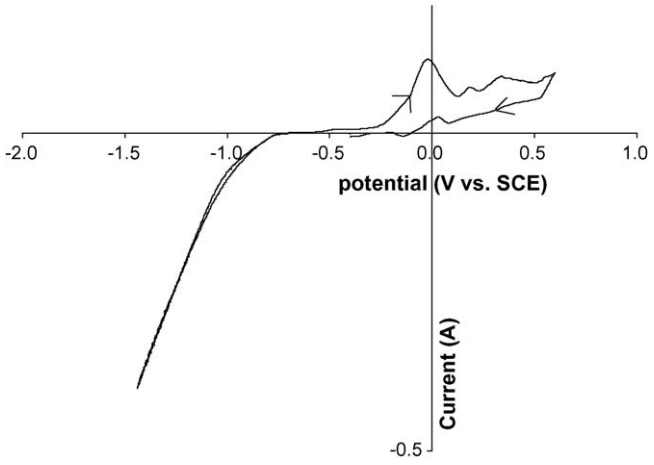

Fig. 9. Voltammetric curve from electrolyte (pH 7.5) containing 0.067 mol dm^{-3} $NiSO_4$, 0.033 mol dm^{-3} $NiCl_2$, 0.2 mol dm^{-3} Na_2WO_4 and 0.3 mol dm^{-3} complexing agent (0.1 mol dm^{-3} citrate, 0.1 mol dm^{-3} triethanolamine and 0.1 mol dm^{-3} glycine (glycine 33.3%)) and 0.01 mol dm^{-3} 1,3,6 naphthalene trisulphonic acid.

ric curve for the electrolyte shows a clear oxidation peak above 0.1 V versus SCE (Fig. 9). Thus, it is suggested that metal dissolution may take place in the anodic cycle during pulse plating, thereby reducing the crack occurrence.

4. Conclusion

The type of complexing agent used has a strong influence on the residual stress level in Ni–W deposits, irrespective of current efficiency. The combination of the three complexing agents citrate, glycine and TEA reduces residual stress in Ni–W deposits. In all cases, an increase in tensile stress with time was observed. The increase in the stress after storage for 24 h is larger for higher current density.

Pulse plating could improve the stress level for the electrolyte containing equal amounts of citrate, glycine and TEA as complexing agents. Pulse plating did not prevent the increase in tensile stress with time, because merely hydrogen is removed from the deposit without metal dissolution in the anodic period.

Addition of 1,3,6 naphthalene trisulphonic acid and partial replacement of nickel sulphate with nickel chloride when combined with pulse plating technique reduced the crack occurrence significantly.

References

[1] A. Brenner, Electrodeposition of Alloys, vol. 2, Academic Press, New York, 1963, p. 347.
[2] O. Younes, E. Gileadi, J. Electrochem. Soc. 149 (2) (2002) C100.
[3] O. Younes, E. Gileadi, Electrochem. Solid-State Lett. 3 (12) (2000) 543.
[4] O. Younes, L. Zhu, Y. Rosenberg, Y. Shacham-Diamand, E. Gileadi, Langmuir 17 (2001) 8270.
[5] Y. Wu, D.-Y. Chang, S.-C. Kwon, D. Kim, Plat. Surf. Finish. (2) (2003) 46.
[6] M. Bratoeva, N. Atanasov, Russ. J. Electrochem. 36 (1) (2000) 60.
[7] H. Cesiulis, M. Donten, M.L. Donten, Z. Stojek, Mater. Sci. (4) (2001) 230.
[8] T. Yamasaki, P. Schloßmacher, Y. Ogino, Nanostruct. Mater. 10 (3) (1998) 375.
[9] T. Yamasaki, Mater. Phys. Mech. 1 (2000) 127.
[10] P. Schloßmacher, T. Yamasaki, Mikrochim. Acta 132 (2000) 309.
[11] K. Itoh, F. Wang, T. Watanabe, J. Jpn. Inst. Metals 65 (11) (2001) 1023.
[12] L. Huang, J.X. Dong, F.Z. yang, S.K. Xu, S.M. Zhou, Trans. IMF 77 (5) (1999) 185.
[13] N. Eliaz, T.M. Sridhar, E. Gileadi, Electrochim. Acta 50 (2005) 2893.
[14] I. Mizushima, P.T. Tang, H.N. Hansen, M.A.J. Somers, Electrochim. Acta 51 (2005) 888.
[15] C.H. Huang, W.Y. She, H.M. Wu, Plat. Surf. Finish. 86 (12) (1999) 79.
[16] C.H. Huang, J. Mater. Sci. 34 (1999) 1373.
[17] C.H. Huang, Plat. Surf. Finish. 4 (1997) 62.
[18] W. Kim, R. Weil, Surf. Coat. Technol. 28 (1989) 289.
[19] J.C. Puippe, N. Ibl, J. Appl. Electrochem. 10 (1980) 775.
[20] A. Marlot, P. Kern, D. Landolt, Electrochim. Acta 48 (2002) 29.
[21] S. Lee, Y. Lee, M. Chang, J. Lin, Corros. Prev. Control 6 (1999) 71.
[22] G.G. Stoney, Proc. R. Soc. Lond. A82 (1999) 172.
[23] S. Armyyanov, G.S. Sotirova-Chakarova, Metal Finish. 91 (4) (1993) 59.
[24] Y. Tsuru, M. Kawamoto, J. Jpn. Inst. Metals 55 (1) (2004).
[25] H. Gerischer, H.E. Stambach, Z. Electrochem. 57 (1963) 604.
[26] M. Monev, M.E. Baumärtener, C.J. Raub, J. Electrochem. Soc. 138 (1991) L16.
[27] C.J. Raub, Plat. Surf. Finish. (9) (1993).
[28] Y. Fukai, The Metal Hydrogen System, Basic Bulk Properties, Springer, 1993.
[29] P.T. Tang, H. Dylmer, P. Møller, An electroplating method of forming platings of nickel, cobalt, nickel alloys and cobalt alloys with reduced stress, DK 172937, EP 0835335 and US 6,036,833, 1997.

Chapter 6

Microstructure Characterization of Ni-W Electrodeposits; Identification of An Anomalous Phase

Summary

In the present work Ni-W layers electrodeposited from electrolytes based on $NiSO_4$, Na_2WO_4, citrate, glycine and triethanolamine are characterized with glow discharge optical emission spectroscopy (GD-OES), X-ray diffraction analysis (XRD) and X-ray photoelectron spectroscopy. XRD showed the occurrence of an anomalous phase in the deposits, associated with the presence of an appreciable amount of carbon as identified with GD-OES. The anomalous phase is metastable at room temperature and vanishes upon annealing at 550°C in air.

1. Introduction

Nickel is a widely applied metal for electroforming due to its relative ease of electrodeposition and the high quality surface finish that can routinely be achieved. For the electroforming of mould inserts for micro-injection moulding of polymers, nanocrystalline nickel would be the preferred material. However, the thermal cycling between room temperature and injection molding temperatures up to 350 °C, leads to rapid deterioration of the nanocrystalline (nc) structure due to recrystallization and associated grain growth. Consequently, the initially nc-Ni mould looses its geometry and strength. Among the metals and alloys which can be electrodeposited, Ni-W is a favorable candidate, because it has high strength, corrosion resistance and a thermal stability superior to nc-Ni. Several authors have investigated electrodeposition of Ni-W alloys [1-13]. A major problem arises due to the formation of precipitates (probably $NiWO_4$) in the electrolyte[13]. This can be overcome by adding a suitable complexing agent, as for example citrate. The influence of such a complexing agent on the current efficiency, the composition of the deposit and mechanical properties, etc., is critical, and electrodeposition from electrolytes containing citrate as the major complexing agent is usually associated with low current efficiencies. In our previous research the influence of the additional complexing agents as glycine and triethanolamine was investigated[14]. Characterization of Ni-W electrodeposits from these baths resulted in the occurrence of an unidentified peak in X-ray diffractograms at a Bragg angle of ≈41°2θ (for Cu Kα radiation). Similar peaks were also reported to occur by other authors for XRD patterns of Ni-W layer. However, regardless of the importance of the microstructure of deposited layer for the properties and performance of electrodeposits, so far the anomalous Bragg

peaks have remained unidentified [5, 11]. The present work aims at identification of this anomalous peak and associated anomalous phase in Ni-W electrodeposits.

2. Experimental procedure

A 25L plastic container was used as electrochemical cell. The electrolyte for Ni electroplating consisted of 0.1 mol dm^{-3} $NiSO_4 \cdot 6H_2O$, a total of 0.3 mol dm^{-3} complexing agents (citrate, glycine and triethanolamine) and 0.44 mol dm^{-3} H_3BO_3. The electrolytes for Ni-W electroplating consisted of 0.1 mol dm^{-3} $NiSO_4 \cdot 6H_2O$, 0.2 mol dm^{-3} $Na_2WO_4 \cdot 2H_2O$, a total of 0.3 mol dm^{-3} complexing agents (citrate, glycine and triethanolamine) and 0.44 mol dm^{-3} H_3BO_3. The electrolyte bath was kept at 60°C and agitated with air bubbling during deposition. As a substrate a copper plate was used, which was cathodically degreased in an alkaline solution and pickled in a commercial acidic solution prior to immersion in the electrolyte.
The contents of Ni and W, in the electroplated layer, were determined semi-quantitatively with energy dispersive X-Ray spectrometry (Oxford Scientific). Phase constitution of the electrodeposits was assessed with X-ray diffraction (M21X TXJ-FO88, Mac Science Co. Ltd.) employing CuK_α radiation. Compositional depth profiling of the layers was obtained with glow discharge optical emission spectroscopy (GD-OES, JY-5000RF, Horiba Ltd.). The effect of thermal annealing of the deposits was tested by heating the specimens conducted for 1 hour at 100°C, 250°C, 400°C and 550°C in air.

3. Results and interpretation

3.1 X-ray diffraction analysis

The semi-quantitative W contents of the Ni-W alloy deposits electroplated at 0.01 A cm^{-2} and 0.05 A cm^{-2} are 7 at. % W and 11 at. % W, respectively. X-ray diffractograms of Ni and Ni-W deposits are shown in Fig.1.
According to the binary Ni-W phase diagram W contents ranging from 0 to 17 W at. % W can be dissolved in solid solution in the f.c.c. Ni lattice. Accordingly, the Bragg peaks for Ni and Ni-W at about 2θ=44°, 51°, 75°, 91° and 97° can be assigned to the diffraction of the {111}, {200}, {220}, {311} and {222} lattice planes of f.c.c., respectively. The dissolution of tungsten atoms in the nickel lattice causes an expansion of the f.c.c. lattice and, accordingly, a shift of the f.c.c. Bragg peaks towards lower

scattering angles. Based on the lattice parameter of 3.524 Å [15] of pure nickel and the difference in atomic radii of Ni and W (Ni=1.246 Å, W=1.371 Å) [15], the average distance between atoms and 111 lattice parameter of Ni-W containing 10 at. % W are 1.259 Å and 3.565 Å, respectively. The peak position of the 111 Bragg peak of the Ni-W containing 10 at. % W is estimated at 2θ=44°. The occurrence of a Bragg peak at 2θ=41.4° (Fig. 1) cannot be attributed to the f.c.c. lattice and corresponds to another phase. In addition to the anomalous peak at 2θ=41.4°, augmented diffracted intensity is observed on the high (and low) angle side of the (111) reflection as well as on both high and low angle sides of the (311) reflection. Among the possible intermetallic phases, Ni_4W, NiW or NiW_2, these peaks may correspond to 224, 510, 448 and 10-2-0 Bragg peaks of NiW_2, in the Ni-W binary system [16].

3.2. Thermal stability of anomalous phase

X-ray diffractograms recorded after 1 h annealing at various temperatures are presented in Fig. 2. The annealed samples were originally taken from same batch. The intensity of the anomalous peak at about 2θ=41° decreases with increasing annealing temperature. Simultaneously, the intensity of the Ni-W (111) line profile increases. These changes are ascribed to grain growth of the nano-sized Ni-W crystallites in the layer as well as to the gradual disappearance of the anomalous phase. Also both peaks in Fig. 2 appear to shift slightly to higher Bragg angles. At the highest annealing temperature applied, 550 °C, nickel tungsten oxide ($NiWO_4$) have developed (Fig. 3). Evidently, the anomalous phase has disappeared

3.3. Glow discharge optical emission spectroscopy

Depth profiles of Ni, W, C, O and Cu corresponding to the samples for which X-ray diffractograms were given in Fig.1, are collected in Fig. 4. GD-OES analysis is not available for precise quantitative analysis; however an intensity drop for a specific element at the interface between the Ni-based deposit and the copper substrate allows positive identification of the presence of this element in the deposit. For the oxygen profiles no such intensity change is observed at the interface. On the other hand, the layers deposited from the electrolytes containing citrate, glycine and triethanolamine as complexing agents contain an appreciable amount of carbon. While the difference of intensity of carbon in Ni and Ni-W layers electrodeposited from this electrolyte at 0.01 A cm^{-2} are similar, the carbon content in the Ni-W layer deposited at 0.05 A cm^{-2} appears high.

4. Discussion

The only match of the anomalous peaks with known phases in the Ni-W system is the intermetallic phase NiW_2. Poulsen et al. [16] mentioned that the NiW_2 phase is extremely sensitive for the presence of oxygen. This would be consistent with the disappearance of the anomalous phase upon annealing and its complete disappearance, associated with the appearance of oxides, after annealing at 550 °C. However, it is difficult to identify this intermetallic phase on the basis of so few Bragg peaks. Also, hitherto none of the intermetallic phases in the Ni-W system have previously been observed to be deposited by electroplating. Thermodynamically NiW_2 is not the first intermetallic Ni-W phase to be expected, since it has the highest W content of the known Ni-W intermetallics. Rather, Ni_4W would be expected, but no correlation could be found between Ni_4W and the anomalous Bragg peaks in the present work. Yamasaki et al. [17] suggested the presence of nano crystalline Ni_4W in Ni-W electrodeposits taking interatomic distances determined by EXAFS as evidence.

The presence of carbon in both the Ni and the Ni-W layers as observed with GD-OES could provide another explanation for the anomalous peaks. In fact, a relatively high intensity difference of GD-OES carbon profile of Ni-W layer deposited at 0.05 A cm $^{-2}$ in Fig. 4d corresponds favourably with the relatively large intensity of the Bragg reflection at about $2\theta=41°$ in Fig.1, which strongly suggests a correlation between the appearance of the anomalous phase and the presence of carbon.

The Gibbs energies of formation of the most stable W and Ni carbides, i.e.WC and Ni_3C respectively, are [18]:

$$\Delta G(T)_{WC} = -38074 + 1.6736T$$
$$\Delta G(T)_{Ni_3C} = 33932 - 7.1128T$$

Clearly, WC is the more stable of these carbides.

Nevertheless, the anomalous Bragg peaks in Figs. 1 and 2 cannot be assigned to any known WC, W_2C, W_3C or WC_X carbides. Consistency could be obtained for a M_6C type carbide Ni_2W_4C (511) or for an M_3C type carbide Ni_3C (006) (see Tables 1 and 2). Possibly the composition of the M_3C carbide is not stoichiometric but of type $(Ni,W)_3C$. The shoulder at about $2\theta=47°$ may correspond to Ni_2W_4C or $(Ni,W)_6C$ (440) or Ni_3C (113). The occurrence of Ni_3C is generally not observed under equilibrium conditions; however, its formation under non-equilibrium conditions has been reported [19-20]. Tanaka [19] observed the formation of metastable Ni_3C by mechanical alloying of nickel and graphite powder. Laidani et al. [20] reported that Ni_3C had developed in a sputter

deposited Ni-C film. In a similar sense electrodeposition is a non-equilibrium process and the occurrence of Ni_3C or $(Ni,W)_3C$ can therefore not be excluded. Nevertheless, no indications were observed for the development of Ni_3C (without W) on electrodeposition of the Ni layers. The anomalous peak at about 2θ=90° would correspond better to Ni_2W_4C (10 22) than to Ni_3C (00 12), but taking the anticipated expanding effect of W on the lattice of M_3C into consideration, $(Ni,W)_3C$ carbide should be considered a possibility.

As a third alternative, the anomalous peak in the XRD pattern could be attributed to the interstitial dissolution of a large amount of C in the f.c.c. Ni-W lattice, leading to an expanded f.c.c. lattice, similar to that occurring for nitrogen or carbon dissolved in austenitic stainless steel [21, 22] and in Ni alloys [23]. Such an interstitial solution derives from anticipated short range ordering of W and C atoms and an associated enhancement of the lattice solubility of C in Ni-W. If this hypothesis applies, the lattice constant of the expanded Ni has increased from 3.568Å to 3.778Å, corresponding to a linear expansion of 5.9 %. For comparison, for stainless steel linear expansions of the lattice parameter up to 11 % have been observed by the incorporation of N [24]. Then, the diffracted intensity at about 2θ=47° and 2θ=91° in the diffractograms of the Ni-W alloy deposit shown in Fig.1 may correspond to the positions of (200) and (222) of the expanded f.c.c. Ni-W-C phase. The occurrence of a constant C content in the deposits could than be explained from a two phase nanocrystalline structure containing f.c.c. Ni(-W) with a relatively low W and C content and expanded Ni-W-C.

Probably, the development of such a phase distribution is tentatively explained from co-deposition of tungsten with nickel. Although electrodeposition of tungsten can be achieved by a presence of nickel ions due to a lowering of the Gibbs energy after mixing of the elements, nickel ions and tungstate do not directly form a complex. The complex formation between nickel and tungstate can be achieved by coordination of the HWO_4^{2-} ion to a site in the complexing agent molecule next to a site occupied by a nickel ion [25]. It is suggested that carbon containing complexing agents with coordination of both nickel and tungstate ions are involved in the co-deposition and electrocrystallization of Ni and W, incorporating C and thus leading to the formation of the anomalous phase. Concurrently, nickel is deposited directly, possibly with a low W content.

The third alternative is considered to be the most likely explanation for the observed anomalous phase, since the appearance of a “far from equilibrium” phase becomes more likely with faster electrodeposition (high current density). The probability for the development of carbides and intermetallic Ni-W phases is considered to become less

likely with faster deposition.

5. Conclusion

In this study the development and stability of a hitherto unidentified phase during electrodeposition of Ni-W layer from an electrolyte containing citrate, glycine and triethanolamine was investigated. Compositional analysis with GD-OES indicates that the anomalous phase is promoted by the presence of both W and C and does not occur in W-free Ni electrodeposits. Three alternative explanations were discussed: the development of Ni_4W, the development of (Ni,W) carbides of M_6C and M_3C types, and the co-deposition of nanocrystalline Ni(-W) and Ni-W-C phases. The latter explanation is considered most likely. Here, Ni-(W) is possibly relatively lean in W and Ni-W-C contains a relatively high interstitial amount of C in the f.c.c. Ni-W lattice, giving rise to an expansion of the f.c.c. lattice.

6. References

1. A. Brenner, "Electrodeposition of Alloys", Vol. 2, p. 347, Academic Press, New York (1963)
2. O. Younes & E. Gileadi, J. Electrochem. Soc., 149 (2) C100-C111 (2002)
3. O. Younes & E. Gileadi, Electrochemical Solid-State Letters, 3 (12) 543-545 (2000)
4. O. Younes, L Zhu, Y Rosenberg, Y. Shacham-Diamand & E. Gileadi, Langmuir, **17**, 8270-8275 (2001)
5. Y. Wu, Do-Y. Chang, Sik-C. Kwon & D. Kim, Plat. Surf. Finishing, (2) 46-49 (2003)
6. M. Bratoeva & N. Atanasov, Russ. J. Electrochem., 36 (1) 60-63 (2000)
7. H. Cesiulis, M. Donten, M.L. Donten & Z. Stojek, ISSN Material Science, (4) 230-234 (2001)
8. T. Yamasaki, P. Schloßmacher & Y. Ogino, Nanostructured Materials, Vol. 10, No. 3 (1998) 375-388
9. T. Yamasaki, Mater. Phys. Mech., Vol. 1 (2000) 127-132
10. P. Schloßmacher & T. Yamasaki, Mikrochim. Acta, 132 (2000) 309-313
11. K. Itoh, Feng Wang & T. Watanabe, J. Japan Inst. Metals, Vol. 65, No 11, 1023-1028 (2001)

12. L. Huang, J. X. Dong, F. Z. yang, S. K. Xu & S. M. Zhou, Trans. IMF, 77 (5) 185-187 (1999)
13. C.A. Schuh, T.G. Nieh, H. Iwasaki, Acta Mater. 51 (2003) 431-443
14. I. Mizushima, P. T. Tang, H. N. Hansen and M. A. J. Somers, Electrochimica Acta, 51, 888-896 (2005)
15. B. D. Cullity; Elements of X-Ray Diffraction, Addison-Wesley Publishing Company, INC (1967)
16. K. E. Poulsen, S. Rubæk and E. W. Langer, Scripta Metallurgica, vol. 8 (1974) 1297-1300
17. T. Nasu, M. sakurai, T. Kamiyama, T. Usuki, O. Uemura and T. Yamasaki, Journal of Non-Crystalline Solids 312-314 (2002) 319-322
18. "Ellingham diagram web tool"; http://www.engr. sjsu.edu/ellingham/
19. T. Tanaka, K. N. Ishihara and P. H. Shingu, Metall. Trans. A, Vol. 23A, 9 (1992) 2431-2435
20. N. Laidani, L. Calliari, G. Speranza, V. Micheli, E. Galvanetto, Surf. Coat. Techn. 100-101 (1998) 116-124
21. T. Christiansen and M.A.J. Somers, Surf. Eng., vol. 21, (2005) 445-455
22. T. Christiansen and M.A.J. Somers, Scripta Mater., vol. 50 (2004) 35-37
23. T. Makishi, K. Nakata, Metall. Mater. Trans. A vol. 35A (2004) 227-238.
24. T. Christiansen and M.A.J. Somers, Metall. Mater. Trans. A, vol. 37A. (2006) 675-682
25. H. Hayashi & M. Kasai, Hyoumen Gijutsu, Vol. 55, No. 1, 85-86 (2004)

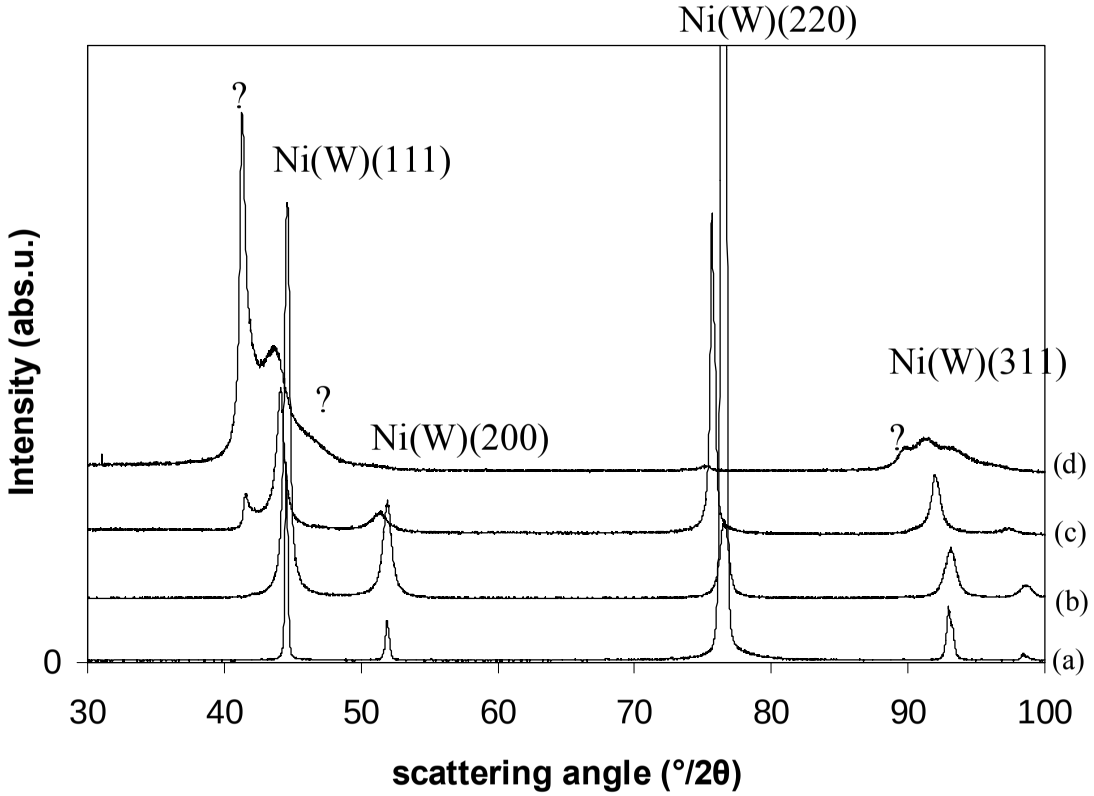

Fig. 1 X-ray diffractograms of Ni deposits electroplated at 0.01 A cm^2 from electrolyte containing no complexing agents (a) and from an electrolyte containing citrate, glycine and triethanolamine (b) and of Ni-W deposits electroplated at 0.01 A cm^2 (c) and 0.05 A cm^{-2} (d) from an electrolyte containing citrate, glycine and triethanolamine.

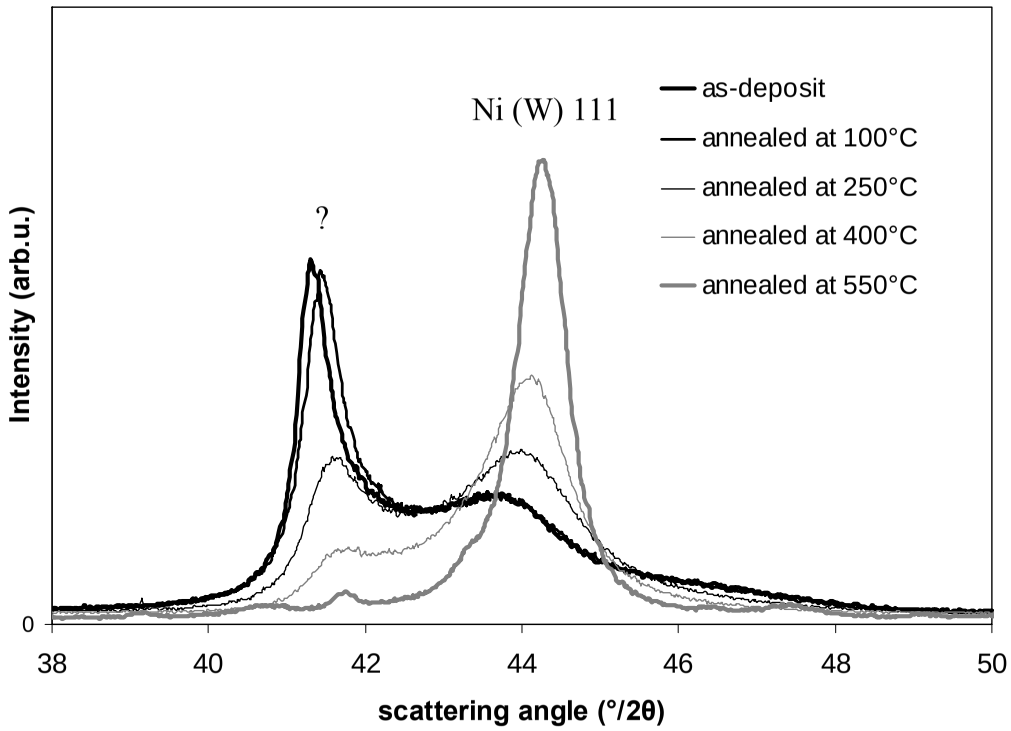

Fig. 2 X-ray diffractogram of Ni-W deposits electroplated at 0.05 A cm^{-2} from electrolyte containing citrate, glycine and triethanolamine and annealed for 1 h at the annealing temperatures indicated.

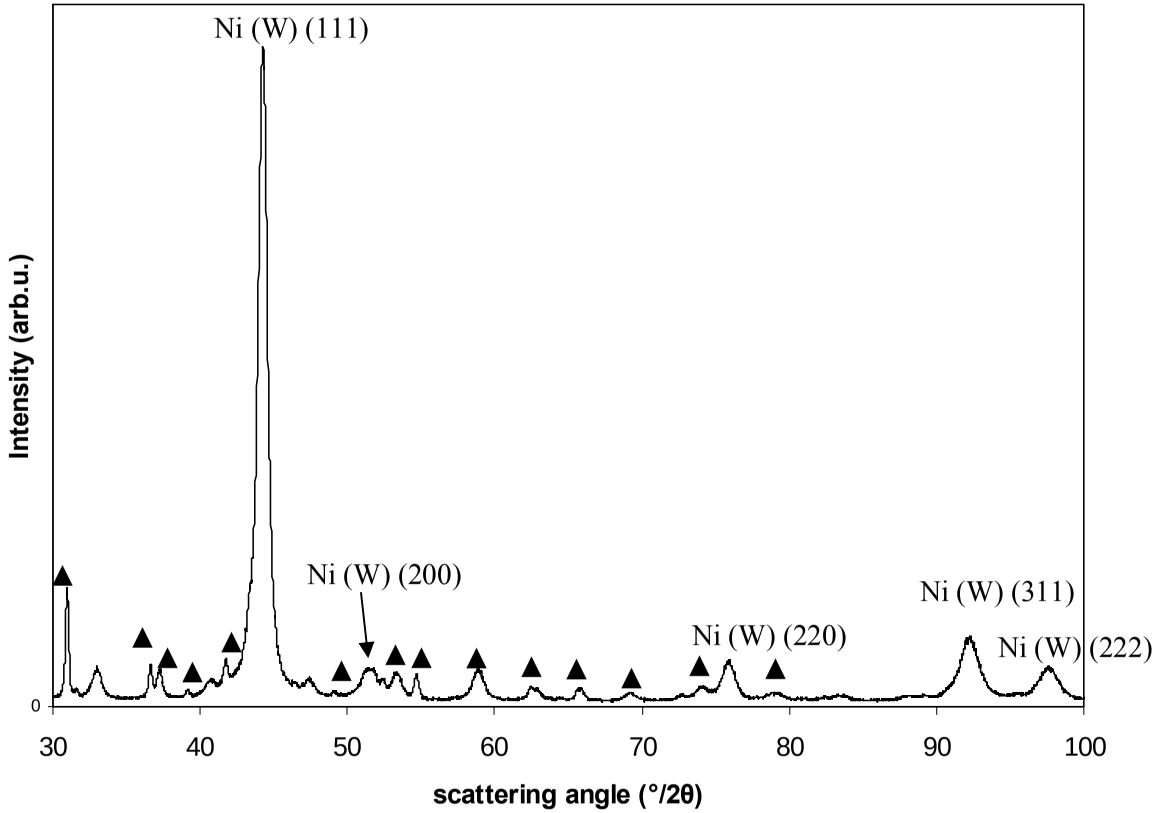

Fig. 3 X-ray diffractogram of Ni-W deposit electroplated at 0.05 A cm^{-2} from electrolyte containing citrate, glycine and triethanolamine and annealed for 1 h at 550°C, ▲=$NiWO_4$

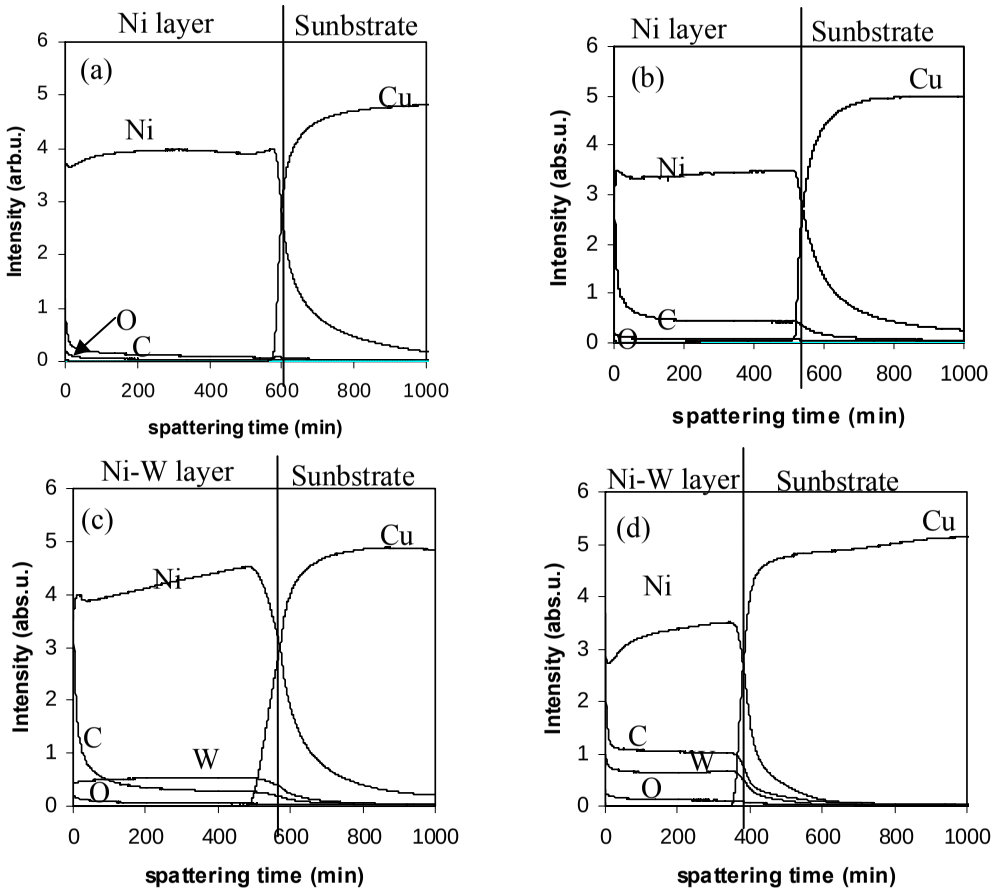

Fig. 4 GD-OES profiles of Ni deposits electrodeposited at 0.01 A cm^{-2} from an complex-free electroyte (a) and an electrolyte containing citrate, glycine and triethanolamine (b), of Ni-W alloy layers deposited at 0.01 A cm^{-2} (c) and 0.05 A cm^{-2} (d) from an electrolyte containing citrate, glycine and triethanolamine

Table 1 Miller indices, lattice spacings and 2θ Bragg angles (for CuKα radiation) for Ni_3C

miller index (hkl)	d	2θ
110	2.2765	39.58
006	2.1533	41.94
113	2.0126	45.03
116	1.5644	59.02
300	1.3143	71.80
119	1.2143	78.79
220	1.1383	85.22
0012	1.0766	91.41
226	1.0063	99.94

Table 2 Miller indices, lattice spacings and 2θ Bragg angles (for CuKα radiation) for Ni_2W_4C

miller index (hkl)	d	2θ
331	2.583	34.72
422	2.298	39.19
511	2.167	41.66
440	1.990	45.57
622	1.696	54.05
731	1.465	63.48
733	1.375	68.18
822	1.327	71.00
751	1.299	72.78
1022	1.084	90.61

Chapter 7

Effect of Age of Glycine-containing Electrolyte on Microstructure of Ni-W Electrodeposit

Summary

In the present work the influence of the age of an electrolyte, containing glycine as complexing agent, on the microstructure of a Ni-W electrodeposit is investigated. The microstructure of the electrodeposits was characterized with scanning electron microscopy (SEM), X-ray diffraction (XRD) analysis and glow discharge optical emission spectroscopy (GD-OES).

It was observed that an anomalous Bragg peak at $2\theta \approx 41.5°$ occurs for layers deposited from aged electrolyte and not for layers deposited from the fresh electrolyte; the intensity of the Bragg peak increases with the age of the electrolyte. Simultaneously, the presence of carbon is observed with GD-OES in layers deposited from the aged electrolyte. The carbon dissolution in the Ni-W alloy deposit is associated with the formation of a new phase in the electrodeposit, giving rise to the anomalous Bragg peak.

1. Introduction

Ni-W is an excellent material due to high corrosion resistance and mechanical strength. Electroplating of the material has potential for applications as micro-injection molding inserts tool and surface finishing. Several authors have investigated electrodeposition of Ni-W alloys [1-13].

In order to overcome precipitate formation in the electrolyte (probably $NiWO_4$) and enable the co-deposition of nickel and tungsten, it is necessary to add a suitable complexing agent to an electrolyte for Ni-W deposition. In our previous work we optimized the complexing agents in the electrolyte for obtaining high current efficiency (>80%) and low residual stress in the deposit [14,15].

The influence of complex formation in the electrolyte on the current efficiency, the composition of the deposit and the mechanical properties is critical. Younes et al. investigated the influence of the pH value of an ammonical citrate electrolyte for Ni-W electroplating on complex formation of tungstate and the tungsten content in the deposit[2]. While the amount of $\left[Ni\left(NH_3\right)_x\right]^{2+}$ complex increased as a consequence of NH_3 formation by the reaction of $NH_4OH \rightarrow NH_3 + H_2O$ with increasing pH value of the electrolyte, the amount of the terminal complex between nickel, citrate and tangstate decreased. Cosequently, the tungsten content in the deposit was reduced owing to less nickel ion assistance for deposition of tungsten.

The conditions for complex formation in the electrolyte might be unstable because of the sensitivity to the pH value and the concentration of metal ions; nevertheless, hitherto

the stability of the electrolyte and its effect on the composition of the electrodeposit has received only limited attention.
In the present work the effect of aging of a glycine containing electrolyte on the phase constitution and the composition of Ni-W electrodeposits is investigated.

2. Experimental procedure

A 1 dm^3 glass beaker was used as the electrochemical cell. The electrolyte for Ni-W electroplating consisted of 0.1 mol dm^{-3} $NiSO_4 \cdot 6H_2O$, 0.2 mol dm^{-3} $Na_2WO_4 \cdot 2H_2O$, 0.3 mol dm^{-3} glycine and 0.44 mol dm^{-3} H_3BO_3. The pH value was adjusted with NaOH. Agitation was conducted with a magnetic stirrer at a rotating speed of 500 rpm. A copper plate substrate was cathodically degreased with an alkaline solution and subsequently pickled in a commercial HCl solution prior to electrodeposition. The electrodeposition time was adjusted to obtain a 12μm thick layer approximately.
The metallic composition in the electroplated layer was determined semi-quantitatively with energy dispersive X-ray spectrometry (Oxford Scientific). Phase identification was conducted with X-ray diffraction (M21X TXJ-FO88, Mac Science Co. Ltd.) using CuK_α radiation. Composition-depth profiles of the layers were determined with glow discharge optical emission spectroscopy (JY-5000RF, Horiba Ltd.). Complex formation in the electrolyte was investigated with UV-spectrophotometry (UV1240 Shimadzu Ltd.).

3. Results and interpretation

3.1. Aging of bath by repeated deposition

The Ni-W layers contain approximately 10 at.%W, regardless of the age of the electrolyte. The appearance of the Ni-W deposit depends on the age of the electrolyte: whilst the surface of the layer deposited from a fresh electrolyte has a mirror-like surface finish, the surface gets darker with aging of the baths. This darkening of the surface is associated with an increase of the number of leaf-like particles on the surface of the Ni-W deposits with age of the electrolyte, which causes an effective surface roughening (Fig.1).

X-ray diffractograms of Ni-W layers deposited from electrolyte of various age are shown in Fig.2. The Bragg peak for Ni-W at about 44°2θ can be assigned to the diffraction of Cu K_α radiation at 111 lattices planes of the f.c.c Ni-W solid solution . [14] The enhanced intensity at 43.3°2θ is attributed to diffraction at the Cu substrate. For a fresh bath no peaks in addition to those expected for the f.c.c. solid solution were observed. After consumption of 1150 Coulombs by deposition a small peak occurs at 41.4°2θ. This Bragg peak indicates the development of another phase. The intensity of the anomalous peak increases slightly with the age of the electrolyte from which the layers were deposited. It is mentioned explicitly that the background intensity level in-between the Ni (111) and the anomalous peak also increases with aging of the electrolyte.

Energy dispersive X-Ray spectrometry did not reveal any significant difference in (semi-quantitative) composition for the various electroplated layers determined semi-quantitatively with. GD-OES composition-depth profiles of Ni, W, C, S, H, O and Cu for layers deposited from both a fresh electrolyte and an electrolyte aged through consumption of 1150 Coulombs are shown in Fig.3. The only noticeable difference between the composition-depth profiles for fresh and aged electrolytes is an enhanced carbon content in the layer deposited from the aged electrolyte. Where the carbon profile for the deposit from the fresh electrolyte gradually decreases with depth and smoothly fades at the interface between deposit and copper substrate, the carbon profile of the deposit from the aged electrolyte maintains a higher level throughout the deposit and shows a discontinuity at the interface with the copper substrate. The layer deposited from the fresh bath contains carbon mainly at the surface, whereas, the layer deposited from the aged electrolyte contains an enhanced carbon content. The presence of carbon in the layer is associated with the observation of the anomalous Bragg peak (Fig.2). Evidently, the formation of the anomalous phase is a consequence of carbon dissolution in the Ni-W deposit.

The only source of carbon in the electrolyte is glycine. Possibly, a change of the complex formation of glycine in the electrolyte with age causes the uptake of higher amounts of carbon. Upon consumption of 1150 coulombs the pH value of the electrolyte increased from 7.0 to 7.8, UV spectro-photometry showed that stronger adsorption occurs at wavelengths of about 600 nm and 1000 nm (Fig.4 a). Intensities of these absorptions are associated to the field strength of glycine coordinating to nickel ions.

The appearance of flakes at the surface and carbon dissolution in the deposit might be ascribed by the change of complex condition in the electrolyte.

3.2. Influence of pH on the microstructure of Ni-W electrodeposits

In order to investigate whether the changes in surface topography and microstructure are a consequence of the increase in the pH value of the electrolyte with age, influence of pH value of a fresh electrolyte was investigated. For the investigation the fresh electrolytes with various pH values adjusted with NaOH were used to distinguish between effects of age and of pH value.

The influence of a change in pH value of the electrolyte on the microstructure of Ni-W alloy deposits is shown in Fig. 6.

Clearly the density of flakes at the surface and the associated surface roughness increases with pH value of the fresh electrolyte (Fig. 5). This observation is consistent with the results in Fig.1.

X-ray diffraction indicates that the anomalous Bragg peak is hardly observed in the layers deposited from the fresh electrolytes regardless of pH value, not even at a high pH value of 8.5.

UV spectro-photometry of *fresh* electrolytes with a pH value ranging from 7.0 to 8.5 are given Fig. 4b. The intensities of absorption at wavelength of 600 and 1000nm of the fresh electrolyte with pH value of 8.5 are similar to the aged electrolyte at pH=7.8.

4. Discussion

The effect of aging of the electrolyte as a consequence of prior electrodeposition is addressed first.

Comparison of the results in Fig. 2 and Fig. 6 proves that the formation of the anomalous phase in the aged electrolyte cannot be attributed to an increase of the pH value. Comparing the UV spectra in Fig.4a and b, it is observed that the increased absorption for the aged electrolyte with a pH value of 7.8 is stronger than for the fresh electrolyte with (a comparable) pH value of 8.0. The increase in strength of ligand field to nickel ion is not caused only by the increase in pH but also by another change.

In a previous article [16] we attributed the anomalous phase to the co-deposition of Ni(W) and Ni-W-C phases. The latter has an expanded f.c.c. lattice as compared to the Ni(W) phase because of the interstitial dissolution of C in the f.c.c. lattice. Such a phase which has an expanded lattice does not exist in a tungsten-free nickel layer deposited from the electrolyte containing same complexing agents, although the nickel layer also contains

carbon as well. The anomalous phase is most likely a consequence of the co-deposition of carbon with both nickel and tungsten.

Younes mentioned [2] that concentration of the complex between tungstate and citrate in the electrolyte decreased with increasing pH value as a consequence of decrease in amount of hydrogen ion coordinating to both citrate and WO_4^{2-}. The concentration of complex between glycine and tungstate is supposed to decrease with increasing pH value as well. The decrease in concentration of the complex might be an opposite effect on the co-deposition and the formation of the anomalous phase.

There is another possibility that the origin of the carbon in the deposit for the aged electrolyte is not incorporation of glycine. The co-deposition of carbon may occur from species which come from decomposition of glycine with reduction reaction at cathode. Accumulation of the unexpected species may give rise to the increase in intensity of absorption in UV spectra for the aged electrolyte.

The mechanisms leading to the co-deposition of carbon will be the topic of future investigations.

5. Conclusion

In the present work an influence of age of electrolyte containing glycine as complexing agent on microstructure of Ni-W alloy electrodeposits was investigated.

Although the layer deposited from the fresh bath contains only a limited amount of carbon close of the surface, the presence of carbon in the layer deposited from the aged electrolyte is identified with glow discharge optical emission spectroscopy (GD-OES). An anomalous Bragg peak at $2\theta \approx 41.4°$ is not observed in the Ni-W layer deposited from the fresh electrolyte, however, the intensity of the peak increases with the age of the electrolyte. The formation of the anomalous phase is associated with carbon dissolution in the Ni-W alloy deposit. PH value of the electrolyte increase with the age, however, the increase of the pH value alone does not lead to the formation of the anomalous phase.

6. References

1. A. Brenner, “Electrodeposition of Alloys”, Vol. 2, p. 347, Academic Press, New York (1963)
2. O. Younes & E. Gileadi, J. Electrochem. Soc., **149** (2) C100-C111 (2002)

3. O. Younes & E. Gileadi, Electrochemical Solid-State Letters, **3** (12) 543-545 (2000)
4. O. Younes, L Zhu, Y Rosenberg, Y. Shacham-Diamand & E. Gileadi, Langmuir, **17**, 8270-8275 (2001)
5. Y. Wu, Do-Y. Chang, Sik-C. Kwon & D. Kim, Plating and Surface Finishing, (2) 46-49 (2003)
6. M. Bratoeva & N. Atanasov, Russian Journal of Electrochemistry, **36** (1) 60-63 (2000)
7. H. Cesiulis, M. Donten, M.L. Donten & Z. Stojek, ISSN Material Science, (4) 230-234 (2001)
8. T. Yamasaki, P. Schloßmacher & Y. Ogino, Nanostructured Materials, Vol. 10, No. 3 (1998) 375-388
9. T. Yamasaki, Mater. Phys. Mech., Vol. 1 (2000) 127-132
10. P. Schloßmacher & T. Yamasaki, Mikrochim. Acta, 132 (2000) 309-313
11. K. Itoh, Feng Wang & T. Watanabe, J. Japan Inst. Metals, Vol. 65, No 11, 1023-1028 (2001)
12. L. Huang, J. X. Dong, F. Z. yang, S. K. Xu & S. M. Zhou, Trans. IMF, 77 (5) 185-187 (1999)
13. C.A. Schuh, T.G. Nieh, H. Iwasaki, Acta Mater. 51 (2003) 431-443
14. I. Mizushima, P. T. Tang, H. N. Hansen and M. A. J. Somers, Electrochimica Acta, 51, 888-896 (2005)
15. I. Mizushima, P. T. Tang, H. N. Hansen and M. A. J. Somers, Electrochimica Acta, 51, 6128-6134 (2006)
16 I. Mizushima, P. T. Tang and M. A. J. Somers, Electrochimica Acta, in chapter 6 in this thesis

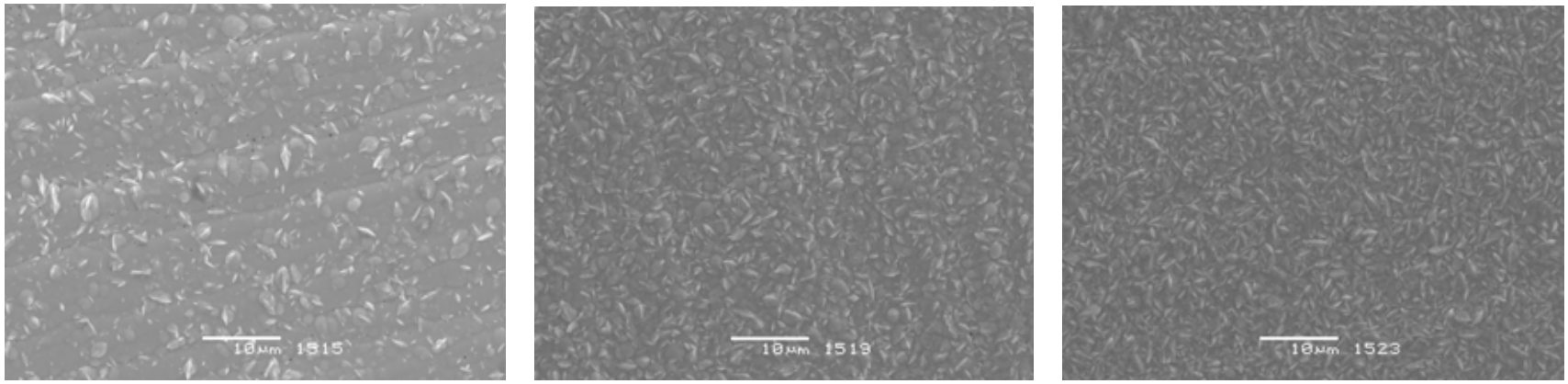

(a) (b) (c)

Fig. 1 Surface topographies of Ni-W layers deposited at 0.01 A cm^{-2} from fresh electrolyte and aged electrolyte (consumption of 330 Coulombs (a), 660 Coulombs (b) and 1150 coulombs (c)) containing glycine

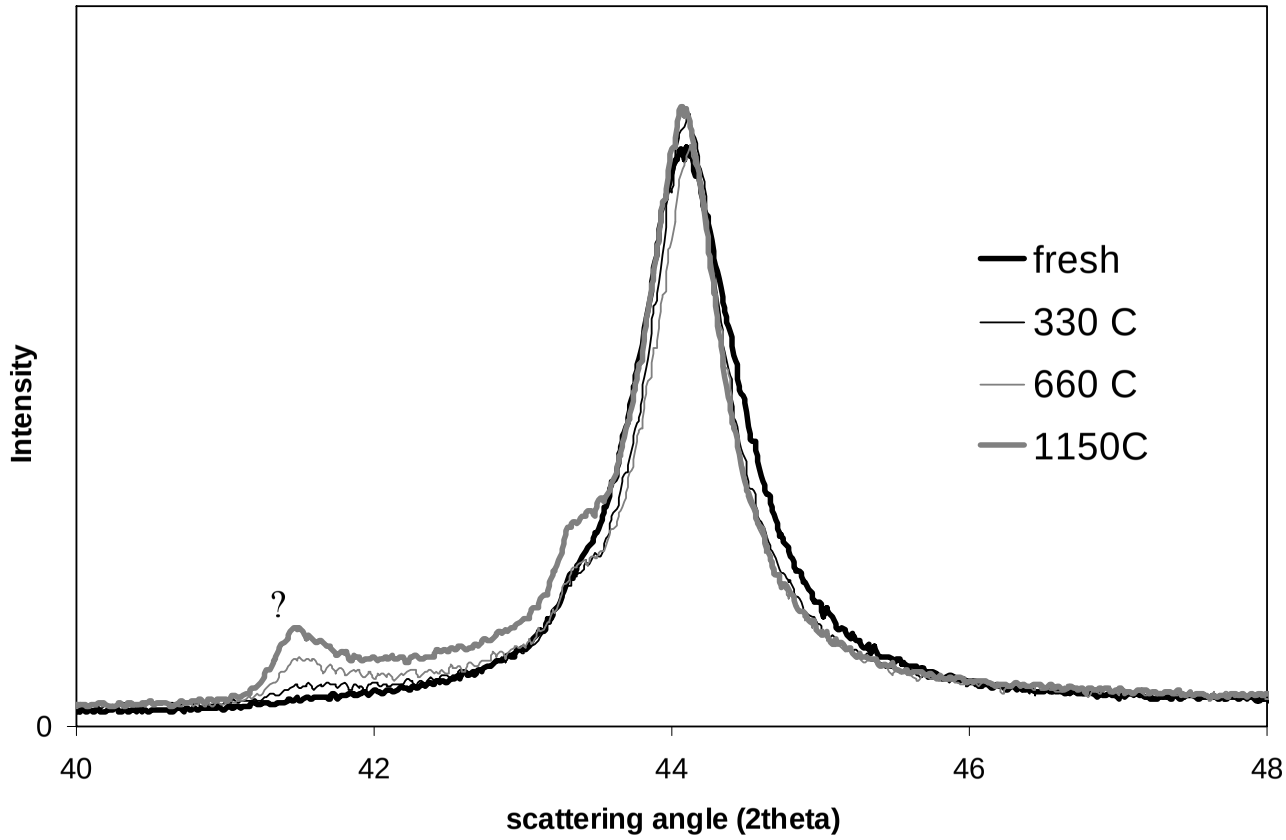

Fig. 2 X-ray diffractograms of Ni-W layers deposited at 0.01 A cm^{-2} from electrolyte aged by prior deposition corresponding to the indicated total charge transfer.

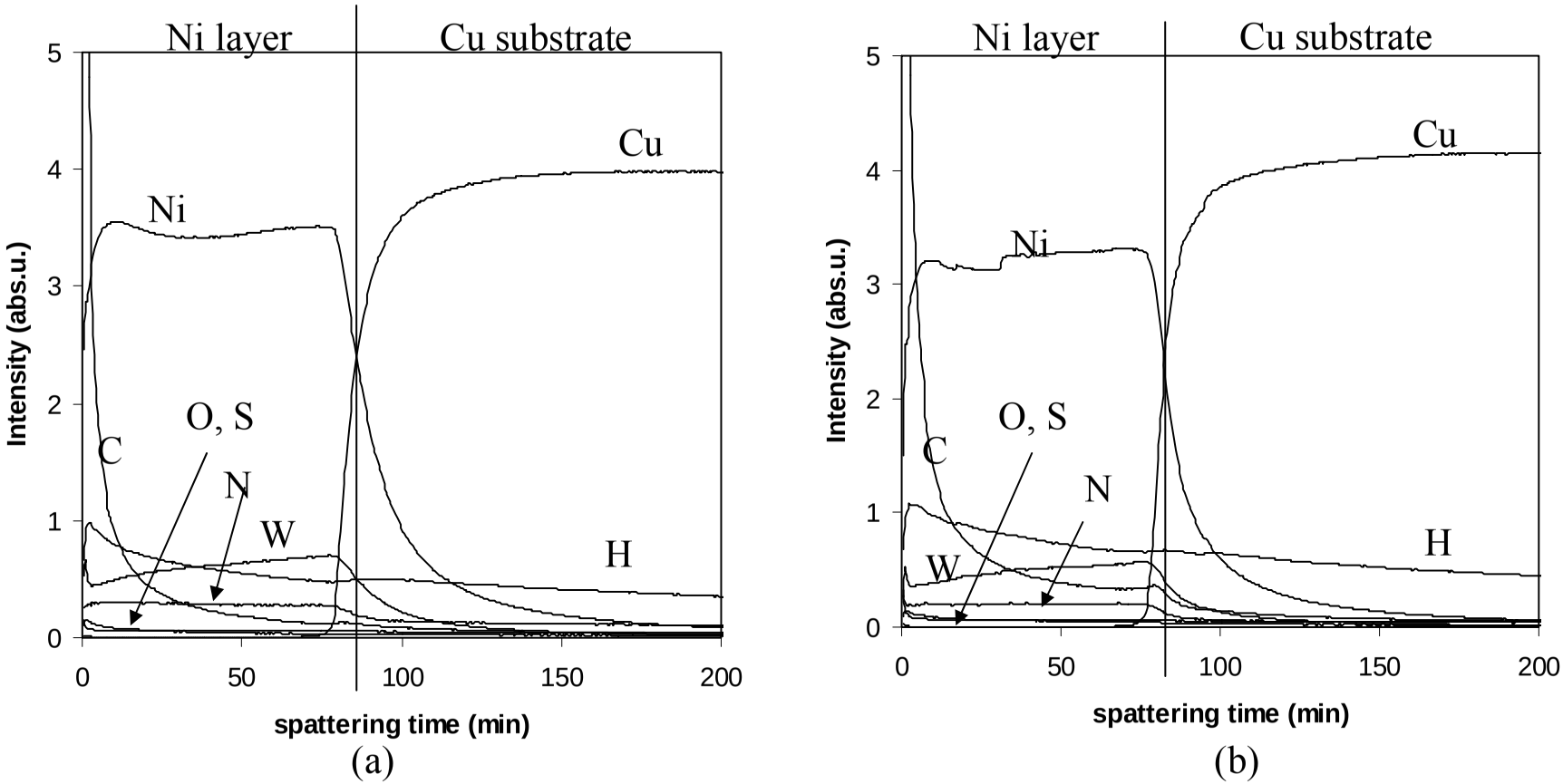

Fig. 3 GD-OES profiles of Ni-W layers deposited at 0.01 A cm^{-2} from fresh electrolyte (a) and aged electrolyte (consumption of 1150 C) (b).

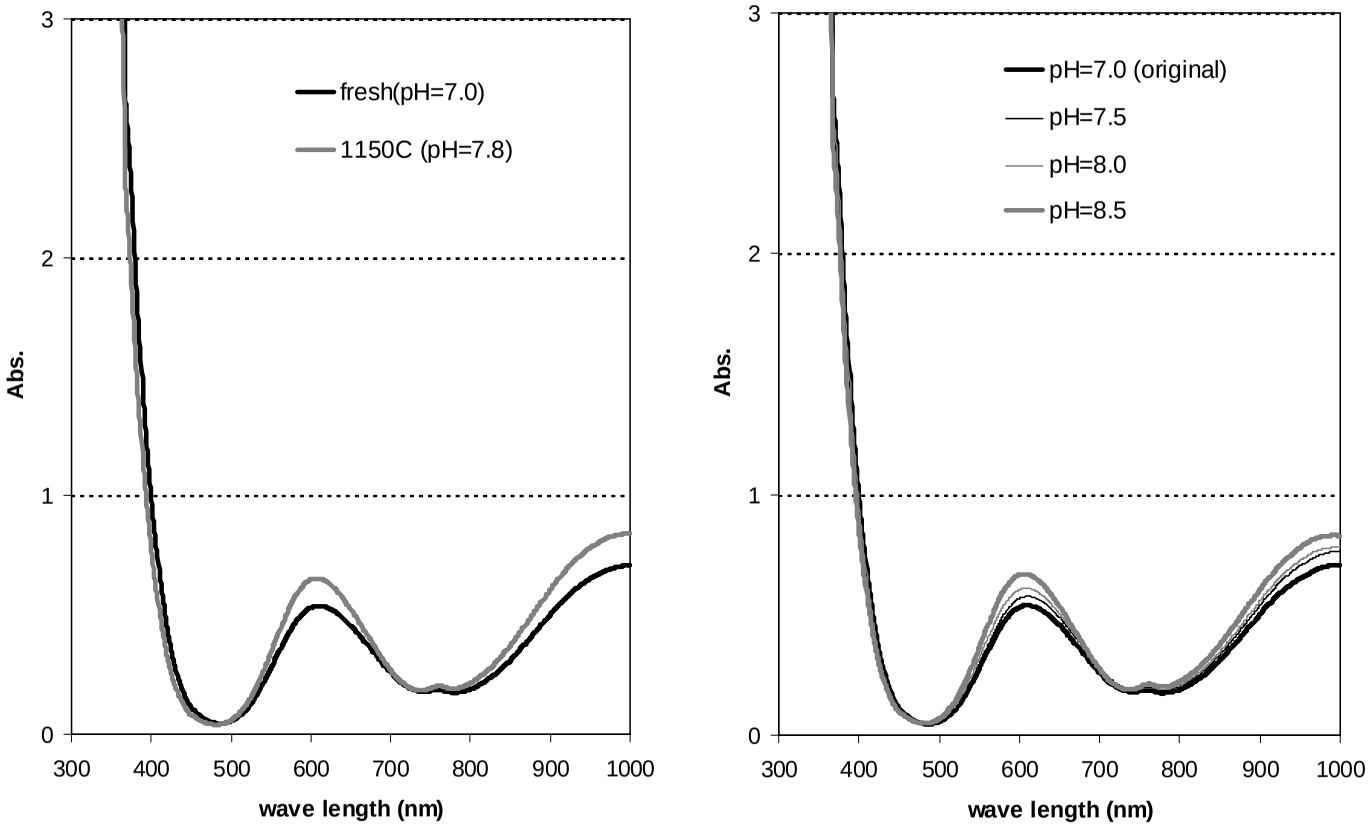

Fig. 4 UV spectra with age of electrolyte after consumption of 1150 Coulombs (a) and with various pH values of the electrolyte.

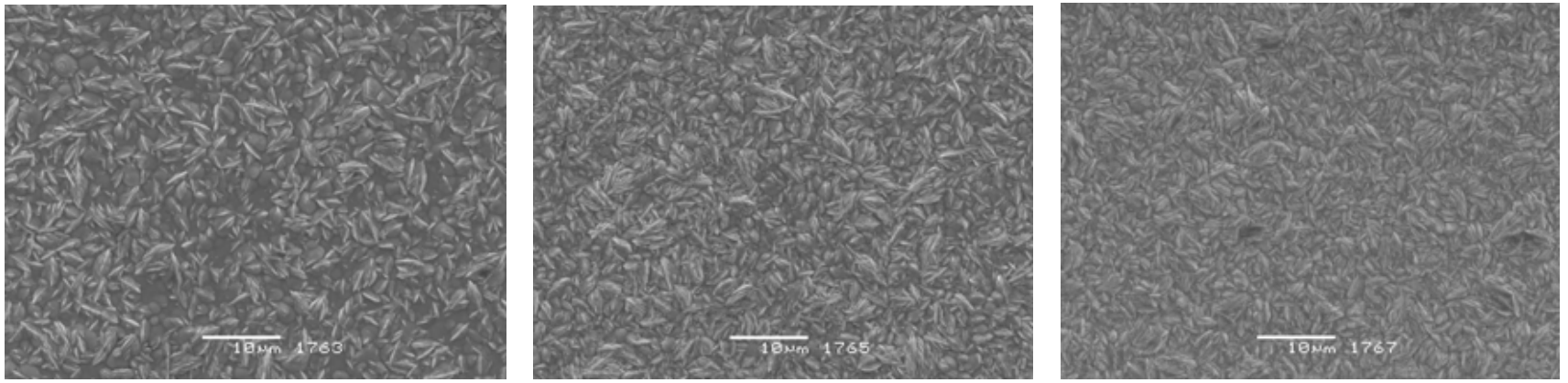

(a) (b) (c)

Fig. 5 Surface topographies of Ni-W deposits at 0.01 A cm^{-2} from fresh electrolyte containing glycine with definite pH values of 7.5 (a), 8.0 (b) and 8.5 (c)

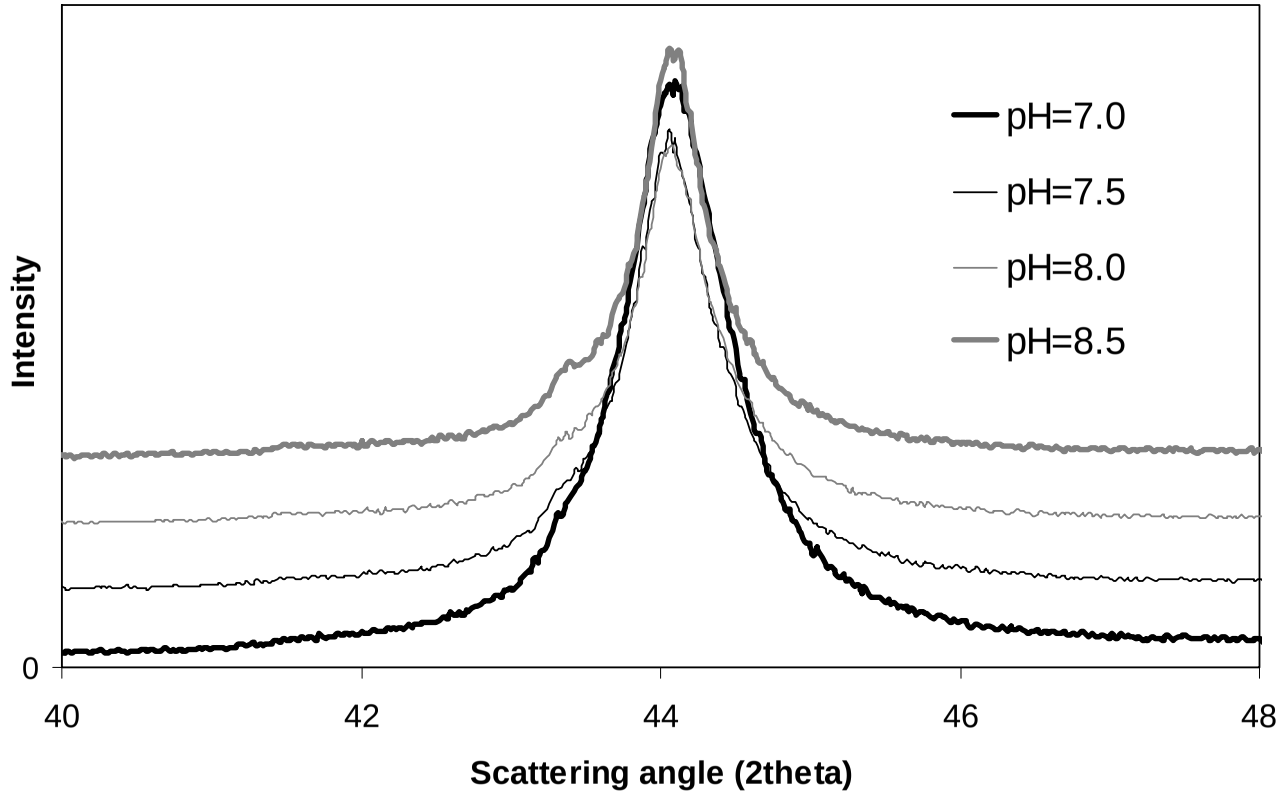

Fig. 6 X-ray diffractograms of Ni-W layers deposited at 0.01 A cm^{-2} from fresh electrolyte with various pH values

Chapter 8

Structure Strength And Stability of Nanocrystalline Ni and Ni-W Layers Electrodeposited from Electrolyte Containing Citrate, Glycine and Treethanolamine

Abstract

In the present work hardness, grain size and thermal stability of nickel and Ni-W alloy layers deposited from electrolytes containing equal amounts of citrate, glycine and triethanolamine are investigated. The hardness of the deposits was investigated in the as-deposited layer as well as after annealing for 1 hour at temperatures up to 550°C. The grain size and microstrains were determined for several crystal orientations by pseudo-Voigt single line analysis of the corresponding X-ray line profiles. The micro Vickers hardness of the nickel deposits depends on the thermal history of the sample. Depending on the microstructure and composition of the electrodeposit the hardness increases or decreases with annealing temperature (for 1 hour). The results are discussed in terms of the possible strengthening mechanisms for nano-crystalline electrodeposits.

1. Introduction

Ni-W alloys possess high corrosion resistance and mechanical strength. This combination of properties allows the application of Ni-W electroplating as micro-injection molding tools.

Strengthening of nano-crystalline electrodeposits cannot be achieved by all the strengthening mechanisms known for bulk materials. The most relevant appear to be solid solution strengthening and grain boundary strengthening. Schuh et al. [1] showed that the high thermal stability of Ni-W electrodeposits is not contributed by solid solution strengthening of W. According to their estimation the dissolution of tungsten in Ni (W=14 at.%) leads to an increment in hardness of only 40 MPa.

The influence of the grain size, d, on the yield strength, σ, (or equivalently hardness) is usually described by the Hall-Petch relation [5-6]:

$$\sigma = \sigma_0 + kd^{-\frac{1}{2}} \qquad (1)$$

where σ_0 and k are material constants. Yamasaki et al. reported that, contrary to Eq.(1), the hardness of Ni-W alloy electrodeposits increased upon annealing, even though the grain size increased from 1.5 nm to 12 nm. [2-4]

This phenomenon is known as the inverse Hall-Petch relation. Several mechanisms have been suggested to explain the inversion of the dependence of hardness on grain size. [1-4, 8-10] Yamasaki et al. [2-4] suggested that in nano-crystalline alloys of Ni-W deposits the deformation does not slip along crystallographic planes within the grains but rather by the sliding of groups of crystals. Grain boundary sliding becomes the

most important, the larger the number of grain boundaries, i.e. the smaller the grains. Consequently, in the range where grain-boundary sliding is the dominant deformation mechanism, the hardness decreases with decreasing grain size. It was observed that the cross-over from dislocation-dominated deformation to sliding-dominated deformation for Ni and Ni-W electrodeposits occurs at a grain size of 15 nm [2-4].

Masumura et al. [7] described the plastic deformation in nanocrystalline materials as a competition between deformation of the grain interior via conventional dislocation motion and a change of the grain shape through grain-boundary diffusion via Coble creep. Scattergood et al. [8] described that at a certain value of the grain diameter, which is comparable to the cut-off distance for the stress field of the dislocations, softening occurs in nano-crystalline materials.

J. Schiøtz et al. [9] reported that atomic-scale analysis of molecular dynamic simulation results showed new dislocations are generated at grain boundaries. glide thorough grains, and are adsorbed at other grain boundaries; i.e., formation of dislocation pileups which causes the Hall-Petch effect. For small grains, the extent of a pileup is limited and the local buildup of stress in a pileup is reduced.

Fan et al. [10] assumed that the grain boundary is composed of a layer of an amorphous phase with disordered atomic arrangement and a low glass-transition temperature, so the deformation at the grain boundary layer occurs visco-elastically in a nano-crystalline material. They described the deformation by the steady-creep depending on the viscosity linked to the diffusivity of the grain boundary and the volume fraction of the grain boundary layer. Accordingly, the higher the diffusivity of a component, the larger is the critical diameter at which the inverse Hall-Petch relation commences. For Cu this critical diameter is at 14-50 nm, whereas for a Ni-W alloy the diameter is 12-15 nm.[9]

Complexing agents in the electrolyte enable the co-deposition of Ni and W and prevent the precipitation of, most probably, $NiWO_4$ [11] in the electrolyte. Several reports exist on the influences of organic additives on the electrocrystallization of nickel. Roth et al.[12] reported that various kinds of organic additives contained in an electrolyte reduced the surface roughness of the nickel deposit and increased the cathode potential of the main deposition reaction $Ni^{2+} + 2e \rightarrow Ni$. Organic additives have been postulated to adsorb at the electrode, inhibit the electrodeposition of nickel, and interfere with the growth of deposited nuclei. The ability to suppress crystal growth depends on the size of the complexing molecule and the number of unsaturated groups in the molecule.[13] Costavaras reported [14], that in the presence of unsaturated organic compounds the texture of nickel electrodeposits degenerates due to a limitation of the lateral extension caused by the organic compounds lying along

the nickel surface. Alternatively, organic compounds adhere preferably at a particular crystallographic plane, as for example a densest packed plane (111), leading to the inhibition of the growth of this specific plane and preferred growth of the other crystallographic planes. Nakamura et al.[15] reported that finer grained crystals were observed in nickel layers deposited from an electrolyte containing saccharin and aliphatic alcohols, as compared to the electrolyte not containing the organic additives.

In the present paper, we report on the crystallographic microstructure, hardness and thermal stability of Ni and Ni-W alloy layers electrodeposited from electrolytes containing equal amounts of the complexing agents citrate, glycine and triethanolamin.[16, 17] The results are compared with investigations of Ni layers deposited from an electrolyte with no complexing agents.

2. Experimental procedure

A 25L plastic container was used as the electrochemical cell. An additive-free electrolyte for Ni electrodeposition consisted of 0.26 mol.dm^{-3} $NiSO_4 \cdot 6H_2O$, 0.04 mol.dm^{-3} $NiCl_2 \cdot 6H_2O$ and 0.44 mol.dm^{-3} H_3BO_3. The electrolyte for Ni electrodeposition containing the complex agents contains in addition to the above constituents 0.3 mol.dm^{-3} citrate, 0.3 mol.dm^{-3} glycine, 0.3 mol.dm^{-3} triethanolamine. For Ni-W electrodeposition the bath consisted of 0.6 mol.dm^{-3} $Na_2WO_4 \cdot 2H_2O$ in addition to the above Ni electrolyte containing the complexing agents.
The electrolyte bath was kept at 60°C and was agitated with air bubbling during deposition. As the substrate for electrodeposition a copper plate, cathodically degreased with an alkaline solution and pickled in a commercial HCl solution, was applied.
The deposits were annealed in air for 1 hour at 100°C, 250°C, 400°C and 550°C in a horizontal tube furnace; temperature control was within ±2 °C.
X-ray diffraction analysis (Discover D8, Bruker AXS) was performed using CuKα radiation. Diffractograms were recorded with a step size of 0.02 °2θ and measuring time 5 sec per step. Scanning electron microscopy (JSM-5900, JEOL) was applied for a qualitative characterization of the surface topography. Composition-depth profiles of the deposits were determined with glow discharge optical emission spectroscopy (JY-5000RF, Horiba Co. Ltd.). Microhardness was measured at a load of 25 g on cross-sections of the electrodeposits with a Hanemann microhardness tester. The cross sections were polished in order to avoid the influence of surface roughness on the measurement. Each reported hardness value is the average of 10 independent

indentations.

3. Results and interpretation

3.1 Topography of Ni and Ni-W alloy layers

The surface topographies of the Ni and Ni-W electrodeposits are shown in Fig. 1. The surface of the Ni deposit from the complex-containing electrolyte is characterized by a large number of fine grains, whereas coarser grains are shown in the layers from the complex-free electrolyte. Cracks are observed in the deposits electroplated at a current density of 0.05 $A.cm^{-2}$ from the electrolyte containing the additives. The micrograph of the Ni-W alloy layer deposited at a current density of 0.01 $A.cm^{-2}$ suggests the presence of fiber-shaped precipitates on the surface. It is not known whether these precipitates are formed during electrodeposition or after finished electrodeposition, for example during cooling from the deposition temperature to room temperature.

3.2. X-ray diffraction analysis of Ni and Ni-W electrodeposits

The X-ray diffractograms of the Ni and Ni-W alloy deposits with thickness of about 100 μm are shown in Fig. 2. Assuming that fiber texture exists in the electrodeposits, the layers electrodeposited from the complex-free electrolyte at 0.01 $A.cm^{-2}$ and 0.05 $A.cm^{-2}$ have a preferred texture of <110> and <100>, respectively. The electrodeposits are sufficiently thick to rule out any influence of a preferred texture in the substrate on the measured textures in the electrodeposits. Generally, the diffractograms of the Ni layers deposited from the complex-containing electrolyte show broader line profiles and lower peak intensities. Also, crystallographic texture appears to be less pronounced than for the Ni deposits from the complex-free electrolyte. The line profiles of the Ni-W alloy deposits are shifted to lower Bragg angles as compared to the Ni deposits. This is attributed to the lattice expansion associated with the dissolution of tungsten in the f.c.c. nickel host lattice. The tungsten content in the Ni-W alloy deposits increases from W=6 at. % to W=11 at. % on changing the current density from 0.01 to 0.05 A cm^{-2}. The line profiles for Ni-W are generally broader than those for the Ni layers deposited from the complex-containing electrolyte, and broadening appears to increase with the tungsten content (i.e. current density). In addition the Bragg reflection identifiable as f.c.c. Ni(-W), there are anomalous Bragg reflections at 41°/2θ, 89°/2θ and 91°/2θ and 93°/2θ as well

as a shoulder at 47°/2θ. The line broadening of the anomalous peak at 41°/2θ of the Ni-W layer deposited at current density of 0.05 A cm^{-2} is relatively small. The origin of these anomalous peaks has been discussed in the previous works [18, 19], and was ascribed to the co-deposition of Ni(-W) and Ni-W-C domains. Interstitial dissolution of carbon, originating from the complexing agents, in the f.c.c. Ni-W lattice gives rise to an expanded f.c.c. lattice. Fig. 3 and Fig. 4 show the X-ray line profiles of Ni and Ni-W alloy electrodeposits upon annealing for 1 hour at 550°C, respectively. Clearly, the line profiles of both the Ni and the Ni-W deposits are narrower than in the as-deposited condition (cf. Fig. 2). Generally, the line-profiles of the Ni-W deposits are broader than the Ni deposits. The peaks associated with the anomalous phase in the Ni-W electrodeposits have disappeared. Instead, peaks associated with the oxide $NiWO_4$ have appeared.

The broadening of all line profiles determined for Ni and Ni-W deposits was interpreted in terms of the size of the coherently diffracting crystallites (i.e. grain size in nano-crystalline materials) and microstrains. To this end the pseudo-Voigt single line analysis [19,20] was applied to the 111, 200, 220 and 311 line profiles. The results of these analyses are collected in Table 2 and Fig.5. For the Ni layer electrodeposited from the complex-free electrolyte the line broadening of 111, 200 and 220 line profiles was comparable to the instrumental broadening of the diffractometer in the corresponding 2θ range. Consequently, an interpretation in terms of grain size and microstrain was not possible for these line profiles. Fig. 5a shows that the grain size determined for 111, 200 and 220 line profiles are comparable for the complex-containing electrolyte; the grain size evaluated from the 311 line profile is significantly smaller.[1] Fig. 5b shows a similar trend as Fig. 5a, but here the evaluated grain sized of both <200> and <311> grains are significantly smaller than <111> and <200>. For the as-deposited Ni-Layers the grain sizes determined for 111 and 311 line profiles is the smaller the higher the current density during deposition, which is in correspondence with the higher driving force for deposition at higher current density. Upon annealing grain growth occurs. Evidently, the rate of grain growth and the "incubation time" depends strongly on the grain orientation. It appears that the <111> oriented grains grow fastest: as compared to the as-deposited state their size has increased by a factor 5 upon annealing for 1 hour at 550 °C.

The grain size determined for the Ni-W deposits shows major irregularities as compared to the Ni layer deposited from the complex-containing electrolyte. This can partly be attributed to interference with overlapping peaks (this only applies for 111 and 311 for the Ni-W layer electrodeposited at 0.05 A cm^{-2}). For the as-deposited condition it is remarkable that particularly the <111> and <200> grains appear to be

significantly smaller in the Ni-W deposits than in the Ni deposits. It was impossible to determine grain size for 200 line profiles for the Ni-W layers electrodeposited at 0.05 A cm^{-2} due to the too low intensity. Regarding the evolution of the grain size upon annealing, it appears that the <111> and <200> grains in the Ni-W deposit grow more slowly than those grains in the Ni electrodeposits do. The <111> and <220> grains in the Ni-W layer electrodeposited at 0.01 $A.cm^{-2}$ appear to shrink upon annealing. As shown in Fig. 6 (a), the 220 and 311 line profiles of the Ni-W layer appear to be broader and are shifted to higher Bragg angles upon annealing. The phenomenon of the change of the line profile is similar to the gradual disappearance of the anomalous Bragg reflection at about $2\theta=41°$ upon annealing for the Ni-W layer, as shown in the previous work [17].

3.3 Compositional analysis of Ni and Ni-W electrodeposits

The composition depth profiles determined with GD-OES are shown in Fig. 7. The carbon profile in the layer deposited from the complex-free electrolyte gradually decreases with depth and no difference is observed between carbon levels in the deposit and in the copper substrate. The carbon profile of the layer deposited from the electrolyte containing the complexing agents decreases at the interface between the deposit and the copper substrate. It indicates that the deposit from the complex bath contains carbon. The origin of the carbon in the deposits is the incorporation of the complexing agents. The complexing agents of citrate, glycine and triethanolamine are also expected to be absorbed on the electrode strongly, leading to interference with the electrocrystallization of the deposit, and influence on the microstructure of the deposit. Ni-W alloy deposits contain carbon as well. In previous studies [19, 20] it was found that the anomalous Bragg reflections are likely to be a consequence of lattice expansion of the f.c.c solid solution Ni(W) due to carbon interstitial dissolution. The dissolution of carbon in pure nickel does not lead to a shift of the Ni Bragg reflections, indicating that carbon is not dissolved interstitially in the nickel f.c.c. lattice. Presumably, short range order of C and W atoms promotes the interstitial incorporation of carbon in the Ni-W(-C) domains. Further, no crystalline phases in addition to nickel was observed. Therefore, it is assumed that carbon in the nano-crystalline Ni deposits is mainly present at grain boundaries.

3.4 Microhardness of Ni and Ni-W electrodeposits

Microhardnesses of the electrodeposits in the as-deposited condition are given in

Table 2. Evidently, the complexing agents cause a substantial increase in the hardness of the nickel deposit, which coincides with a significant decrease in the grain size (cf. Table 1 and Fig. 5).

Upon annealing the hardness of the Ni layers deposited from the complex-free electrolyte decreases progressively with annealing temperature (Fig. 8). On the other hand, the hardness of the Ni layers electrodeposited from the electrolyte containing the complexing agents increases for annealing temperatures up to 250 °C and decreases beyond this temperature (Fig. 8). The hardness of the carbon-containing Ni layers deposited from the complex-containing electrolytes (both Ni and Ni-W) is higher than for those deposited from the complex-free electrolyte, irrespective of the annealing temperature. For the Ni-W electrodeposits the hardness increases gradually with annealing temperature up to 550 °C. Only for the highest annealing temperature, the hardness of the Ni-W deposits is higher than for the corresponding Ni layers. In the as-deposited condition and the annealing temperature lower than 550 °C the hardness of the Ni-W deposits is always lower than for the Ni layers deposited from the complex-containing electrolyte.

4. Discussion

The determined grain sizes in the various electrodeposits clearly show that the grain size depends on the grain orientation. In this respect it should also be recognized that the grain size is determined along the direction of the diffraction vector, i.e. perpendicular to the plane of the layer. The spread among the grain size values is modest for the as-deposited Ni layers as well as the annealed Ni layers up to, say, 400 °C. A quantitative evaluation of hardness in terms of grain size is therefore considered to be allowed for these deposits. For the highest annealing temperature as well as for the Ni-W electrodeposits, which show a large spread among the determined grain sizes, such a quantitative comparison is doomed to fail. Therefore only a qualitative evaluation will be given for these deposits.

In order to arrive at an average grain size from the orientation specific grain sizes in Table 1, the grain size values were weighted according to their relative texture weight in the diffractogram:

$$d_{ave} = \sum_j f_j d_j = f_{111} d_{111} + f_{200} d_{200} + f_{220} d_{220} + f_{311} d_{311} \qquad (2)$$

where f_j is the texture fraction of $j = hkl$ and d_j is the grain size of $j = hkl$.

The fraction is defined as

$$f_j = \frac{I_j / I_{0,j}}{\sum I_j / I_{0,j}} \qquad (3)$$

where I_j is the integrated intensity of the Bragg reflection $j = hkl$ and $I_{0,j}$ is the relative intensity of a random Ni powder, as given by JCPDS standard 04-850.
A comparison of the grain size values thus determined and the microhardness is given in Fig. 9.
The hardness of the Ni layer deposited at higher applied current density of 0.05 A cm^{-2} as a function of grain size in range of d <25 nm is higher than for 0.01 A cm^{-2}, while the hardness values of both layers deposited at 0.01 A.cm^{-2} and 0.05 A.cm^{-2} with large grains (corresponding to the samples annealed at 550 °C) coincide.

According to the values given in references 1-3, the hardness for grain sizes up to 15 nm depends on the composition of electrodeposit. With increasing tungsten content in the deposit the hardness increases. The tungsten content in the deposit has an influence on sliding-dominated deformation. Probably, tungsten dissolution in nickel gives rise to an increase of the diffusivity of the grain boundary and resistance to the sliding-dominated deformation. The hardness of the Ni with grain diameter of < 20 nm deposited at higher applied current density of 0.05 A cm^{-2} is higher compared to 0.01 A cm^{-2}, and that for 10 nm coincides with the Ni-W layer with W=13 at.% as given in the literature[1]. The high hardness is ascribed to the presence of carbon in these electrodeposits. Most probably, along with the smaller as-deposited grain size in the Ni layer deposited at 0.05 A.cm^{-2}, a higher amount of carbon is incorporated in the deposit. The presence of carbon may also increase the diffusivity of the grain boundary as well as tungsten.
The lower hardness of the Ni-W deposits obtained in the present work is ascribed by the irregular grain size distribution. Probably, the increase in hardness upon annealing is ascribed by compositional change of grains. It is assumed that carbon is also dissolved interstitially in the solid solution Ni(W) and, particularly, in the anomalous phase. Upon annealing a redistribution of carbon atom over Ni-W and Ni-W(C) domains may occur. Indeed, increases in micro-stress determined from the 220 and 311 line profiles upon annealing were observed. Compositional gradients might be responsible for the higher microstrains. The carbon redistribution may change structure of the grain boundary and increase the hardness of the Ni-W deposits where grain-boundary sliding is the dominant deformation mechanism.

5. Conclusion

A Ni layer electrodeposited from an electrolyte containing equal amount of citrate, glycine and triethanolamine is characterized by smooth surface, high hardness and

small grain size. For the as-deposited Ni-layers from the complex-containing electrolyte the grain sizes are the smaller the higher the current density during deposition. The grain sizes of both <200> and <311> grains are significantly smaller than <111> and <220>. Upon annealing grain growth occurs. The rate of grain growth and the "incubation time" upon annealing depend strongly on the grain orientation. The <111> oriented grains grow fastest. The hardness of the Ni layers electrodeposited from the electrolyte containing the complexing agents increases with annealing temperature for annealing temperatures up to 250 °C and decreases beyond this temperature. The inverse Hall-Petch relation occurs for the Ni layer deposited from the complex-containing electrolyte. The hardness as a function of grain size of the Ni layer deposited at 0.05 A cm^{-2} is higher than for 0.01 A cm^{-2}.

Generally, the line-profiles of the Ni-W deposits are broader than the Ni deposits. The grain size determined for the Ni-W deposits shows major irregularities as compared to the Ni layer deposited from the complex-containing electrolyte. Both the Ni and Ni-W layers deposited from the complex-electrolytes contain carbon. Only for the highest annealing temperature applied, i.e. 550 C, the hardness of the Ni-W deposits is higher than for the corresponding Ni layers.

Acknowledgement

Financial support from the Danish Research Council for Technology and Production Sciences (under grant 26-03-0276) is gratefully acknowledged.

5. References

1. C.A. Schuh, T.G. Nieh, H. Iwasaki, Acta Mater. 51 (2003) 431-443
2. T. Yamasaki, P. Schloßmacher & Y. Ogino, Nanostructured Materials, Vol. 10, No. 3 (1998) 375-388
3. T. Yamasaki, Mater. Phys. Mech., Vol. 1 (2000) 127-132
4. P. Schloßmacher & T. Yamasaki, Mikrochim. Acta, 132 (2000) 309-313
5. E.O. Hall, Proc. Ohys. Soc. London, 1951, vol. B64, 747-753
6. N.J. Petch, J. Iron Steel Inst., 1953, vol. 174, 25-28
7. R. A. Masumura, M.P. Hazzledine,, and C.S. Pande, Acta Mater. 46, (1998) 4527-4537
8. R. Scattergood and C.C. Koch, Scripta Matall. Mater. 27 (1992) 1195-1200
9. J. Schiøtz and W. Jacobsen, Science vol. 301 (2003) 1357-1359
10. G.J. Fan, H. Choo, P.K. Liaw, and E.J. Lavernia, Metallurgical and Material

Trans. A, 36A (2005) 2641-2649
11. N. Eliaz, T. M. Sridhar, E. Gileadi, Electrochimica Acta, 50, 2893-2904 (2005)
12. Clayton C. Roth and Henry Leidheiser, J. Electrochem. Soc. 12 (1953) 553-565
13. B. D. Cullity; Elements of X-Ray Diffraction, Addison-Wesley Publishing, Company, INC (1967)
14. Th. Ap. Costavaras, M. Froment, and A. Hugot-Le Goff, J. Electrochem. Soc., 7 (1973) 867-874
15. Y. Nakamura, N. Kaneko, M. Watanabe and H. Nezu, J. Appl. Electrochem., 24 (1994) 227-232
16. I. Mizushima, P. T. Tang, H. N. Hansen and M. A. J. Somers, Electrochimica Acta, 51, 888-896 (2005)
17. I. Mizushima, P. T. Tang, H. N. Hansen and M. A. J. Somers, Electrochimica Acta, 51, 6128-6134 (2006)
18. I. Mizushima, P. T. Tang, and M. A. J. Somers, ”Microstructure characterization of Ni-W electrodeposits ; identification of an anomalous phase” in this thesis
19. I. Mizushima, P. T. Tang, and M. A. J. Somers, “Influence of age of electrolyte containing glycine as complexing agent on microstructure of Ni-W alloy electrodeposit” in this thesis
20. T.H. Keijser, J.I. Langford, E.J. Mittemeijer and A.B.P.Vogels, J.Appl. Cryst., 15 (1982) 308
21. J.I. Langford, J. Appl. Cryst. (2004) 37, 381-390

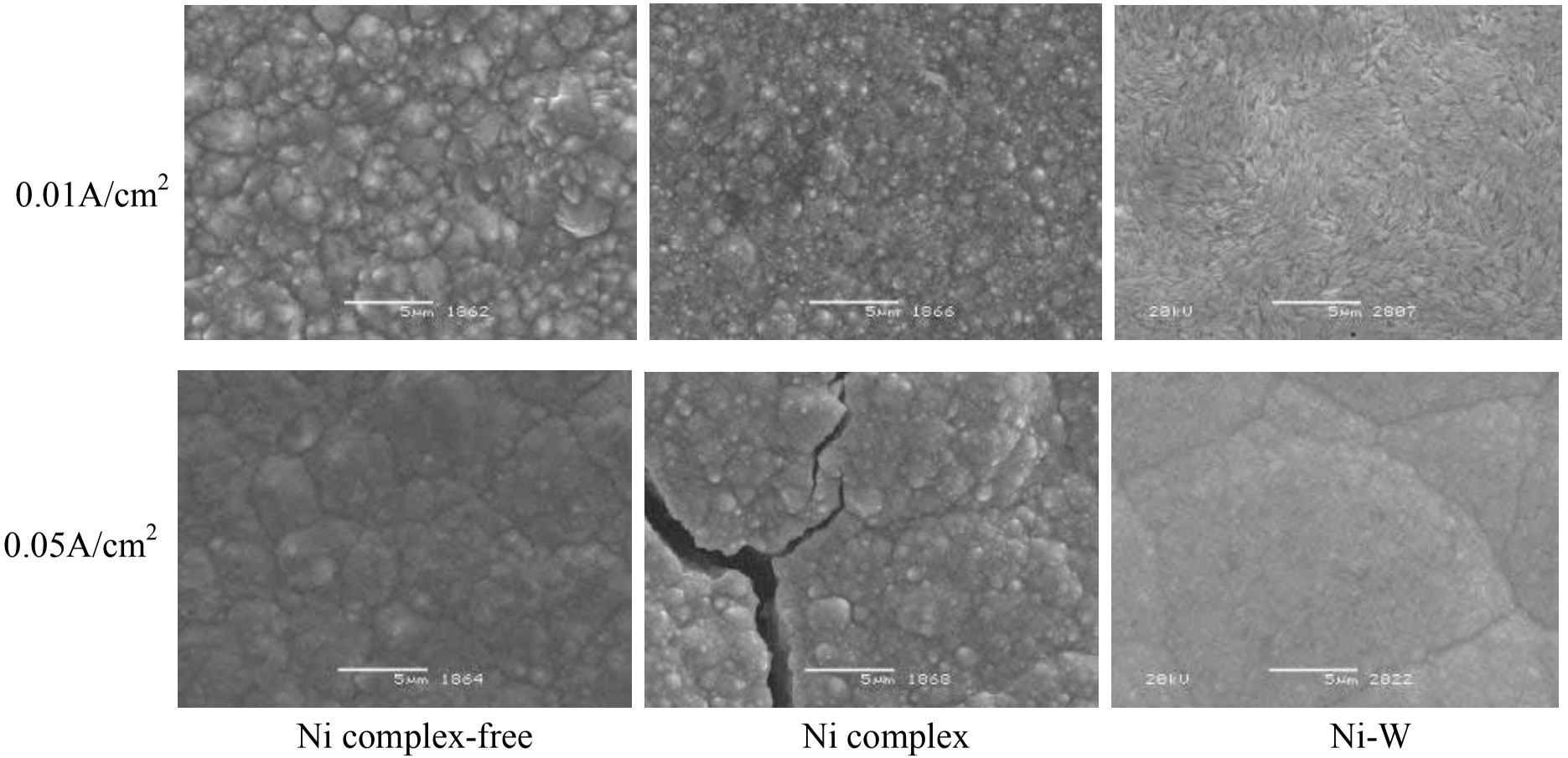

Fig. 1: Surface topographies of Ni layers deposited from complex-free electrolyte and complex-electrolyte and Ni-W alloy electrodeposits

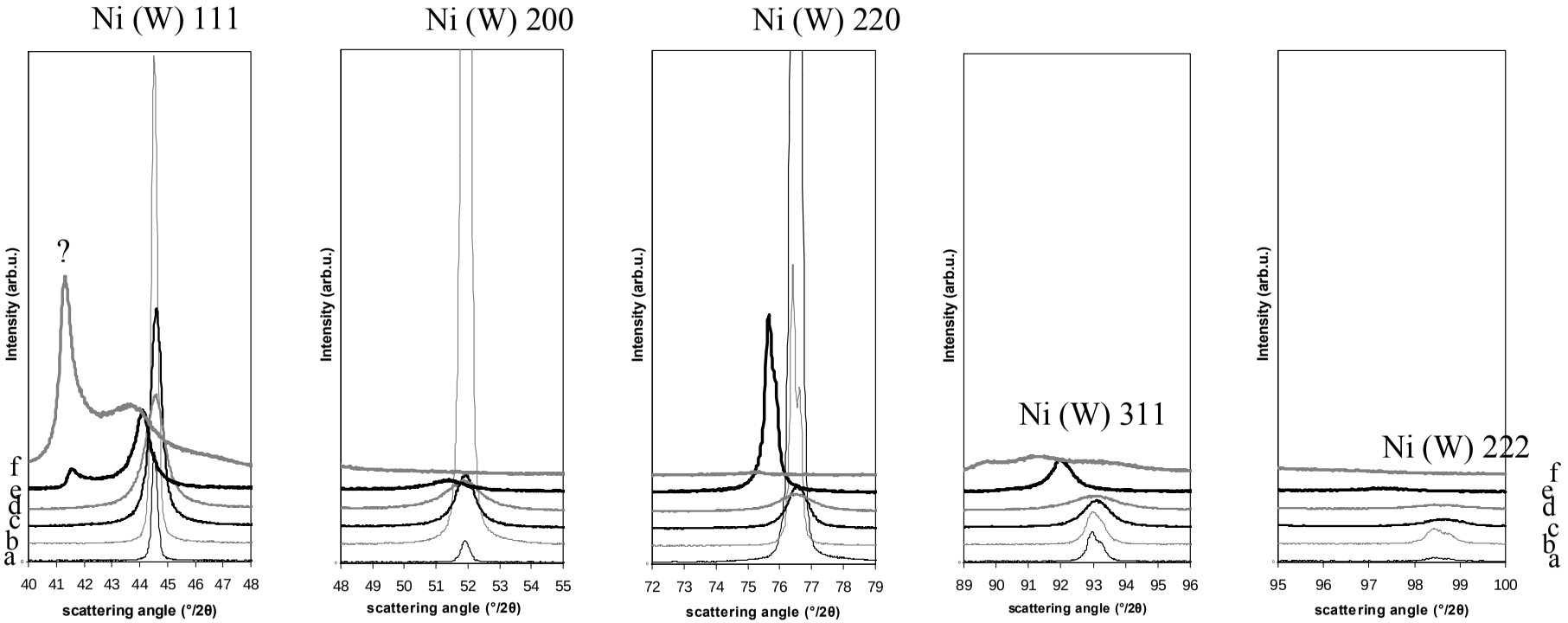

Fig. 2: XRD patterns of Ni and Ni-W layers electrodeposited at 0.01 A cm^{-2} (black line) and 0.05 A cm^{-2} (gray line)

a —— :Ni-complex agent free, 0.01 A cm^{-2}, b—— :Ni-complex agent free, 0.05 A cm^{-2},

c —— :Ni-complex agent, 0.01 A cm^{-2}, d—— :Ni-complex agent, 0.05 A cm^{-2},

e —— :NiW-complex agent, 0.01 A cm^{-2}, f—— :NiW-complex agent, 0.05 A cm^{-2}

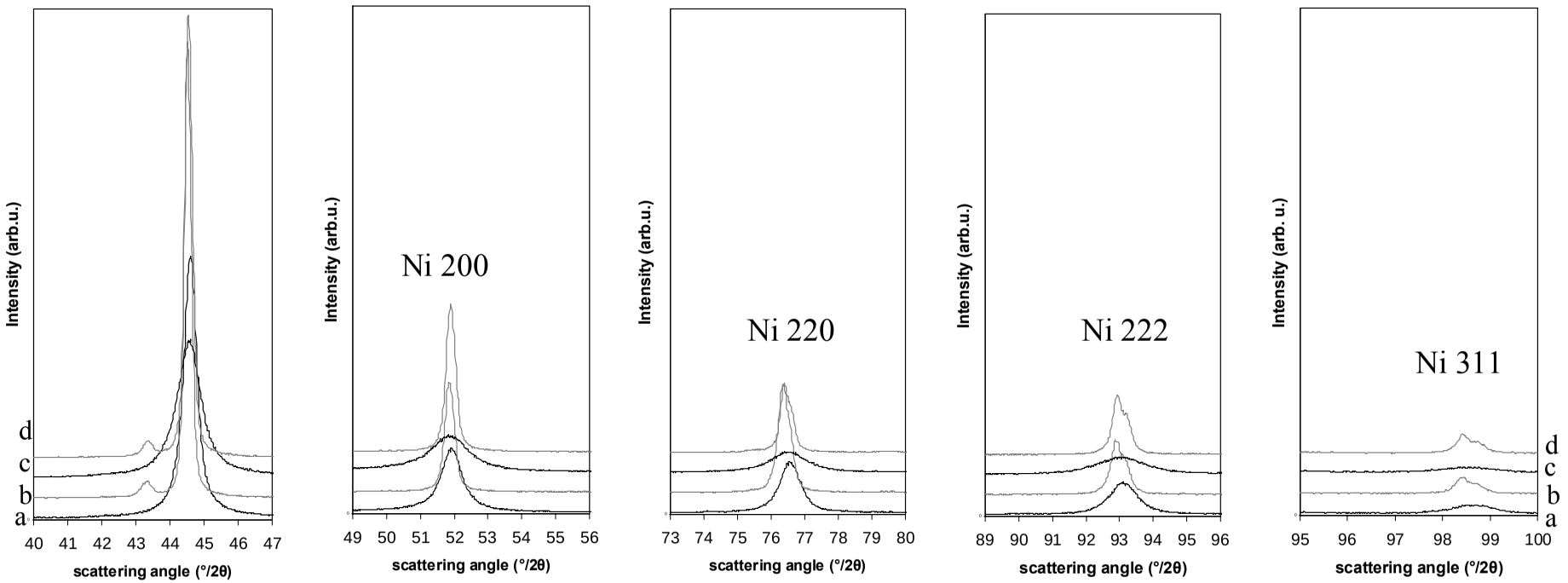

Fig. 3: Change of X-ray diffractograms of Ni layers with annealing for one hour at temperatures of 550 °C (as-deposit : black, annealed layer : gray)
a: 0.01 A cm^{-2} as-deposit, b: 0.01 A cm^{-2} annealed at 550°C
c: 0.05 A cm^{-2} as-deposit, d: 0.05 A cm^{-2} annealed at 550°C

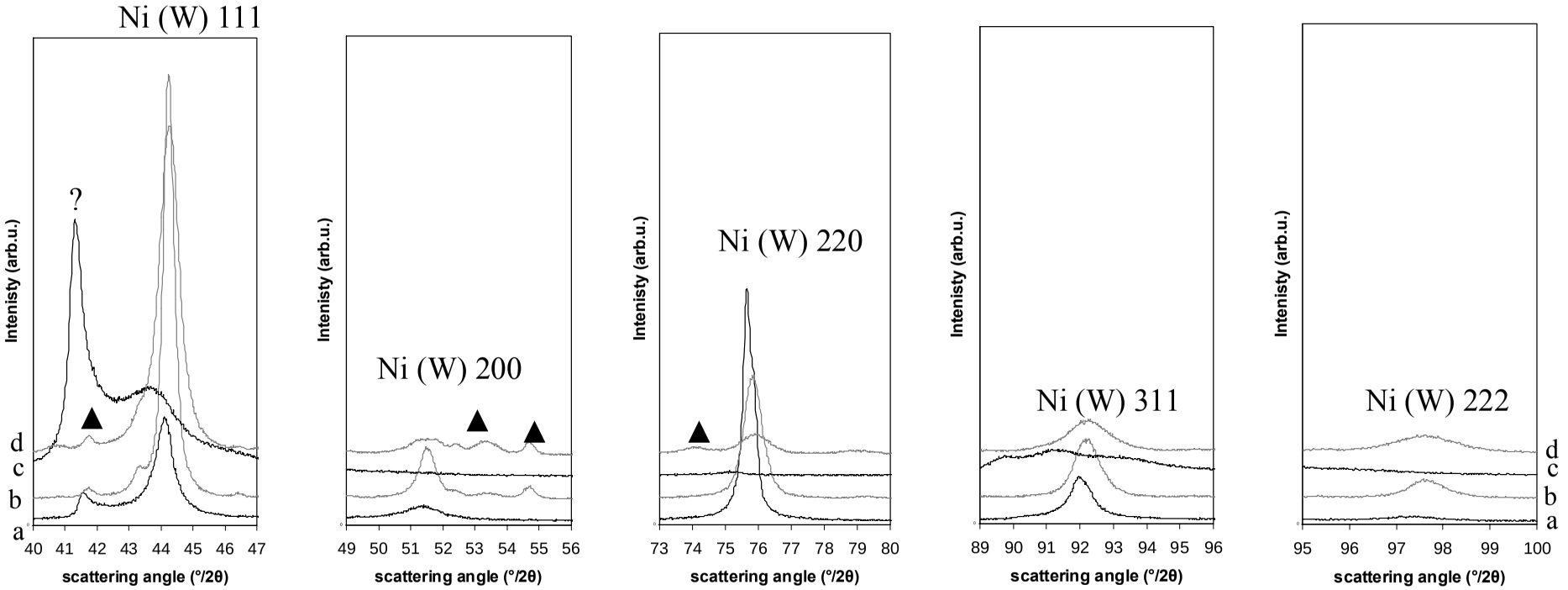

Fig. 4: Change of X-ray diffractograms of Ni-W layers with annealing for one hour at temperatures of 550 °C (as-deposit : black, annealed layer : gray)
a: 0.01 A cm^{-2} as-deposit, b: 0.01 A cm^{-2} annealed at 550°C
c: 0.05 A cm^{-2} as-deposit, d: 0.05 A cm^{-2} annealed at 550°C
? : anomalous phase, ▲: $NiWO_4$

Table 1: Values of grain size of Ni electrodeposits assessed from XRD line-profile broadening

		Ni- complex-free		Ni-complex		NiW-complex	
		0.01 A cm^{-2}	0.05 A cm^{-2}	0.01 A cm^{-2}	0.05 A cm^{-2}	0.01 A cm^{-2}	0.05 A cm^{-2}
111	As deposit			18	12	18	
	100°C			20	14	10	
	250°C			26	17	13	
	400°C			37	21	20	6
	550°C			110	81	30	18
200	As deposit			17	10	6	
	100°C			20	10	6	
	250°C			21	11	7	
	400°C			25	16	7	
	550°C			41	47	8	
220	As deposit			19	11	38	
	100°C			23	14	23	
	250°C			23	15	25	
	400°C			29	23	22	27
	550°C			53	65	32	30
311	As deposit	72	44	13	9	14	
	100°C	70	55	13	9	14	
	250°C	110	84	15	12	23	
	400°C	>200	>200	20	17	27	
	550°C	>200	>200	31	33	30	5

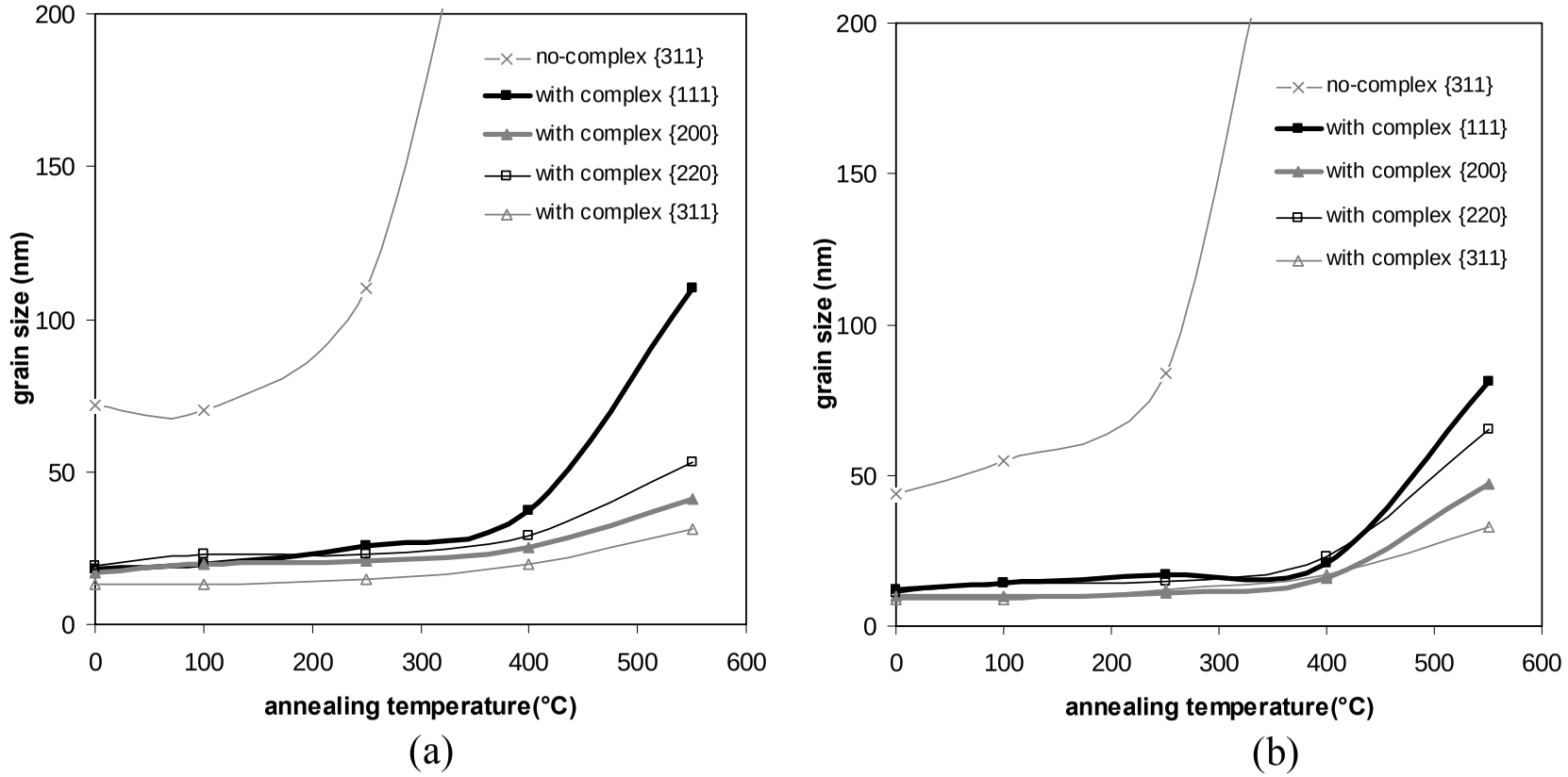

Fig. 5: Change in grain size with annealing of Ni layers deposited at 0.01 A cm^{-2} (a) and 0.05 A cm^{-2} (b) from the additive-free electrolyte and the electrolyte containing citrate, glycine and triethanolamine and Ni-W alloy deposits

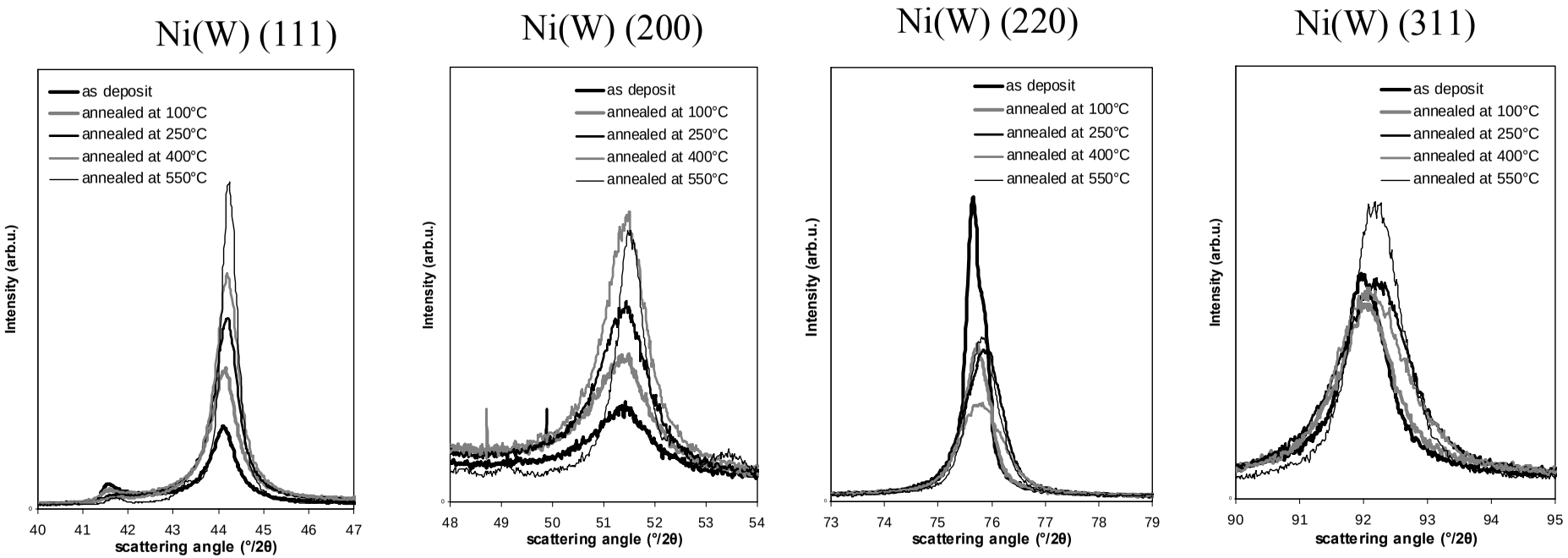

Fig. 6: X-ray diffractograms of Ni-W deposit electroplated at 0.01 A cm^{-2} from electrolyte containing citrate, glycine and triethanolamine and annealed for 1 h at the annealing temperatures indicated

Table 2: Hardness of Ni layers deposited from complexing agent-free electrolyte and electrolyte containing the complexing agents and Ni-W alloy electrodeposits

electrolyte	Current density A cm^{-2}	Hardness HV-25g, MPa
Ni-complex free	0.01	280±10
	0.05	290±15
Ni-complex	0.01	560±10
	0.05	660±20
Ni-W-complex	0.01	420±20
	0.05	390±25

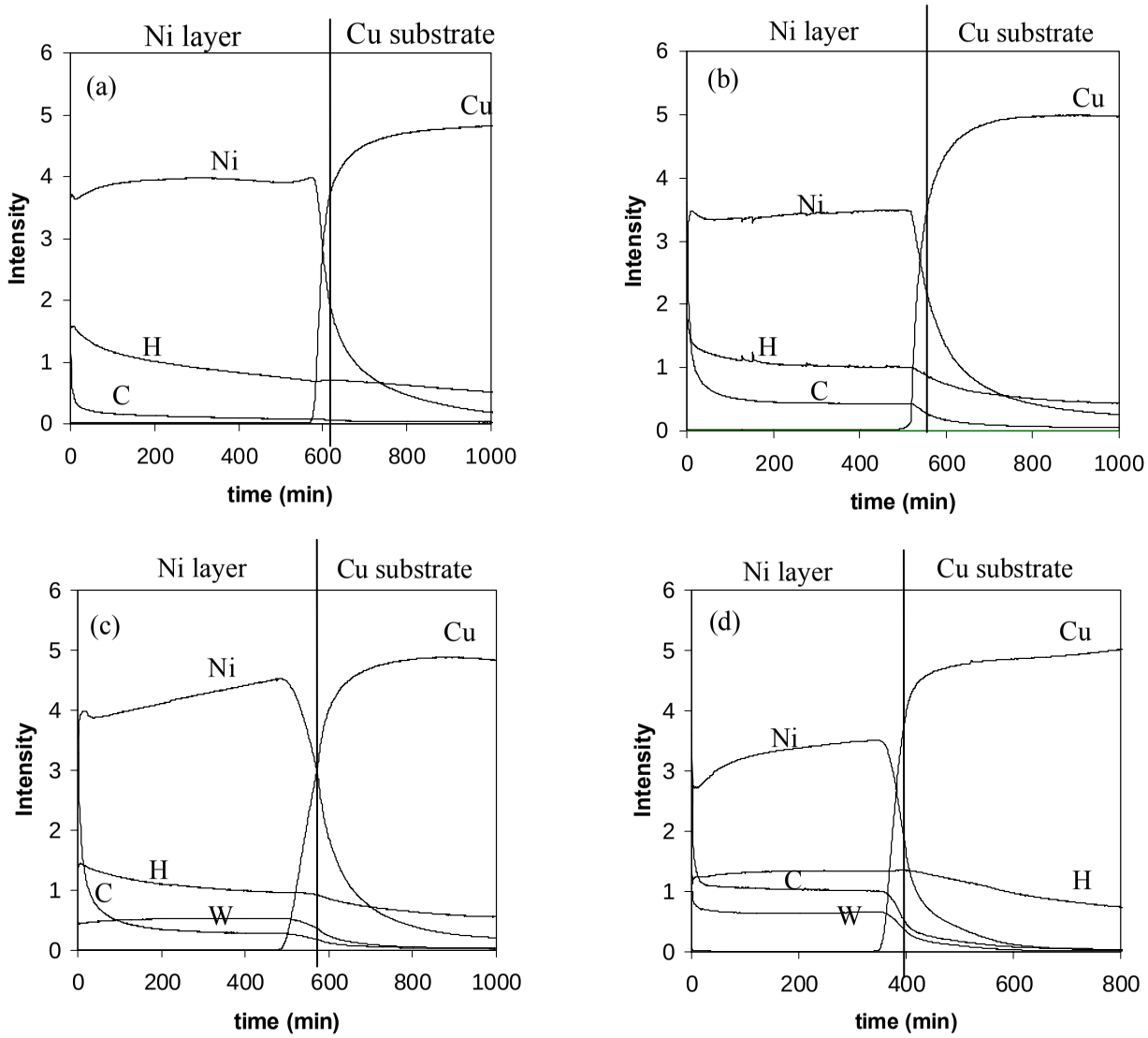

Fig. 7: GD-OES profiles of Ni deposits electroplated at 0.01 A cm^{-2} from electrolyte containing no complexing agent (a) and from electrolyte containing citrate, glycine and triethanolamine (b) and for Ni-W deposits electroplated at 0.01 A cm^{-2} (c) and 0.05 A cm^{-2} (d) from an electrolyte containing citrate, glycine and triethanolamine

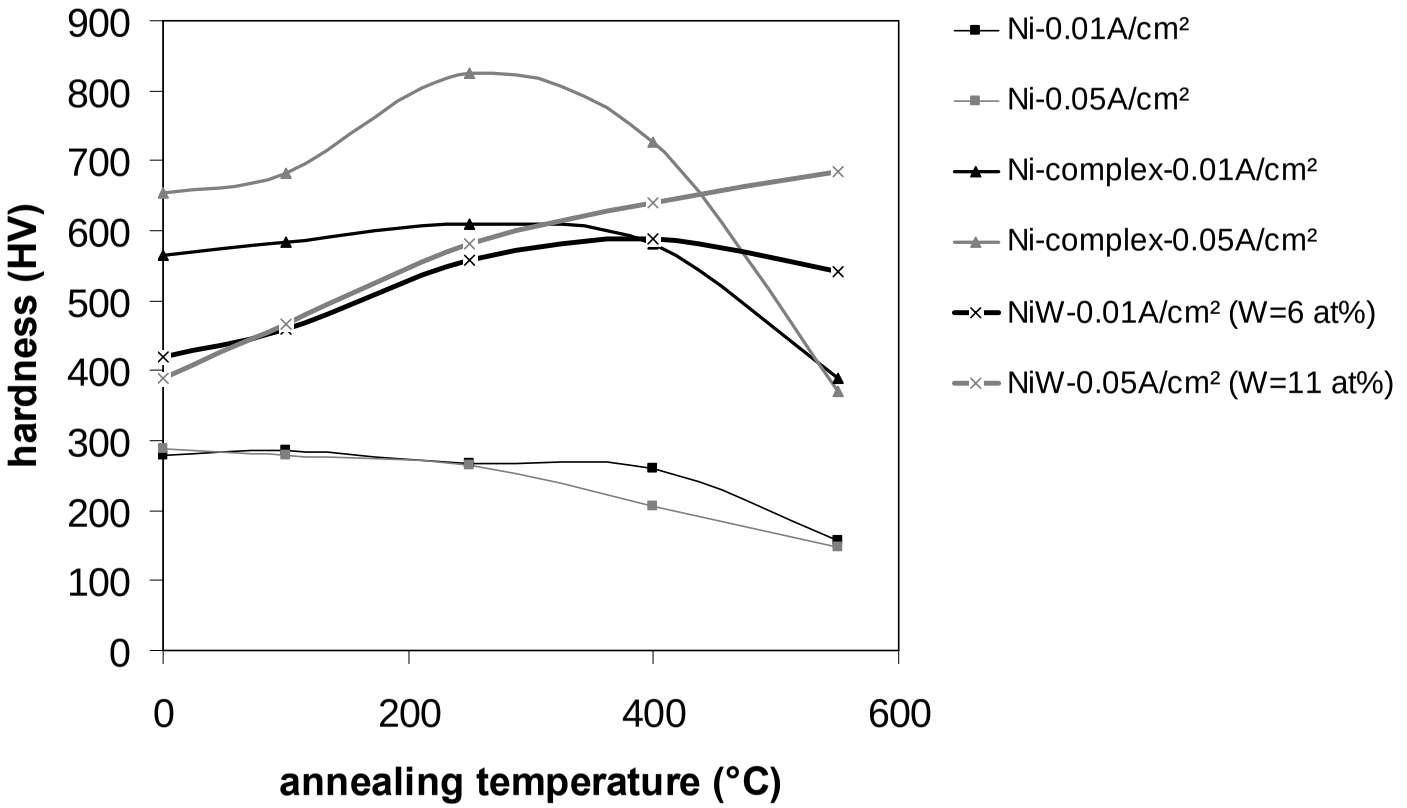

Fig. 8: Change in hardness with annealing of Ni layers deposited from the additive-free electrolyte and the electrolyte containing citrate, glycine and triethanolamine and Ni-W alloy deposits

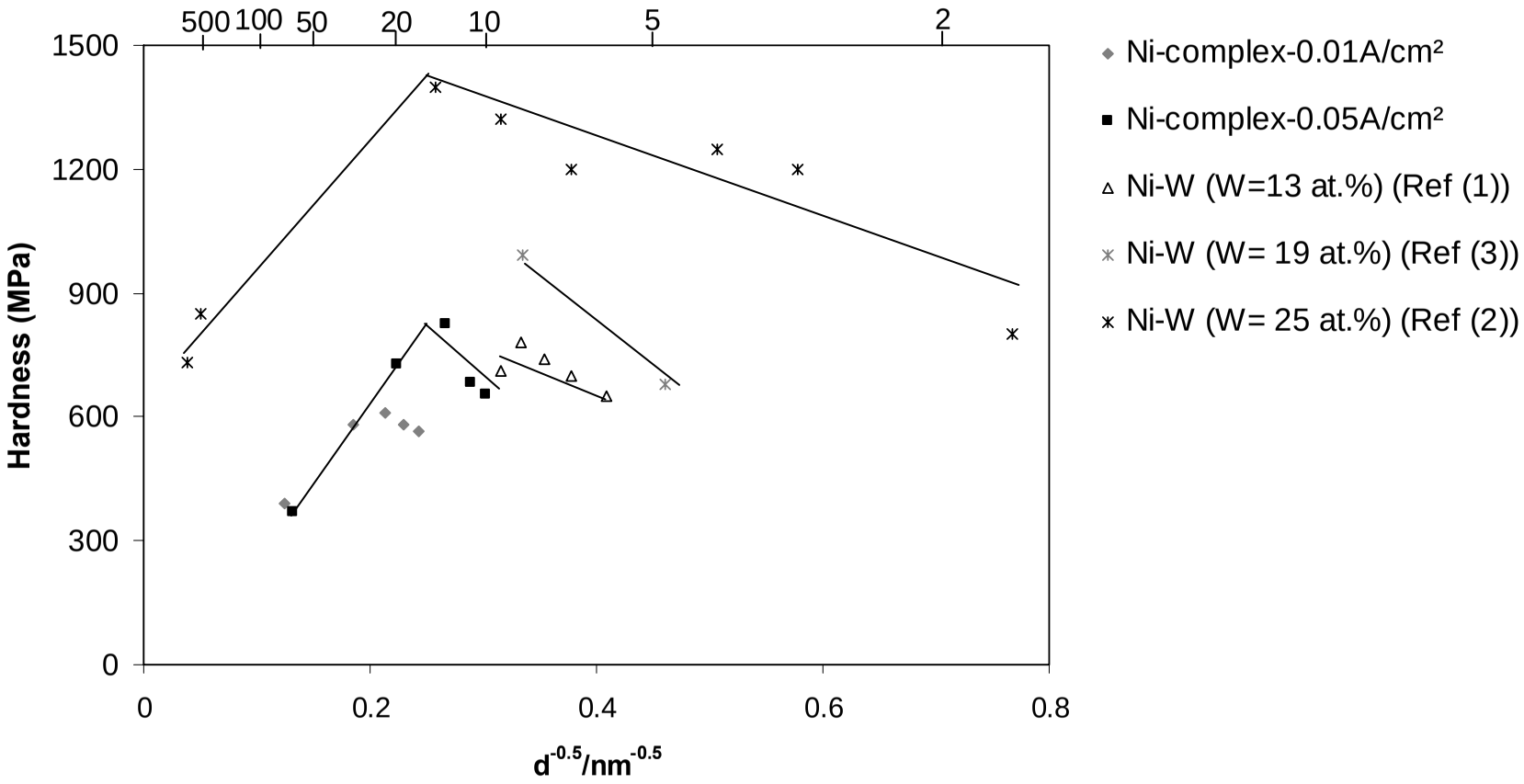

Fig. 9: Vickers microhardness as a function of $1/d_{ave}^{2}$ (d=grain diameter) of nickel layers deposited from electrolyte containing citrate, glycine and triethanolamine.

Chapter 9

Evolution of Residual Stress in Ni-W electrodeposits

Summary

In the present work the evolution of residual stress in Ni-W layers electrodeposited from electrolytes based on $NiSO_4$ and Na_2WO_4 upon storage at room temperature is investigated. Citrate, glycine and triethanolamine were used as complexing agents in the electrolyte to enable the co-deposition of Ni and W. Residual stress averaged over the thickness of the 5-µm-thick Ni-W layers was determined applying the bent-strip method, taking Cu-Be strips as the substrate.

An increase in tensile stress in the Ni-W electrodeposit during storage at room temperature was observed; the increase in tensile residual stress is the larger the higher the current density during electrodeposition.

For one selected current density the electrical resistivity of a Ni-W layer was measured as a function of storage time. The evolutions of stress increase and reduction of electrical resistivity are equal for the first three hours.

1. Introduction

Ni-W is an excellent material due to its high corrosion resistance combined with high mechanical strength and relatively straightforward manufacturing by electroplating of the material.

Usually electroplating of Ni-W alloys is associated with poor current efficiency[1-3]. In previous work we reported on the development of a new electrolyte on the basis of $NiSO_4$ and $NiWO_4$, containing citrate, glycine and triethanolamine (TEA) as complexing agents [4]. Upon electrodeposition it was observed that residual stress in the layers changed significantly within the first 24 hours, from relatively low tensile values to moderate values of (several) hunderd(s) of MPa's. An increase of tensile stresses in the Ni-W layer upon storage at room temperature may induce failure by cracking of the electrodeposit [5]. It was demonstrated that modifying the bath composition could result in effectively stress-free electrodeposits.

Hydrogen incorporation in electrodeposits and its subsequent release is considered an important mechanism for the occurrence of tensile stress in electrodeposited Ni layers. Monev explained [6] a time-dependent decrease of the hydrogen concentration in Ni electrodeposits from the decomposition of an unstable compound between Ni and H, that had formed during electrodeposition. Then, it would be expected that the level of tensile residual stress is the higher, the lower the current efficiency during deposition. Accordingly, generally higher residual stresses are expected for higher current

densities, since the current efficiency tends to decrease with current density. Nevertheless, in our previous work a large spread was observed among various layers electrodeposited at high current densities, while the current efficiency was effectively kept constant at about 80%.[5] A significant increase in tensile stress was measured upon storage, eventually leading to cracking. Huang et al. reported that tensile stress in Ni-W deposits increased with current density as well, even though the current efficiency increased[7-9]. Apparently, current efficiency is not the only parameter that affects the evolution of residual stress upon storage.

Possibly, Ni-W electrodeposits also contain hydrogen. With respect to our work a current efficiency below about 80% is considered sufficiently low to cause hydrogen dissolution during deposition; subsequent hydrogen release from the deposit would then lead to the development of tensile stress.
In fact, an increase in the tensile stress was seen even after drying the specimen at room temperature in the previous study [5]. The diffusion rate of hydrogen in solid nickel is 80 μm per hour. Possibly, an increase in residual stress after drying is related to the fast hydrogen diffusion, which gives rise to quick desorption of hydrogen and shrinkage of the deposit.
Possibly, the tensile stress level caused by hydrogen incorporation and its subsequent release depends on the current density. Fukai et al. estimated the gas pressure that would correspond to the hydrogen activity at the surface of the electrode as a function of the overpotential [10]. As the overpotential increases with current density, the amount of dissolved hydrogen in the deposit is expected to increase with current density as well[10].

So far limited attention has been devoted to the evolution of residual stress with time after deposition. In the present work we focus on the time-dependence of residual stress in Ni-W deposits. Layer thickness averaged residual stress was determined intermittently with the bent strip method. Also, electrical resistivity was measured to monitor continuously the occurrence of (possible microstructural) changes in the electrodeposit.

2. Experimental procedure

A 1 dm^3 beaker was used as the electrochemical cell. The electrolytes consisted of 0.1 mol dm^{-3} $NiSO_4 \cdot 6H_2O$, 0.2 mol dm^{-3} $Na_2WO_4 \cdot 2H_2O$, 0.1 mol dm^{-3} citrate, 0.1 mol dm^{-3} glycine, 0.1 mol dm^{-3} triethanolamine and 0.44 mol dm^{-3} H_3BO_3. Agitation was

conducted with a magnetic stirrer. The bath was kept at 70°C during deposition. Layer thickness was adjusted at 5 μm for both stress and resistivity measurements.

The mechanical stress in the deposits was estimated from the deflection of one side deposited test strips (Specialty Testing & Development Co.) with known elastic constants (E=130GPa, ν=0.350). The test strip is made from a CuBe foil and is approximately 60 μm in thickness, consists of a 15 mm wide base and has two "legs" of 76 mm long and 5 mm wide. The base and legs of the strip are covered with a resist layer that prevents deposition on facing sides of the legs. The cell for stress measurement has two anodes and one cathode (the test strip) which is located centrally between the anodes, such that the opposite sides of the test strip experience identical deposition conditions. Internal stress in the deposits makes the two legs bend in opposite directions. The distance between the ends of the deflected beams of the test strip, equaling twice the deflection of a single beam, gives an average value of deflection due to stress in the electrodeposit. The average value was converted into mechanical stress using a Perakh's equation that can be applied for measurement of a deflection on the free end of a cantilever substrate [11]. Mechanical stress values were determined immediately after drying in air at room temperature and sometimes after finished deposition. The measurement interval was accessed from the absolute change in residual stress. Immediately after deposition the distance between the deflected legs was measured at short intervals, because of a relatively fast change of the stress.

The difference between deposition temperature and room temperature (where the stress measurements were conducted) introduces a thermal stress between the Ni electrodeposit and the CuBe substrate. Taking the thermal expansion coefficients for Ni and CuBe as 13.3 10^{-6} K^{-1} and 17.0 10^{-6} K^{-1}, respectively a thermal strain of 1.665 10^{-4} is introduced on cooling from 70 °C to room temperate. For a thin Ni layer on an infinitely thick substrate this strain would correspond to a compressive stress of -48 MPa (elastic constants for Ni were taken as: E=199.5 GPa; ν=0.312). The composition in the layer deposited on the test strip was determined semi-quantitatively with energy dispersive X-Ray spectroscopy (Oxford Scientific).

Electric resitivity of the layers was measured with a Tinsley Micro Ohmmeter in four-point-probe geometry. A non-conductive silicon wafer coated with Ti and gold was used as a substrate of specimen for the resistivity measurement.

3. Results and discussion

Fig. 1 shows the time-dependent residual stresses of 5-μm-thick Ni-W layers electrodeposited at 0.005 A cm^{-2}, 0.01 A cm^{-2} and 0.05 A cm^{-2}.

The development level of the residual stress in the deposit depends on the applied current density. Even though the initial stress of the deposit at 0.05 A cm^{-2} is high, the increase in stress is small and stops at 4 hours, whereas, the increase in tensile stress of the deposit at 0.05 A cm^{-2} is extremely high. An exponential curve is seen in the time-dependence of stress for 0.005 A cm^{-2}. Especially, an increase for the first 10 minutes is enormous, and the stress increases from 20 MPa up to 80 MPa. The increase for all the applied current densities has not been over 50 days later yet, as shown in Fig. 2. For the applied current densities of 0.005 A cm^{-2} and 0.01 A cm^{-2} values of tensile stress seem to be stable after the first 15 hours. Actually, the stress in the layers for 0.005 A cm^{-2} and 0.01 A cm^{-2} continue to increase slightly, which results in an increase in slope at a storage time of 15 hours in the Fig. 2.

Fig. 3 shows both changes in the stress and resistivity of the layer for 0.01 A cm^{-2}. The axes of resitivity and stress are scaled as the changes in both the values upon storage for 24 hours are fitted. While a positive change is seen for the stress, the resitivity changes negatively. The resistivity change indicates a change of the amount of defects in the electrodeposit (point, line, plane and volume defects). The difference in fitting the curves between for first 3 hours and 4 hours indicates several kinds of possibilities what happen in the electrodeposit upon storage after electroplating.

The time dependence is assumed to be caused by hydrogen release from the deposit which results in shrinkage of the deposit and the introduction of tensile stress in the deposit, according to several reports on dissolved hydrogen in Ni electrodeposits. The decrease in resistivity can also be caused by release of hydrogen from point defect in deposit. Especially, the enthalpy of solution of hydrogen in nickel, ΔH, is only 0.17 eV per atom[12], and the solubility of hydrogen in nickel is relatively low as compared to other metals. Besides, differing from hydride formation of solid metal under high pressure in hydrogen gas, electrodeposition might facilitate solution of hydrogen in metal deposit due to simultaneous co-deposition of hydrogen and metal atoms.

Fukai et al. suggested sites which could dissolve hydrogen atoms in nickel from the thermal desorption spectrum [13]. The stability of the hydrogen depends on the type of the site. A desorption peak at 100 °C of hydrogen atoms occupying the interstitial sites disappeared after storage at room temperature for a few hours, whereas; hydrogen atoms trapped by vacancies, which are released upon heating at 350 °C, stay for longer time [13].

The deviation of the stress curve from one of resistivity after 4 hours in Fig. 3 indicates a difference in type of stress development between within the first 3 hours and 4 hours. The development may depend on the type of site that the dissolved hydrogen atoms occupy.

The decrease in resistivity within the first 3 hours may be attributed to release of interstitial dissolved hydrogen which gives rise to lattice expansion. The stability of the hydrogen is low and stress relaxation with shrinkage occurs immediately after the release of the hydrogen. The increase in stress at a time of 4 hours may be caused by the release of hydrogen trapped at sites where H has a higher binding energy for the lattice parameter is less sensitive than the electric resistivity. It is suggested that the release of H from grain boundaries, vacancies and dislocations occurs in this stage.

Fractional volume of grain boundary of the Ni-W electrodeposit increases with increasing applied current density owing to the decrease in the grain size [14]. Probably, the large volume of the intercrystalline regions also gives rise to an increase in amount of hydrogen staying in the deposit for long time. Indeed, the exponential slope in stage II in Fig. 2 for 0.05 A cm^{-2} is higher as compared to 0.005 A cm^{-2} and 0.01 A cm^{-2}.

The slope in stage I also increases with applied current density as well. Fukai et al. mentioned the amount of dissolved hydrogen increased with applied current density, associated with hydrogen activity. Probably, applying high current density facilitates also interstitial dissolution of hydrogen in metal. Besides, tungsten content in deposit may also influence stability of the dissolved hydrogen. Solubility of hydrogen in tungsten is much lower as compared to nickel. Values of the enthalpy of hydrogen solution for nickel and tungsten are 0.17 eV and 1.05 eV, respectively. [10] Tungsten content increased from 6 at.% up to 11 at. % with varying current density 0.005 A cm^{-2} – 0.05 A cm^{-2}. Interstitial dissolved hydrogen may release faster from deposit with higher tungsten content due to lower stability of dissolved hydrogen.

4. Conclusion

An increase of tensile stress in Ni-W deposit with storage time at room temperature was observed. The increase in the stress after storage for twenty-four hours is the larger the higher current density. The tensile stress for 0.05 A cm^{-2} continues to increase even for storage longer than one week.

Fitting curve of change in resistivity with the stress increase indicated that there were two stages of hydrogen release upon storage at room temperature.

5. References

1. O. Younes & E. Gileadi, J. Electrochem. Soc., **149** (2) C100-C111 (2002)
2. O. Younes & E. Gileadi, Electrochemical Solid-State Letters, **3** (12) 543-545

(2000)
3. N. Eliaz, T. M. Sridhar, E. Gileadi, Electrochimica Acta, 50, 2893-2904 (2005)
4. I. Mizushima, P. T. Tang, H. N. Hansen and M. A. J. Somers, Electrochimica Acta, 51, 888-896 (2005)
5. I. Mizushima, P. T. Tang, H. N. Hansen and M. A. J. Somers, Electrochimica Acta, 51, 6128-6134 (2006)
6. M. Monev, M. E. baumgärtner, and C. J. raub, J. Electrochem. Soc., 138, L16 (1991)
7. C. H. Huang, W. Y. She & H. M. Wu, Plating and Surface Finishing, Vol.86 Issue. 12, 79-83 (1999)
8. C. H. Huang, J. Materials Science 34, 1373-1377 (1999)
9. C. H. Huang, Plating & Surface Finishing, 4, 62-65 (1997)
10. Y. Fukai, The Metal Hydrogen System, Basic Bulk properties (Springer, 1993)
11. M. Perakh, Surface Technology, 8 (1979) 265-309
12. E. Fromm, G. Hörz, Intern. Metals Rev. 25, 269 (1980)
13. Y. Fukai, M. Mizutani, S. Yokota, M. Kanazawa, M. Miura and T. Watanabe, J. Alloys Comp., 270, (2003) 356-357
14. I. Mizushima, P. T. Tang, H. N. Hansen and M. A. J. Somers, ”Thermal stability of hardness of Ni-W electrodeposited layers” in this thesis

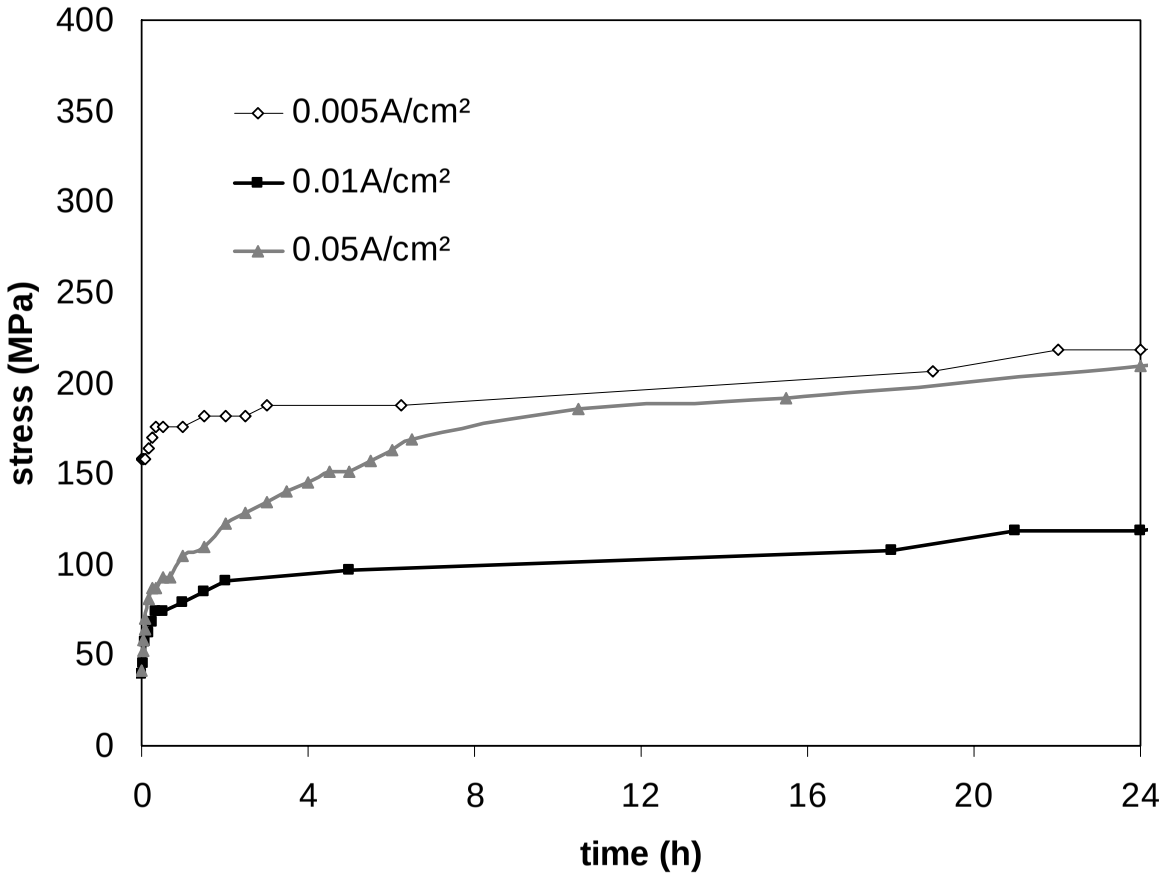

Fig. 1 Time-dependence of residual stress of Ni-W layers electrodeposited at applied current densities of 0.005, 0.01 and 0.05 A cm^{-2} for 24 hours

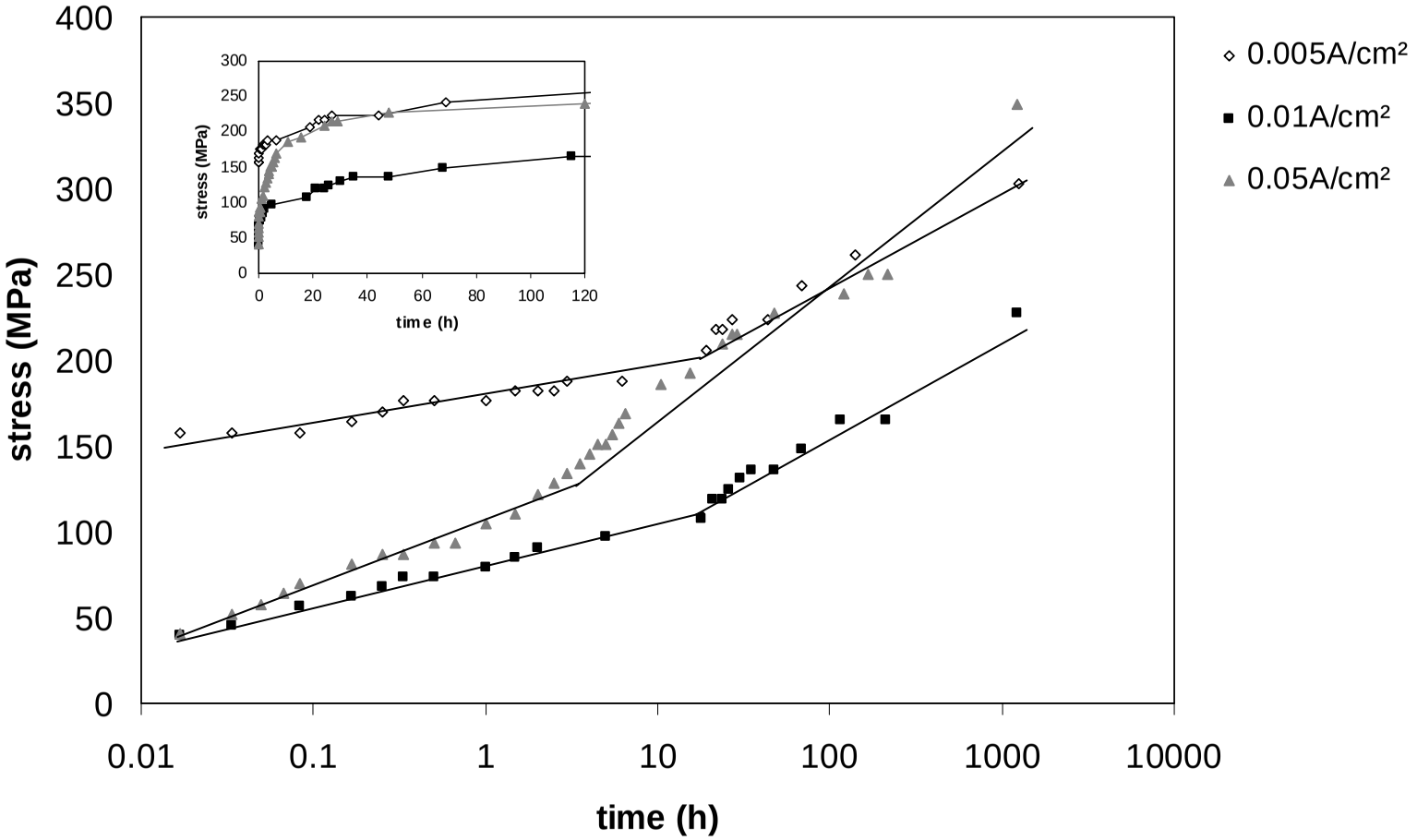

Fig. 2 Time-dependence of residual stress of Ni-W layers electrodeposited at applied current densities of 0.005, 0.01 and 0.05 A cm^{-2} for 50 days

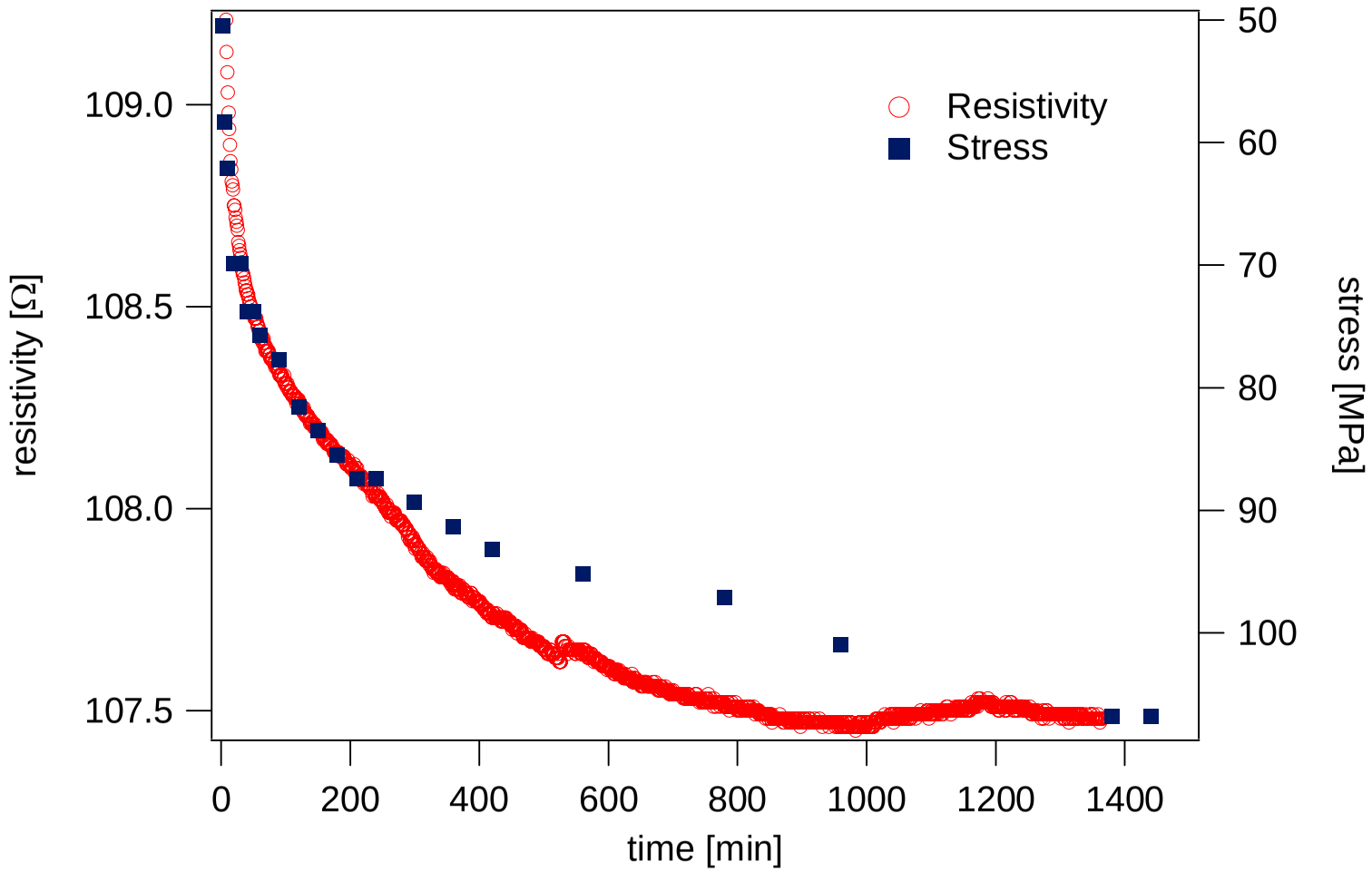

Fig. 3 Time-dependence of residual stress and electric resistivity of Ni-W layers electrodeposited at an applied current densities of 0.01 A cm^{-2}

Conclusion

In the present work development of a new electroplating process for Ni-W alloys possessing high hardness and thermal stability is attempted and some facts are shown.

According to the theoretical comments and literature reviews described in Chapter 2, Ni-W alloy electrodeposits with tungsten content of 13-25 at. % is nanocrystalline material and possesses high hardness and thermal stability, however; it is difficult to obtain a combination of high current density and reasonable tungsten in the conventional electrolyte containing citrate and ammonia as complexing agent.

The development of a new electrolyte containing additional complexing agents was attempted first. High tungsten contents combined with high current efficiencies could be realized by applying electrolytes containing a combination of three complexing agents of citrate, glycine and triethanolamine. The predominant phase of the deposits is a solid solution of tungsten in nickel.

The type of complexing agent used has a strong influence on the residual stress level in Ni-W deposits, irrespective of current efficiency. The combination of the three complexing agents citrate, glycine and TEA reduces residual stress in Ni-W deposits. In all cases, an increase in tensile stress with time was observed. The increase in the stress after storage for twenty-four hours is larger for higher current density. The tensile stress for 0.05 A cm^{-2} continues to increase even for storage longer than one week.

Both the Ni and Ni-W layers deposited from the complex-electrolytes contain carbon, and have nanocrystalline structure. The Ni-W layers have an anomalous phase, which is indicated to be promoted by the presence of both W and C by GD-OES analysis and does not occur in W-free Ni electrodeposits, in addition to the Ni-W solid solution. Carbon can be dissolved interstitially in the Ni-W alloy deposits. Generally, the line-profiles of the Ni-W deposits are broader than the Ni deposits. The grain size determined for the Ni-W deposits shows major irregularities as compared to the Ni layer deposited from the complex-containing electrolyte. The hardness of the Ni layers electrodeposited from the electrolyte containing the complexing agents increases with annealing temperature up to 250 °C and decreases beyond this temperature. The inverse Hall-Petch relation occurs for the Ni layer deposited from the complex-containing electrolyte. The hardness as a function of grain size of the Ni layer deposited at 0.05 A cm^{-2} is higher than for 0.01 A cm^{-2}. Only for the highest annealing temperature applied, i.e. 550 C, the hardness of the Ni-W deposits is higher than for the corresponding Ni layers. The anomalous phase which contains carbon in the Ni-W deposits has disappeared upon annealing at applied temperature of 550°C.

Appendix

Fabrication of forming tool

1. Introduction

Fabrication of the forming tool is preferably performed by electroforming in order to be able to control the reproduction of microscale geometrical details. Nickel is a widely applied material for electroforming, but pure nanocrystalline nickel electrodeposits cannot withstand the relatively high pressure during forming. Among the metals and alloys which are expected to possess higher mechanical strength than nickel and which can be electrodeposited, Ni-Co and Ni-W a favourable candidate.
Then, we developed a new process for producing small component using electroforming.

2. Investigation Procedure

2.1 Fabrication of small cast

The investigation procedure is shown in Fig.1. The fabrication flow of the tool is shown in Fig. 2. The tool must be able to withstand high pressure during forming, so hardness and tensile strength of the electroformed deposits were also examined.

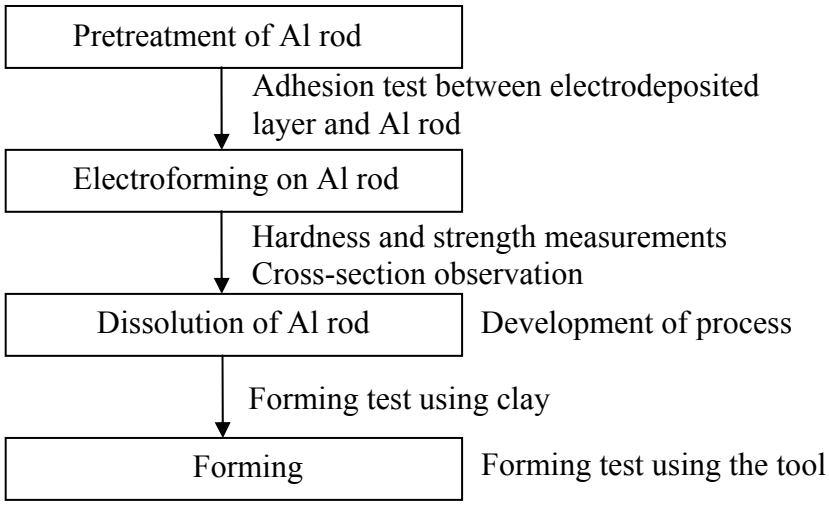

Fig.1 Fabrication flow of tool for forming by electroforming

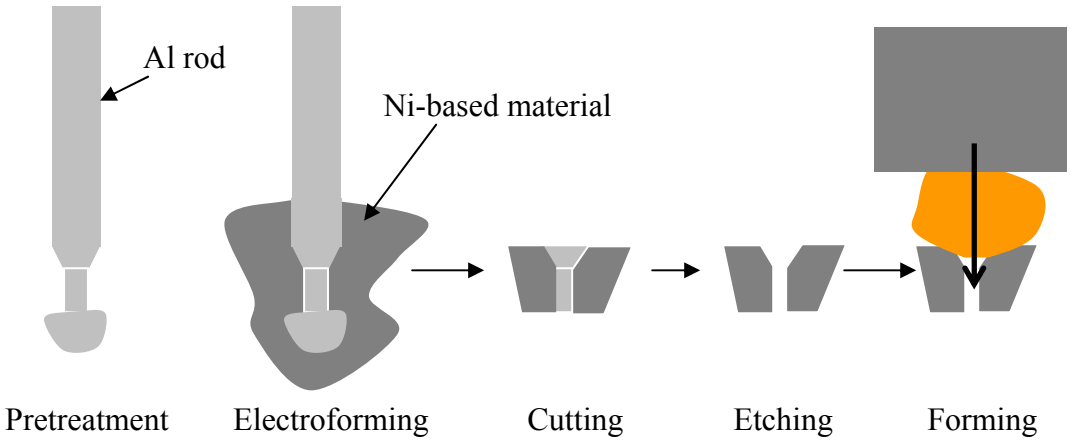

Fig.2 A schematic drawing of fabrication flow of tool for forming by electroforming

An Al rod was used as substrate for electroforming. (Fig.3)

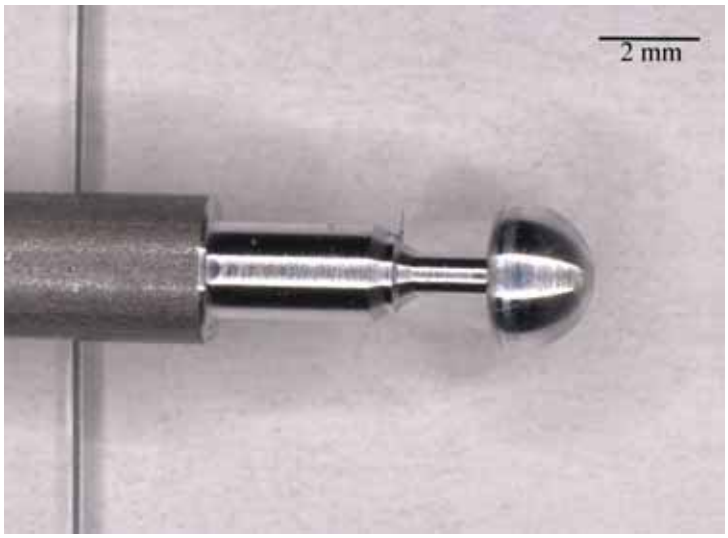

Fig.3 Photograph of Al rod

For all electroforming of Ni, NiCo and NiW a 25L plastic container was used as electrochemical cell. Agitation was conducted with air bobbling. The electrolyte compositions and electrodeposition conditions for Ni, Ni-Co and Ni-W electroplatings are described in Table 2, 3 and 4, respectively. The electroplating was performed after the pretreatment as described in Table 1 in order to ensure high adhesion between Ni layer and Al.

Table 1 Pretreatment process

1	Electropolishing in cyanide-alkaline solution at 4V
2	Treatment with 60g/ℓ NaOH solution at 60 °C
3	Activation with 30g/ℓ HNO_3 and 20g/ℓ NH_4F solution
4	Zincate treatment using commercial chemical

Table 2 Conditions for Ni electroplating

Composition of electrolyte	310 g dm^{-3} $Ni(NH_2SO_3)_2 \cdot 4H_2O$, 35 g dm^{-3} $NiCl_2 \cdot 6H_2O$, and 35 g dm^{-3} H_3BO_3.
Current density	$4A/dm^2$
Temperature	40 °C

Table 3 Conditions for NiCo electroplating

Composition of electrolyte	66 g dm^{-3} $NiSO_4 \cdot 6H_2O$, 238 g dm^{-3} $NiCl_2 \cdot 6H_2O$, 16 g dm^{-3} $CoCl_2 \cdot 4H_2O$, 3 g dm^{-3} 1,3,6 naphthalene trisulphonic acid (NTS) and 35 g dm^{-3} H_3BO_3.
Current density	pulse plating $4A/dm^2/-6A/dm^2$, Qa/Qc=0.5, f=12.5
Temperature	40 °C

Table 4 Conditions for NiW electroplating

Composition of electrolyte	0.26 mol dm^{-3} $NiSO_4 \cdot 6H_2O$, 0.04 mol dm^{-3} $NiCl_2 \cdot 6H_2O$, 0.6 mol dm^{-3} $Na_2WO_4 \cdot 2H_2O$, 0.3 mol dm^{-3} citrate, 0.3 mol dm^{-3} glycine, 0.3 mol dm^{-3} triethaolamin (TEA)) and 0.44 mol dm^{-3} H_3BO_3.
Current density	$1A/dm^2$
Temperature	60 °C

Microhardness was measured at a load of 25g on cross-sections of the electrodeposits with a Hanemann microhardness tester. For the preparation the specimens were mounted in epoxy resin (Seriefix 20), and the cross sections were polished in order to avoid the influence of surface roughness on the measurement. Each reported hardness value is the average of 10 independent indentations.

For tensile strength measurement specimens of $10 \times 90 \times 0.5$ mm^3 were prepared. For the preparation a $130 \times 100 \times 5$ mm^3 aluminium plate was used as substrate for electroplating. After treatment of the whole surface in order to avoid corrosion, 130×100 mm^2 area was electroplated. After cutting the plate, the electrodeposited layer was taken from the Al plate. The measurement was conducted after obtaining a thickness profile as distance in order to calculate the strength precisely, because the thickness of electrodeposited layer is not uniform.

A 2L beaker was used for dissolution of Al rod. The Al rod fixed with stainless wire was hung in the beaker. Al rod was dissolved in 200g/L KOH solution at 90°C with agitation by a magnetic stirrer.

3. Result

3.1 Hardness of electrodeposits

The values of hardness of Ni and Ni-W layers deposited on the Al rod almost coincide to those on Al plate, whereas the hardness of the Co deposit is lower seriously. (Table 5) The decrease was caused not by electrolyte aging but by change of substrate geometry. Probably part current density on thin part of the Al rod is lower, but Co content in the layer is similar. Co content does not have so critical influence on hardness. However, carbon content in the deposit may decrease with changing current density.

Table 5 Hardness of Ni, Ni-Co and Ni-W electrodeposited layers

	on Al plate composition	hardness	on Al rod composition	hardness
Ni			Ni 100%	440
Ni-Co	Ni 62-Co 38%	520	Ni 64-Co 36%	400
Ni-W			Ni 90-W10%	430

3.2 Tensile strength of electrodeposits

Tensile strength of the pure Ni was 10^5N, whereas Ni-Co seems to have higher strength. Ni-W layer is so brittle like stone that the layer was broken during cutting, so it was impossible to prepare specimen for strength measurement any more. Electroformed Ni-W deposit should be annealed for using as a tool for forming.

3.3 Cross-section observation of electroforming on Al rod which has complicated geometry

A Ni layer is deposited on the Al rod without void. (Fig.4 and 5)

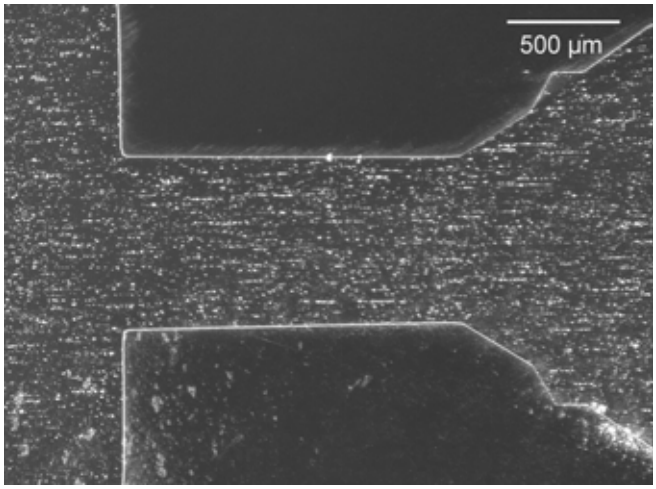

Fig. 4 Cross-section optical microscope image of pure Ni layer on Al rod

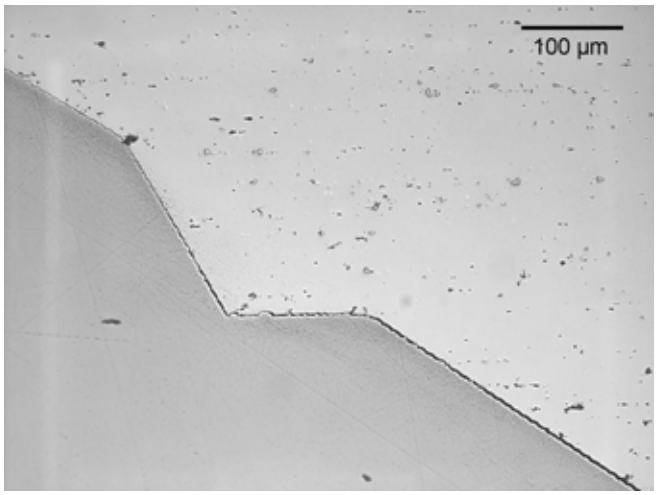

Fig. 5 Cross-section optical microscope image of pure Ni layer on Al rod (high magnification)

After dissolution of the Al rod in the specimen mounted in the mould the surface of the electroformed Ni deposit can also be observed. (Fig. 6) Reproduction of the geometrical detail of the Al rod could be realized.

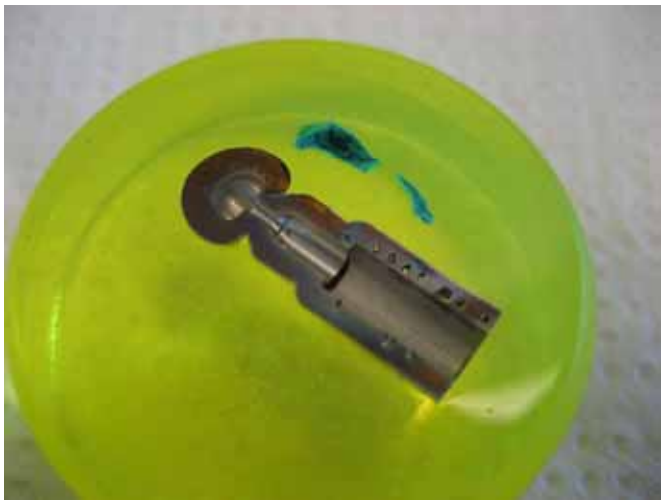

Fig.6 Photograph of specimen of electroformed Ni deposit after dissolution of Al rod

4. Conclusion

According to the process flow, production of a small tool by Ni electroforming was succeeded in.